https://doi.org/10.35662/unine-thesis-2670

Faculty of Science
Centre for Hydrogeology and Geothermics
Laboratory of Geothermics and Geodynamics

Dissertation

High performance computing for hydrothermal systems or geothermal reservoirs using MULTI-GPU technology: Application to the Lusi geyser system in Java, Indonesia

for the degree of
Doctor of Science (Dr. Sc.)

presented by
Reza Sohrabi Zadeh

Accepted on the recommendation of

Prof. Dr. Stephen A. Miller
Centre for Hydrogeology and Geothermics, Laboratory of Geothermics and Geodynamics
University of Neuchâtel

Prof. Dr. Benoît Valley
Centre for Hydrogeology and Geothermics, Laboratory of Geothermics and Reservoir Geomechanics
University of Neuchâtel

Prof. Dr. Yury Y. Podladchikov
Faculty of Geosciences and Environment, Swiss Geocomputing Centre
University of Lausanne

Dr. Benjamin Malvoisin
Faculty of Geosciences and Environment, Swiss Geocomputing Centre
University of Lausanne

Dr. Adriano Mazzini
Faculty of Mathematics and Natural Sciences, Centre for Earth Evolution and Dynamics
University of Oslo

Defended on May 7, 2018

Reza Sohrabi Zadeh

High performance computing for hydrothermal systems or geothermal reservoirs using MULTI-GPU technology: Application to the Lusi geyser system in Java, Indonesia

Dissertation, May 7, 2018
Reviewers: Prof. Dr. Stephen A. Miller, Prof. Dr. Benoît Valley, Prof. Dr. Yury Y. Podladchikov, Dr. Benjamin Malvoisin and Dr. Adriano Mazzini

University of Neuchâtel
Faculty of Science
Centre for Hydrogeology and Geothermics
Laboratory of Geothermics and Geodynamics
Rue Emile-Argand 11
2000 Neuchâtel

UNIVERSITÉ DE NEUCHÂTEL

Faculté des Sciences
Secrétariat-décanat de Faculté
Rue Emile-Argand 11
2000 Neuchâtel – Suisse
Tél : + 41 (0)32 718 21 00
E-mail : secretariat.sciences@unine.ch

IMPRIMATUR POUR THESE DE DOCTORAT

La Faculté des sciences de l'Université de Neuchâtel autorise l'impression de la présente thèse soutenue par

Monsieur Reza SOHRABI ZADEH

Titre:

"High performance computing for hydrothermal systems or geothermal reservoirs using MULTI-GPU technology: Application to the Lusi geyser system in Java, Indonesia"

sur le rapport des membres du jury composé comme suit:

- Prof. Stephen A. Miller, directeur de thèse, Université de Neuchâtel, Suisse
- Prof. ass. Benoît Valley, co-directeur de thèse, Université de Neuchâtel, Suisse
- Prof. Yury Y. Podladchikov, Université de Lausanne, Suisse
- Dr. Benjamin Malvoisin, Université de Lausanne, Suisse
- Dr. Adriano Mazzini, Université d'Oslo, Norvège

Neuchâtel, le 24 mai 2018

Le Doyen, Prof. R. Bshary

Professor: “In Geology, name the three types of rock.”

Me: *1. Classic*

2. Punk

3. Hard

Abstract

Hydrothermal systems and geothermal reservoirs are of major interest for natural and engineering sciences. Their fascinating complexity spurs multidisciplinary efforts for supplying society with heat and electricity production. Their applications require the correct simulation of fluid dynamics and thermodynamics processes in fractured media, and many of these media host a certain degree of complexity. This thesis aims to understand the heat transfer and fluid dynamics within a newborn geyser system, named Lusi, which began erupting in 2006 in East Java, Indonesia.

Geyser systems are ubiquitous, with a wide-range of processes, making the development of a general model difficult. My goal is to establish 3D conceptual and numerical models capable of simulating fluid dynamics and thermodynamics within large-scale geyser reservoirs such as the Lusi region, considering porosity and permeability evolution through time. These models can also address a number of other renewable applications, including Enhanced Geothermal Systems (EGS) and CO2 sequestration (Carbon Capture and Storage CCS).

I developed a new mesh algorithm to create hexahedral octree meshes to transfer the structural geological information using binary space partitioning (BSP) of the input geometry and octree refinement on the grid. The algorithm provides a new method for hexahedral mesh generation for any 3D numerical simulations to quantify Thermal-Hydraulic-Mechanical-Chemical (THMC) physical processes.

Further, I present a new high performance 3D tool using Graphics Processing Unit (GPU) workstations or cluster technology. The physical processes implemented into the code are those associated with deep hydrogeological complexes where high fluid pressures generated by dehydration reactions can be sufficient to induce hydro-fractures that significantly influence porosity and permeability structures within geological formation.

Finally, I use the developed numerical models to investigate Lusi using 3D geological context and complexity with multiphysics processes considering High Performance Computing (HPC) on parallel computing. I present the first 3D numerical model of the Lusi geyser system using multi-GPU technology.

Key words:

High Performance Computing (HPC), Graphics Processing Unit (GPU), 3D Numerical Modelling, Adaptive Mesh Refinement, Geyser, Hydrothermal Systems, Geothermal Reservoirs, Lusi

Résumé

Les systèmes hydrothermaux et les réservoirs géothermaux sont d'un intérêt majeur pour les sciences naturelles et les sciences de l'ingénierie. Leur fascinante complexité intéresse de plus en plus les recherches multidisciplinaires en relation avec la société actuelle pour la demande d'approvisionnement de chaleur et d'électricité. Leur application nécessite la simulation exacte des processus liés à la dynamique des fluides et de la thermodynamique du sous-sol, ceux-ci pouvant être relativement complexes. Le but de ce travail est de comprendre le transfert de chaleur et la dynamique des fluides contrôlant le fonctionnement d'un geyser nommé Lusi. Ce système prit forme, en 2006, sur l'Est de l'île de Java en Indonésie.

Les geysers sont répandus à travers le monde et engendre des processus physiques multiples et difficiles à comprendre. Le développement de modèles pour les étudier est très complexe. Mon but ici, est de créer des modèles conceptuels et numériques en 3D, à grande échelle, capables de simuler la dynamique des fluides et la thermodynamique de ces systèmes en tenant compte de l'évolution de la porosité et la perméabilité de la roche du milieu. Ces modèles peuvent aussi être mis en pratique pour des applications renouvelables tel que les systèmes géothermaux stimulés (EGS) et la séquestration du CO_2 (CCS).

C'est pourquoi, j'ai développé un nouvel algorithme pour la création de meshs hexahedraux qui transfère l'information structural de modèle géologique dans un grid numérique, en utilisant une méthode de « Binary Space Partitioning » (BSP) et d'« octree refinement ». L'algorithme fournit une nouvelle méthode pour la création de meshs hexahedraux pour tous types de simulations numérique en 3D quantifiant les processus physiques Thermique-Hydraulique-Mécanique-Chimique (THMC).

Par la suite, je présente un nouvel outil 3D de « High Performance Computing» (HPC) se basant sur la technologie des « Graphic Processing Units » (GPU). Les processus physiques implémentés dans le code sont associés aux systèmes hydrogéologiques profonds et complexes où les fluides sous-pressions génèrent une réaction de déshydratation de la roche suffisante pour induire de l'hydro-fracturation. Ces processus influencent fortement les structures de la porosité et de la perméabilité au sein même des formations géologiques.

Au final, pour comprendre Lusi, il me faut faire appel aux modèles numériques développés, tout en tenant compte du contexte géologique et de sa complexité. De ce fait, j'utilise des techniques informatiques de « High Performance Computing (HPC)» pour procéder aux calculs des processus multiphysiques. Dans ce travail, je vous présente le premier modèle numérique en 3D du geyser Lusi utilisant la technologie de GPU multiples en parallèles.

Mots clés:
Calcul à haute performance (HPC), Processeur Graphique (GPU), Modélisation Numérique 3D, Raffinement de Maillage Adaptif (AMR), Geyser, Systèmes hydrothermaux, Réservoirs Géothermiques, Lusi

Acknowledgements

I would like to express my sincere and deep gratitude to Prof. Dr. Stephen A. Miller for letting me obtain my computational learning in geofluids and geothermics letting me do a doctorate, and supervising it. He guided and supported me through many discussion during my work and cooperated with me on challenging modelling ideas at the Centre for Hydrogeology and Geothermics (CHYN) in the Laboratory of Geothermics and Geodynamics. I admire his fresh and amazing look on science and the enjoyable atmosphere he created during these years.

I would like to thank Prof. Dr. Benoît Valley for his support and expert knowledges in geomechanics and geothermics from the engineering geology and feasibility of the application of my computational models during my work at the Centre for Hydrogeology and Geothermics (CHYN) in the Laboratory of Geothermics and Reservoir Geomechanics.

I would like to thank Prof. Dr. Yury Y. Podladtchikov, who kindly accepted to examine my dissertation and for many useful discussions on High Performance Computing (HPC) with multi-GPU and for letting me use the “Octopus” supercomputer at the Faculty of Geosciences and Environment, Swiss Geocomputing Centre at the University of Lausanne.

Furthermore, I would like to thank Dr. Benjamin Malvoisin for many useful discussions on physics and computational approach for hydrothermal systems and geothermal reservoirs. Finite Difference (FD) is the way! I would like to thank Dr. Adriano Mazzini for all the support and useful discussion on the “LusiLAB” project at the Centre for Earth Evolution and Dynamics (CEED) at the University of Oslo and conveying to me how Lusi is interesting for pluridisciplinary sciences.

Also, I would like to thank Dr. Samuel Omlin who showed me the way with High Performance Computing (HPC), supercomputing and multi-GPU technology and convinced me that computer science is awesome! I would like to thank Ludovic Raess for many useful discussions on parallel computing and who guide me with the “Octopus” supercomputer.

Additional thanks go to all my colleagues and the students (M.Sc. and B.Sc.) at the CHYN.

I would like to particularly thank my friend and “Master Yoda” Gunnar, for the amazing work and fun we got together passing these years: “Built and Run, you must”.

I would particularly like to thank my Mum, my brother Sina and my sister in law Melania for their support and guidance in my life. My nephew Nima showed me what’s most important in life during the final countdown of this dissertation…and thanks Iago, you make me laugh every single day!

Finally, I am especially thankful to my friend, my partner in crime, my love Aline who was always there for me and without whom nothing would have been possible in my life.

The work presented in this dissertation was financially supported by a grant from the Swiss National Science Foundation (SNSF n° 200021-16005/1).

Contents

Motivations

"Success consists of going from failure to failure without loss of enthusiasm"

- Winston Churchill

Think globally, act locally (Geddes, 1915). Understanding nature for human needs is a current topic where human society is finally taking into account that our mother Earth can help us to survive. Hydrothermal systems and geothermal reservoirs can be used for heat and energy supply concerning the energy need in relation to the entirety of humanity during the next century (Photo 1). However, understanding the design of power plants and modelling of such large scale and complex hydrogeological system poses significant technical issues in assessing their risks and consequences. Deep hydrothermal systems or geothermal reservoirs involves several physical mechanisms. Therefore, complete simulation and modelling of these complex systems requires the coupling of many processes, including fluid flow, thermal and geochemical effects, and the transport of multiple reactive chemical types at multiple temporal and spatial scales. On the other hand, the reliability of these predictive simulations is adversely affected by poor conceptual models and by limitations in site characterization data. Moreover, these models require a large number of parameters to be determined. Thus the development of accurate, efficient and robust simulation tools supporting hydrogeological and geothermal efforts represents a formidable modelling challenge. In this thesis, I present a series of articles with mathematical formulations of computational models entailing coupled and nonlinear flow, mass and heat transportation, and deformation in heterogeneous geological media. In addition, I present ensemble-based simulators using High Performance Computing (HPC) which can be powerful tools to understand such natural or engineered systems.

Photo 1: The Svartsengi geothermal power plant by the Blue Lagoon in Iceland. (Photograph: Paul A. Souders, Corbis)

Groundwater in geological process formations is driven by capillary trapping, dissolution, and geochemical mineralization under highly permeable or impermeable hydrogeological formations. Assessment, design, and monitoring of these activities involving subsurface reservoirs and aquifers require large-scale simulations of physical processes over long time periods. Predictive computational models may be the only means to compensate for the lack of a complete characterization of the subsurface environment, the multiple scales of the various interacting processes and the need for long time predictions. Modelling and simulation of hydrothermal systems or geothermal reservoirs are a difficult challenge for numerical modellers. There are several reasons for these difficulties, including the need for higher order algorithms, conservation of mass locally, large time steps, and numerical diffusion. Likewise, simulating multiphase flows in geologic formations requires a better understanding of phase behavior. The effects of temperature, pressure, and salt concentration on interfacial tension and its effect on hysteretic relative permeability and capillary pressure, porosity and permeability evolution, are among the current challenges that scientists and engineers face in the development of models of fluid flow in porous media. Due primarily to their inaccessibility, subsurface formations are poorly characterized, so techniques for estimating model parameters and for quantifying uncertainty are additional challenges numerical modellers must face. These difficulties are essential to overcome for all geosystems, but particularly for modelling hydrothermal systems and geothermal reservoirs in deep geological formations, which is the focus of this thesis.

The consequences of hydrothermal systems and geothermal reservoirs depend on a complex set of interactions in which phase behavior and flow are coupled with geochemical and geomechanical processes that are far from equilibrium. They are under extreme heterogeneity, and exist over a wide range of timescales. Moreover, fluid properties such as diffusion, density, viscosity, and interfacial tension are keys to modelling and understanding the importance of different mechanisms for short-term and long-term geothermal behaviors across the different scales. In this thesis, through several articles, I discuss mathematical and computational formulations for describing reservoir characterization and evaluation of long term natural hydrothermal systems, as well as current computational capabilities and challenges. Validation is demonstrated by providing comparisons with field scale observation.

Thesis structure

This thesis is organized in 6 chapters. Chapter 1 gives a brief introduction of the theoretical and numerical background used for hydrothermal systems and geothermal reservoirs using HPC. Chapter 2 presents an advance 3D meshing tool, to numerically discretize any 3D geological models, which can be used in any numerical simulator based on Finite Difference (FD), Finite Volume (FV) or Finite Element (FE) methods. Chapter 3 introduces a 3D numerical simulator using multi-GPU technology for simulating the main physical processes in deep hydrothermal systems or geothermal reservoirs. Chapter 4 and 5 treat the application of the two numerical tools, using High Performance Computing (HPC) technology, developed above with an application on a real case study in East Java, Indonesia where a geyser named “Lusi” came into

existence twelve years ago. Finally chapter 6 presents the conclusions of this thesis and outlooks towards future research possibilities.
This cumulative thesis is organized as a series of papers submitted to international journals linked to computational and geothermal sciences. Each chapter from two to five are complete articles.

Chapter 2:
HULK: Simple and fast generation of structured hexahedral meshes for improved subsurface simulations

Short for *H*exahedra from *U*nique *L*ocation in (*K*)convex Polyhedra: *HULK*. This chapter introduces a simple and efficient algorithm to generate hexahedral meshes from generic STL files describing a geological model to be used in simulation tools based on the finite element, finite volume or finite difference methods. Using binary space partitioning of the input geometry and octree refinement on the grid, a successive increase in accuracy of the mesh is achieved. I present the theoretical basis as well as the implementation procedure with three geological models of varying complexity, providing the basis on which the algorithm is evaluated. *HULK* generates high accuracy discretizations with cell counts suitable for state-of-the-art subsurface simulators and provides a new method for hexahedral mesh generation in geological settings.

Chapter 3:
GEYSER: 3D thermo-hydrodynamic reactive transport numerical simulator considering porosity and permeability evolution on multi-GPU technology

GEYSER, an acronym for *G*PU cluster computing for *E*nhanced h*Y*drothermal *S*yst*E*ms with *R*eactive transport, is a 3D simulator that includes porosity and permeability evolution for mass and heat transport processes in fractured geological media. The simulator also includes mass porosity and permeability evolution in response to dehydration reactions of hydrous minerals. *GEYSER* utilizes a finite difference scheme to solve the governing PDEs associated with 3D large-scale hydrothermal systems or geothermal reservoirs. This tool is a high performance code using Graphic Processing Units (GPU) workstations or cluster technology. The physical processes implemented into the code are those associated with deep hydrogeological complexes where high fluid pressures generated by dehydration reactions can be sufficient to induce hydro-fractures that significantly influences the porosity and permeability structures within geological formation. The governing equations are described and implemented, and applied to a simplified 3D model of a magmatic intrusion at depth underlying a deep sedimentary cover. Close to ideal weak scaling is demonstrated on GPU clusters with up to 128 GPUs. The numerical model can be used to investigate and understand coupled and time-dependent hydromechanical and thermodynamic processes at high resolution of the 3D computational domain. Applications include the hydrogeology of volcanic environments or exploitation of sediment-hosted geothermal resources. The code can be also suited for porosity and permeability evolution regarding pressure and temperature reaction rate to rock decarbonization for CO_2 sequestration in deep sedimentary formations.

Chapter 4:
Numerical modelling of the Lusi hydrothermal system: Initial results and future challenges

In East Java, Indonesia, the Lusi mud eruption is an active clastic-dominated geyser and a sediment-hosted hydrothermal system that has generated wide interest across many disciplines. In this chapter, I show that this moderate-to-high enthalpy system is driven by multiphase and multicomponent processes, fluid and rock mechanics, and heat transport processes, all which present challenges in developing realistic numerical models of the underlying physics. I develop a hydrogeological conceptual model for this deep and complex hydrothermal system, and construct an appropriate 3D geological model using the available data. This geological model then serves as the basis for numerically simulations that include some of the dominant processes driving Lusi. I adopt a flexible continuum approach with an efficient numerical simulator based on the 3D geological model representing the deep structures of this hydrothermal system and geothermal reservoir by incorporating borehole information and seismic data obtained in the framework of the LUSI Lab project. The geological model is transformed into a computational grid using binary space partitioning (BSP) of the input geometry and octree refinement on the grid to perform multi-physics simulations. Thermodynamic calculations using the equation of state for a CO_2-bearing aqueous NaCl solution suggest that Lusi is a two-phase flow system (Water/CO_2). Finally, I present initial results from a simple hydro-mechanical multiphase numerical model that simulates processes that likely contributed to the initiation of Lusi.

Chapter 5:
Multi-GPU based 3D numerical modelling of the Lusi geyser system in Java, Indonesia

This chapter presents a fully coupled 3D model of the Lusi hydrothermal system with clay dehydration and considering mass and heat transport for calculation of the evolution of the fluids outflow over time at the Lusi site. I use multi-GPU parallel processing to efficiently calculate the 3D time evolution of pressure, temperature, porosity, permeability and water liberation in deep hydrothermal system at large-scale and at high resolution. Simulations indicate that high-pressure fluids are generated by dehydration reactions and can be sufficient to induce hydro-fractures that significantly influence the porosity and permeability structures within geological formations. This phenomenon is essential to understand the Lusi system in 3D, because a long term increase in temperature due to hydrothermal groundwater flow and in fluids outflow may have a considerable impact for the engineering maintenance of the Lusi site during the coming years. These processes combined with High Performance Computing (HPC) are fundamental for time evolution of such system as natural interest and potential geo-resource development for the surrounding population. I conclude the chapter with an outlook for prospect development and main attentions needed for the future.

1. Introduction

"My dyslexia allowed me to be bad at everything ... and to understand those with difficulties."

Nobel Prize in Chemistry 2017, Prof. Dr. Jacques Dubochet

1.1 Hydrothermal systems and geothermal reservoirs

Hydrothermal systems and geothermal reservoirs are driven by the Earth's interior (Figure 1). It may be stated that the planetary crust, about 6 km thick under the ocean and as much as 35 km under continents, is underlain by the mantle passing down into the core. The plate tectonic model in which the planetary surface, including the sea floor, is divided into several rigid plates in motion relative to each other (Press & Siever, 2004).

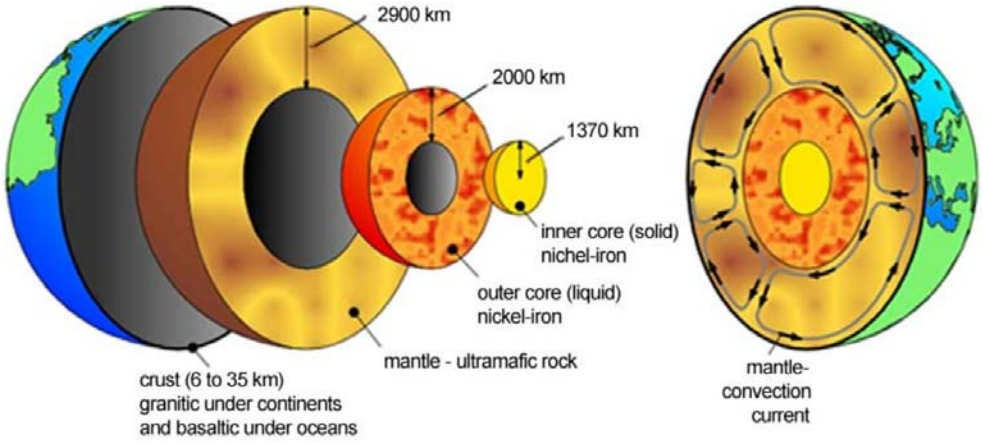

Figure 1: Divisions in the Earth's interior with mantle convection and its relation to plate tectonics (Colman-Sadd and Scott, 1994).

The driving mechanism for plate motion is not fully understood, but seems to be connected with convective movements in the mantle (Figure 2). The internal heat of the Earth is the source of energy. The terrestrial heat flows occur along the spreading and converging plate boundaries. The mass transfer of heat by magmas generated from the mantle carries heat to shallower levels of the crust. Hydrothermal systems and geothermal reservoirs are developed from such heat sources.

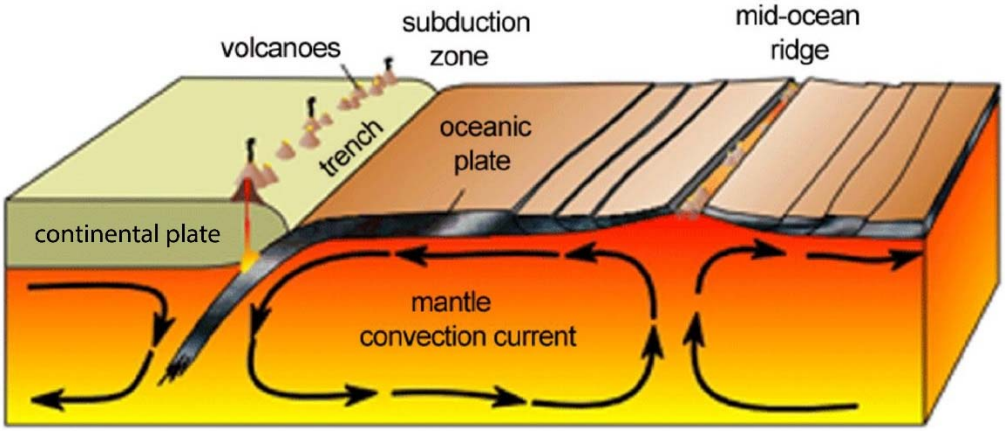

Figure 2: Mantle convection driving the mechanism of plate motion (Colman-Sadd and Scott, 1994).

All prospective high enthalpy geothermal regions of the planet are to be found within belts of geologically young volcanism and crustal deformation produced by lithospheric plates in motion (Figure 3).

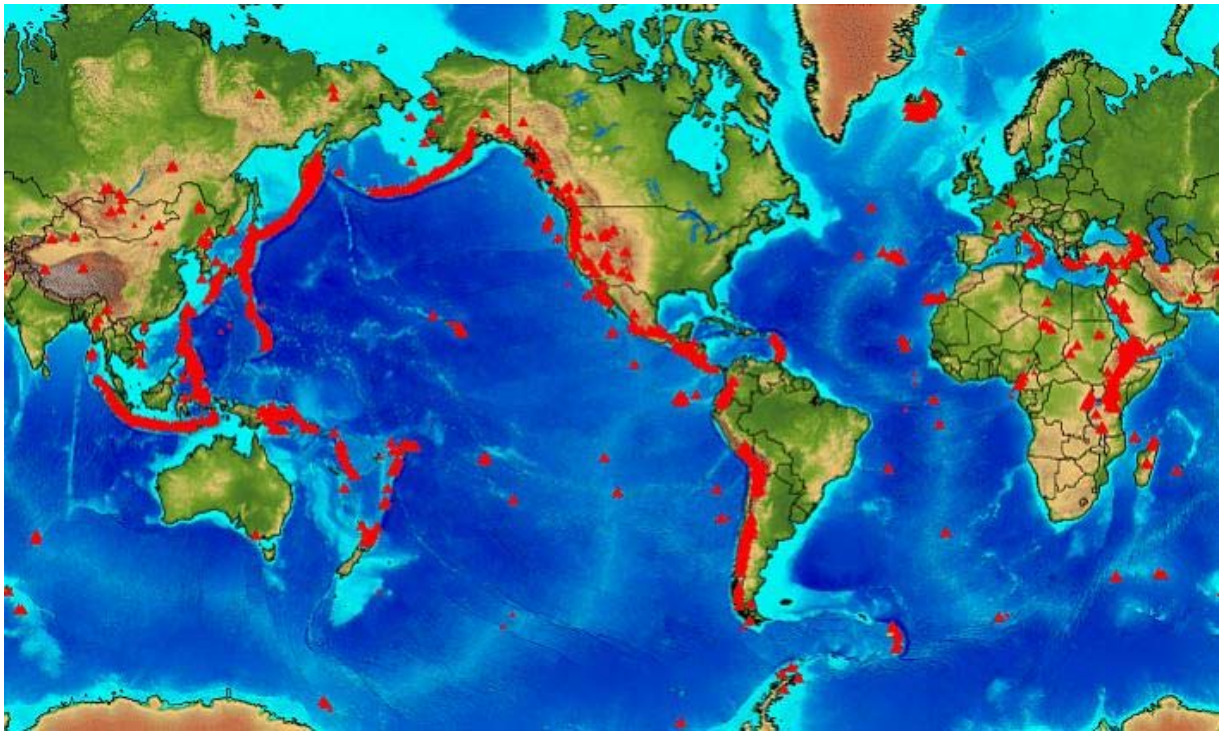

Figure 3: Hydrothermal systems, geothermal reservoirs, volcanic regions, folded mountain zones of the Earth are represented (red dots) on this map (Smithsonian Institution, 2017).

1.2 Conceptual models

Geothermal resources can be classified by enthalpy. Enthalpy is the measure of energy in a thermodynamic system. It can be grouped in two categories:

- Low-enthalpy systems (water-dominant)
- High-enthalpy systems (water/steam-dominant, T° > 150°C reservoir directly heated by magma)

After several meters through the Earth or even in specific tectonic conditions (e.g. hot springs), we find ourselves in the presence of low enthalpy systems, where the underground temperature is constant and, it is possible to extract or store thermal energy for heating or even cooling (Figure 4). The groundwater is a crucial criteria for which kind of engineered system should be used for the exploitation of this energy. Indeed, the groundwater increases the thermal conductivity of the ground and allows a better energy extraction from underground. If the condition for energy production is not reached, we need to enhance deep hydrothermal systems

using a petrothermal process called EGS (Enhanced Geothermal System) which today has gained wide interest across many disciplines for the production of electricity.

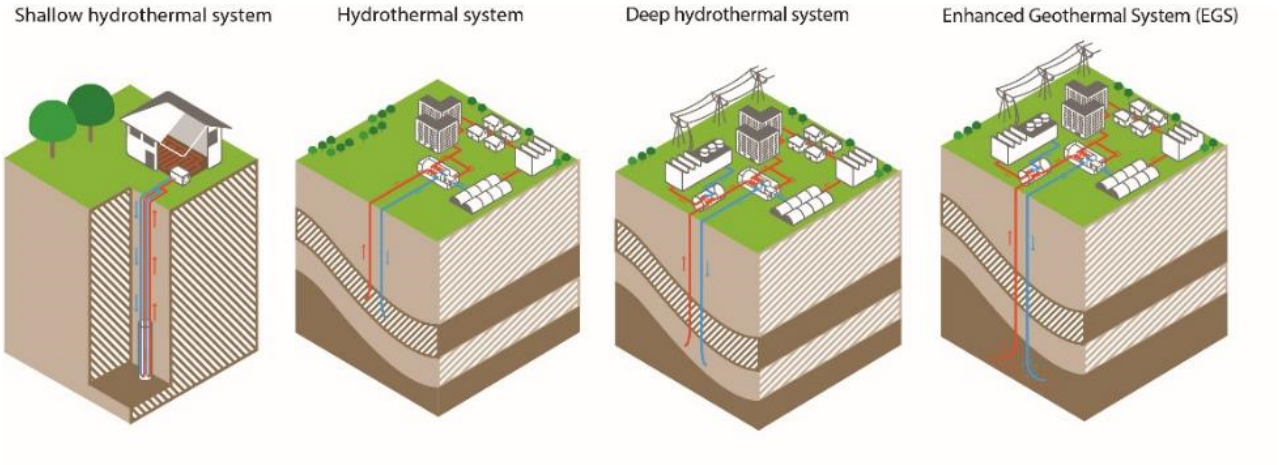

Figure 4: Different sorts of engineering hydrothermal systems in low enthalpy conditions (modified after, Suisse Energie, 2017).

In contrast, high enthalpy systems (e.g. hot springs, sediment-hosted hydrothermal system or geysers) are driven by groundwater in deep geological processes near volcanic complexes or active tectonic zones (Figure 5). These systems are very efficient due to their high temperature, hydrological flow and steam produced by the underground. The production of heat or electricity can be made "easily" with a production of several gigawatts from one power plant.

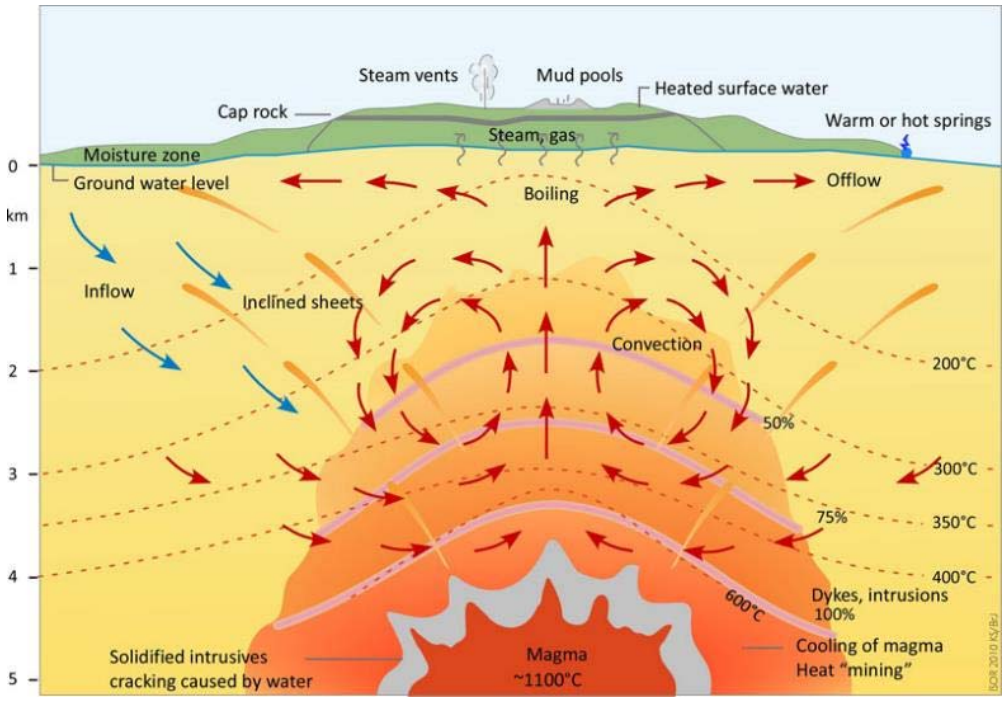

Figure 5: Hydrothermal system in high enthalpy conditions (ISOR, Iceland Geosurvey).

The physical behaviors of hydrogeological processes are the same in both cases. The physics for low and high enthalpy systems are similar, with different level of complexity. Thermal, hydrodynamics, mechanical or chemical processes involved in both systems have to be studied in the same way to gain better knowledge of our underground.

The complexity of such systems is interesting for many different scientific disciplines, but the difficulty is to achieve a good comprehension of the underground and the heated groundwater flow. Numerical modelling becomes a powerful tool to include most of the relevant physics in these processes and catch the complexity of hydrothermal systems or geothermal reservoirs (Figure 6).

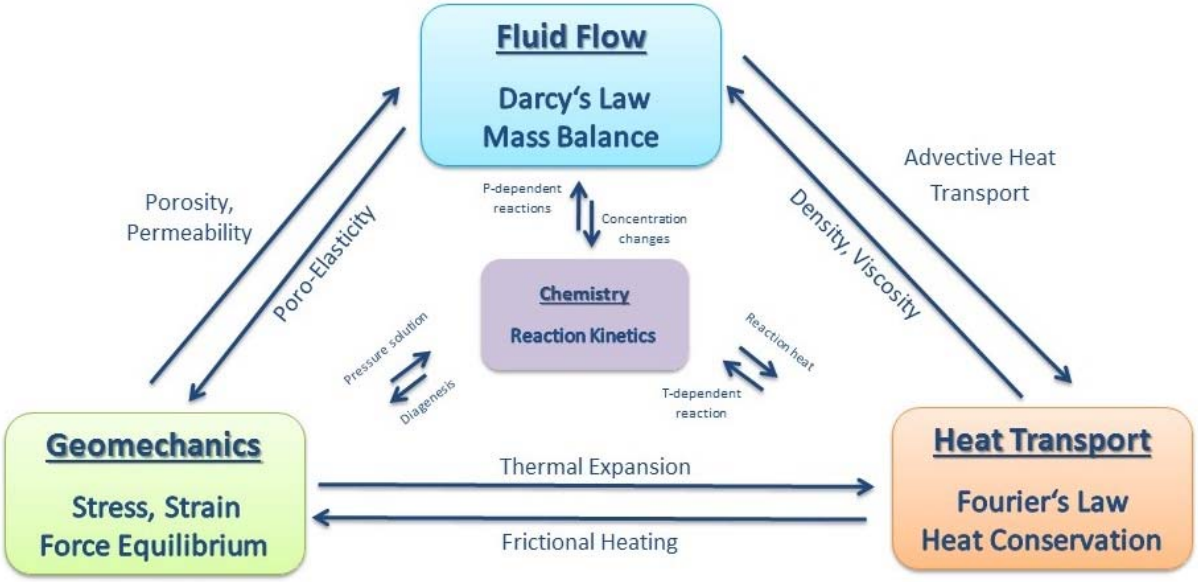

Figure 6: Schematic representation of the coupled thermal-hydrodynamic-mechanical-chemical (THMC) processes relevant in hydrothermal systems or geothermal reservoirs.

1.3 Numerical modelling of flow and transport for fluid dynamics in geological processes

Fundamental hydrogeological and geothermal concepts derive from groundwater motion equations. The physical behavior of large-scale hydrothermal systems or geothermal reservoirs entails coupled and nonlinear flow, mass and heat transport, and deformation in highly heterogeneous geological media. These complex systems depend mainly on numerical solutions coupled with partial differential equations (PDEs) and complementary equation of state (EOS). For decades, natural and engineering sciences have seen a growth of computational power for numerical models which have eliminated or minimized various simplification like physical processes, 3D structures of conceptual models or time scale assumption. Hydrothermal systems have immense scientific and engineering significance and have been studied with many disciplines to understand their geothermal potential (e.g. Bowen, 1979; Ingebritsen et Sanford, 1999; Ingebristen et al., 2010; Jeanne et al., 2014; Karyono et al., 2017; Lizarralde et al., 2010; Mazzini et al., 2012; Pruess, 1991; Svensen et al. 2009; White, 1957). The physical understanding of these deep complex systems is challenging where data acquisition is difficult or sometime impossible and where numerical modelling is the "*cheapest*" and "*fastest*" way, compared to deep borehole campaigns, to understand what occurs at depth.

1.3.1 Mathematical model for fluid flow

Natural convection is the phenomenon of fluid flow driven by density variations in a fluid subject to body forces. Therefore, there are two necessary conditions to be met in order to obtain natural convective flow. Firstly, the existence of density variations within the fluid and secondly the fluid must be subjected to body forces. Density is a function of pressure, temperature or solute concentration (in the case of a binary mixture) and its variation with respect to pressure is much smaller than that with respect to temperature or concentration. Hence, the convection can be driven either by temperature variations or by variations in solute concentration or by both. The solute or heat transport equation should be included in the model and should be extended as well to account for the solute effect on density. The formulation of the governing transport equation is expressed in terms of fluid pressure, temperature or concentration. It has to be assumed that the system is in thermodynamic equilibrium, heat conduction is predominant in the rock and can be described by a bulk thermal conductivity and that capillary pressure effects are negligible (Bear, 1972). The subscripts *'s'* and *'f'* refer to the solid and the fluid phase.

1.3.1.1 Mass conservation

The basic equation describing filtration of a fluid through a porous medium is the continuity equation which states that mass is conserved:

$$\frac{\partial \phi \rho}{\partial t} = -\nabla \cdot (\rho \mathbf{v}) + q \tag{1.1}$$

where ϕ, ρ, $\mathbf{v}$, q are the porosity (volume fraction of fluid) $[-]$, the density $\left[\frac{kg}{m^3}\right]$, the velocity $\left[\frac{m}{s}\right]$ and a source term $\left[\frac{kg}{s}\right]$ respectively.

1.3.1.2 Conservation of momentum

The Navier-Stokes equations govern the conservation of momentum, but for low velocity flow in porous media, the conservation of fluid momentum is expressed by the Darcy's law:

$$\mathbf{v} = -\frac{k}{\mu} \nabla p \tag{1.2}$$

where k $[m^2]$ is the permeability, μ the fluid viscosity $\left[\frac{1}{s}\right]$and p $[Pa]$ is the fluid pressure.

For well-sorted, unconsolidated granular porous media, the terms porosity and permeability are correlated and expressed by the Kozeny-Carman equation (Carman, 1956):

$$k = \frac{\phi^3}{5 s_0^2 (1-\phi)^2} \tag{1.3}$$

where s_0 is the solid surface exposed to the fluid per unit volume of solid matrix.

In hydrogeological settings the permeability can vary over a large range. Many authors consider it as stress and pressure dependent (e.g. Caricione and Tinivella, 2001; Miller et al., 2004; Rice, 1992). These studies use an exponential function of permeability in dependence of normal stress σ_n:

$$k = k_0 \cdot exp^{\left(-\frac{\sigma_n}{\sigma_0}\right)} \tag{1.4}$$

where k_0 is the permeability at zero stress, σ_0 is a scaling constant and σ_n can be expressed with maximal and minimal principal stresses σ_1 , σ_3 and dip angle θ:

$$\sigma_n = \frac{\sigma_1 + \sigma_3 - 2P_f}{2} + \frac{\sigma_1 - \sigma_3}{2}\cos(2\theta)$$

(1.5)

Substituting Darcy's equation (1.2) into the mass conservation equation (1.1) and considering the gravity force:

$$\frac{\partial(\emptyset\rho)}{\partial t} = \nabla \cdot \left(\rho \frac{k}{\mu}\nabla p - \rho g\right) + q$$

(1.6)

The left hand side of this equation may be given as:

$$\frac{\partial(\phi\rho)}{\partial t} = \rho \frac{\partial \phi}{\partial t} + \phi \frac{\partial \rho}{\partial t}$$

(1.7)

Porosity and density are function of pressure only at a constant temperature, the expressions are expanded such that:

$$\frac{\partial \phi}{\partial t} = \frac{\partial \phi}{\partial p}\frac{\partial p}{\partial t}$$

(1.8)

and

$$\frac{\partial \rho}{\partial t} = \frac{\partial \rho}{\partial p}\frac{\partial p}{\partial t}$$

(1.9)

The pressure dependence of the porosity is given through the rock compressibility β_r $[Pa^{-1}]$ at constant temperature:

$$\beta_r = \frac{1}{\phi}\left(\frac{\partial \phi}{\partial p}\right)_T$$

(1.10)

A comparable definition can be defined for the fluid compressibility β_f $[Pa^{-1}]$ at constant temperature:

$$\beta_f = \frac{1}{V}\left(\frac{\partial V}{\partial p}\right)_T = \frac{1}{\rho}\left(\frac{\partial \rho}{\partial p}\right)_T$$

(1.11)

Where V is the volume occupied by the fluid. After substitution of these relationship into equation (1.6) and (1.7), the equation becomes:

$$\phi\rho(\beta_r + \beta_f)\frac{\partial p}{\partial t} = \nabla \cdot \left[\rho \frac{k}{\mu}\left(\nabla p - \rho_f g\right)\right] + q \tag{1.12}$$

Considering the definition of the fluid compressibility and considering that the fluid compressibility is generally very small, the equation (1.12) can be expressed for groundwater flow for slightly compressible flow and rock:

$$\phi\rho(\beta_r + \beta_f)\frac{\partial p}{\partial t} = \nabla \cdot \left[\frac{k}{\mu}\left(\nabla p - \rho_f g\right)\right] + q \tag{1.13}$$

1.3.1.3 Multiphase flow

To test several hypothesis, for one study of the presented work (cf. Chapter 4) I used the physical approach regarding multiphase flow (water/CO_2). An appropriate mathematical model must respect the physical and chemical processes occurring at the macro-scale of a porous media. I use the Representative Elementary Volume (REV) averaging theory (Hassanizadeh & Gray, 1990; Hassanizadeh & Gray, 1997). In REV averaging theory, macroscopic quantities are obtained from local volume averaging of corresponding microscopic quantities. Exchange of mass, momentum and energy between the constituents are explicitly accounted from interfacial effects. The averaging process is conducted by integrating the involved microscopic quantities over a REV of volume *dv* and area *da*. The REV is chosen larger than the constituent individual size scales and at the same time smaller than the size scale of the physical system (Figure 7).

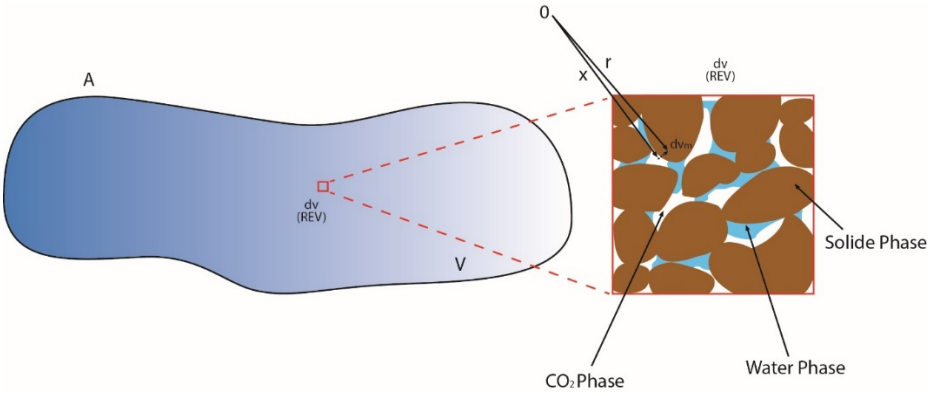

Figure 7: REV of a multiphase medium (Water/CO_2 flow) of a porous medium consisting of three constituents.

I consider that two immiscible fluids simultaneously flow in the pore space with the mass conservation equation for each phase given by:

$$\phi \frac{\partial}{\partial t} S_\alpha + \nabla \cdot \mathbf{v}_\alpha = -q_\alpha \qquad \alpha = Water, CO_2 \tag{1.14}$$

where α is the phase index, S_α [-] is the phase saturation; $\emptyset$ [-] is the porosity; and q_α is the source term. It is assumed that the phase velocity $\mathbf{v}_\alpha$ is governed by the generalized of Darcy's Law for multiphase flow:

$$\mathbf{v}_\alpha = -\frac{1}{\mu_\alpha} \mathbf{K}_\alpha \cdot (\nabla p_\alpha - \rho_\alpha g) \tag{1.15}$$

With the definition of the relative permeability $k_{r\alpha}$, a relation between the conductivity for the phase α, K_α and the intrinsic permeability, **K**, which is fluid independent can be set-up:

$$\mathbf{K}_\alpha = k_{r\alpha} \mathbf{K} \tag{1.16}$$

The relative permeability $k_{r\alpha}$ can be considered as a scaling factor that depends on the saturation of the phases present and satisfies the following constraint (Bear, 1972; Helmig, 1997):

$$0 \leq k_{r\alpha}\left(S_1, \ldots, S_{nphase}\right) \leq 1 \quad \forall \alpha \tag{1.17}$$

The generalized Darcy's Law is therefore:

$$\mathbf{v}_\alpha = -\frac{k_{r\alpha}}{\mu_\alpha} \mathbf{K} \cdot (\nabla p_\alpha - \rho_\alpha g) \tag{1.18}$$

If I consider an H_2O-CO_2 flow system under isothermal conditions, I can apply the pressure-saturation formulation with modifications (Helmig, 1997). With a constitutive relationship for the relative permeabilities of $k_{r\alpha} = k_{r\alpha}(S_\alpha)$, and the saturation constraint $S_{water} + S_{CO2} = 1$. Here, I have a complete system of equations for the unknown variables p, S_{water} and S_{CO2}.

I employ a pressure-saturation formulation to solve this system of equations. Summing up the two mass-balance equations for water and CO_2, we obtain the pressure equation:

$$\nabla \cdot (\lambda_{tot} \nabla p) = q_{tot} \tag{1.19}$$

where $\lambda_{tot} = \lambda_{water} + \lambda_{CO2}$ is the total mobility tensor and $q_{tot} = q_{water} + q_{CO2}$ the total source term. Once the pressure is computed, the saturation is obtained by solving the mass-balance equation for one of the two phases (e.g., water phase):

$$\emptyset \frac{\partial}{\partial t} S_{water} + \nabla \cdot [f_{water}(S_{water}) v_{tot}] = -q_{water} \tag{1.20}$$

where the total velocity is defined as:

$$\mathbf{v}_{tot} = \mathbf{v}_{water} + \mathbf{v}_{CO2} = -\lambda_{tot} \nabla p \tag{1.21}$$

and the fractional flow function is given by:

$$f_{water} = \frac{\frac{k_{rwater}}{\mu_{water}}}{\frac{k_{rwater}}{\mu_{water}} + \frac{k_{rCO_2}}{\mu_{CO_2}}} \tag{1.22}$$

1.3.2 Mathematical model for heat transfer

Nield et al., 2006 present that heat transfer in porous media is mainly driven by two basic processes, thermal conduction and convection. Thermal conduction is the transfer of heat by microscopic collisions of particles without movement of the transferring medium. In thermal convection, heat is transferred by movement of fluids. Thermal convection takes place through advection, diffusion or both.

The energy heat conservation over an elemental volume of medium for a solid and a fluid phase and considering thermal equilibrium so that $T = T_s = T_f$, is (Nield et al. 2006):

$$\begin{aligned} \Big((1-\emptyset)\rho_s c_s + \emptyset(\rho_f c_f)\Big)\frac{\partial T}{\partial t} + (\rho_f c_f) v_f \cdot \nabla T \\ = \nabla \cdot \Big(\big((1-\emptyset)\lambda_s + \emptyset\lambda_f\big)\nabla T\Big) + \big((1-\emptyset)q_s + \emptyset q_f\big) \end{aligned} \tag{1.14}$$

where c is the specific heat of the phase, λ is the thermal conductivity and q is the heat production per unit volume.

1.4 Challenges and solutions for modelling hydrothermal systems or geothermal reservoirs

Hydrothermal systems and geothermal reservoirs are multiscale systems. The correct simulation of the multiphase, multicomponent and fracture porous media should cast different size of complexity. The large-scale and time dependence of such complex systems post problems from the numerical modelling point of view. There are two main problems. Firstly, the multiphysics involved in these kind of systems are complex and if we want to consider most of the main processes, the cost in computational time is high. Secondly, if modelling of the thermo-hydromechanical evolution considering chemical reaction is intended, then the numerical grid must be able to follow the development mass and heat transport flow with porosity and permeability evolution. A way to overcome this difficulty, could be to increase the numerical resolution in a specific area or to remesh when new physics occur. In realistic modelling of deep complex geological media, many factors controls the thermal, hydrodynamics, mechanical and chemical development. Determining specific areas is problematic because non-localized porosity evolution might develop hydro-fractured networks. In these circumstances, previous numerical zooming cannot be accurately prescribed and constant remeshing is extremely expensive in terms of computing. One approach used in this work (Chapter 3) is to decompose the numerical domain spatially into a local problem (Figure 12) with enough points to resolve thermo-hydromechanical processes. By doing so, the model is able to follow the evolution of porosity and permeability network in the whole domain at every iteration. The main drawback in this approach is the increment on the computation time. Implicit methods would require the inversion of very large matrices and heavy matricidal operations that require long computational time.

To solve the problem in 3D, I use explicit difference finite methods. Explicit methods have the advantage of being computationally light but time steps are very restrictive, increasing again the overall computation time. Parallel computation allows fast computation over large data sets. In particular Graphical Processor Units (GPU) have become a reference in parallel computing over the last decade. The video games and the artificial intelligence industries move billions of dollars every year. This requires better software and hardware to be able to manage the amount of information per frame and the high velocity frame rates. Real time, high resolution 3D graphics rendering, requires parallel intensive computation over large data sets. In order to achieve this, multi-GPU architecture gives more importance to data processing than to data catching or control flow.

1.4.1 Graphical Processing Units (GPU) in numerical modelling

Multi-GPU computing is the use of a graphics processing unit (GPU) together with a CPU to accelerate deep analytics and engineering applications. Pioneered in 2007 by NVIDIA, GPU accelerators now power energy-efficient data centers in government labs, universities, companies, and businesses around the world. They play a huge role in accelerating applications in platforms ranging from artificial intelligence to cars (e.g. autonomous driving), drones, and

robots. Multi-GPU computing offloads compute-intensive portions of the application to the GPU, while the remaining code still runs on the CPU. From a user's perspective, applications simply run much faster. A simple way to understand the difference between a CPU and a GPU is to compare how they process tasks. A CPU consists of a few cores optimized for sequential serial processing while a GPU has a massively parallel architecture consisting of thousands of smaller, more efficient cores designed for handling multiple tasks simultaneously (NVIDIA, 2017).

Figure 8: CPU architecture is designed for serial computations. For this reason it dedicates more chip space to flow control and memory operations. Multi-GPU architecture gives priority to arithmetic intensive operations. Much more Arithmetic Logic Units (ALUs) are built in GPU chips. Cache memory for memory operations and flow control units are limited causing GPUs to be inefficient in comparison to CPUs for serial processes (NVIDIA, 2017).

The job is performed by including many “streaming processor” cores that execute the same instruction stream in parallel. Thus, streaming processor cores produce light-weight arithmetic operations over the data in an intensive way (i.e. much more arithmetic operations are performed as memory operations), so that a limited cached memory is needed. A comparison of the CPU vs GPU architectures is presented on Figure 8. The difference in the performance of CPU vs GPU during the last year has grown exponentially and will not decrease in the future (NVIDIA, 2017). Figure 9 show the number of floating points operations (FLOPs) per second in a GPU is orders of magnitude higher than a CPU and Figure 10 shows the memory bandwidth for GPU and CPU (NVIDIA, 2017). Since 1999, Graphics Processing Units (GPU) have been successfully applied to accelerate non-graphical computations. Their suitability was strongly limited by the complexity and constrains of the graphical programming languages available at that time.

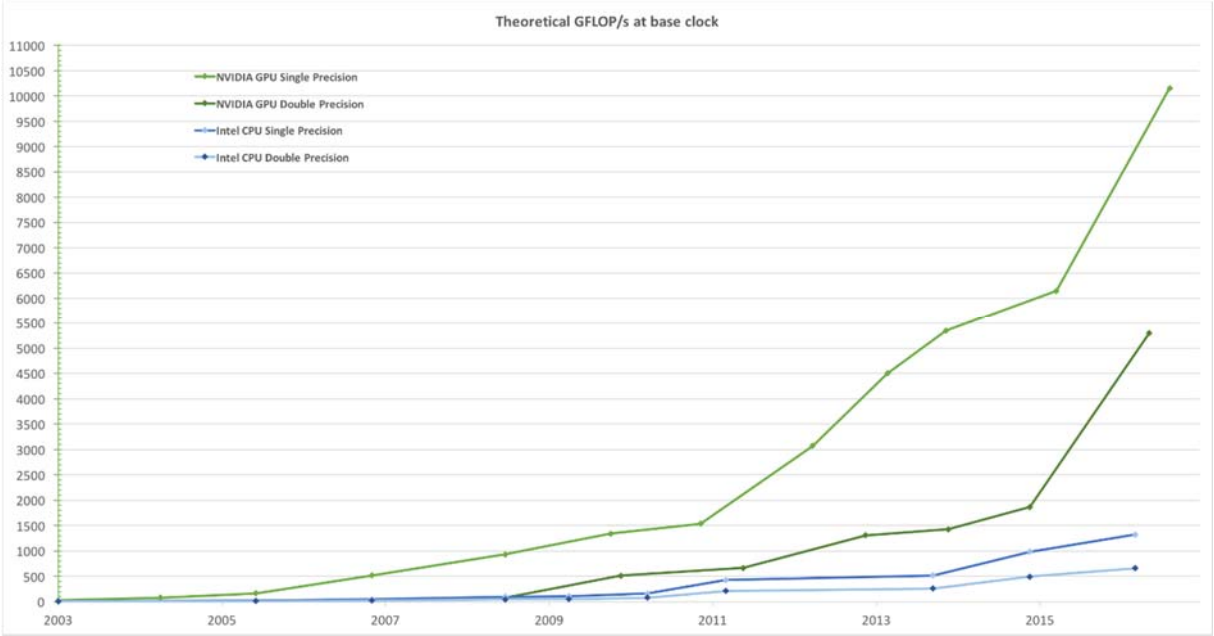

Figure 9: Floating-point operations per second for the CPU and GPU (NIVIDIA, 2017).

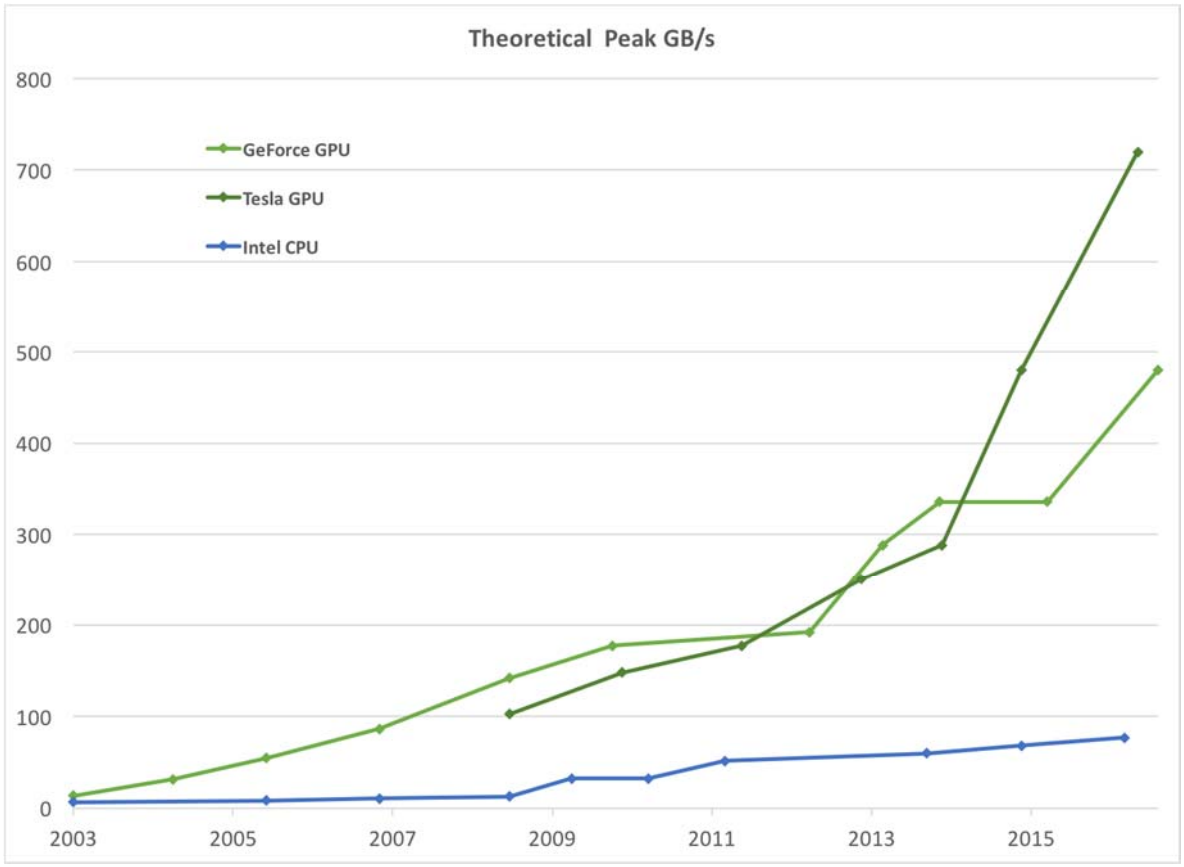

Figure 10: Memory bandwidth for the CPU and GPU (NIVIDIA, 2017).

Beginning 2007, NVIDIA released CUDA (Compute Unified Device Architecture), a massive parallel architecture and programming language based in a C-like programming model that facilitates GPU usage in physical modelling (NVIDIA, 2017). Since then, GPU based scientific modelling has increased over the years (Griebel and Zaspel, 2010; Michéa and Komatitsch, 2010). The introduction of the CUDA architecture made the GPU usage vital for universal computing. Today, most of the best supercomputers on the Earth are GPU based (e.g. Piz Daint at the Swiss National Supercomputing Centre, Lugano, Switzerland is the third fastest supercomputer in the world in 2017 (Top500.org)). GPU clusters are more energy efficient, they consume less electrical power, they require less cooling and they are smaller than CPU clusters. Today, GPU computing is the main tool for high resolution scientific and engineering real world purpose.

1.4.2 GPU architecture

CUDA programs run part on CPU and part on GPU. The kernels, the CUDA functions running on GPU, are executed as block of threads. Threads within the same block execute the same instructions. Every thread in a block has access to its own memory register and to a cached shared memory accessible by all threads of the block. The cached global memory is not available to all the threads, even if they are from the same block or not. Shared memory and global memory are read or write memories accessible by the GPU threads (NVIDIA, 2017). The 32 threads called warps are grouped in blocks to be executed (Figure 11). To pass data from CPU to the GPU device, constant memory and texture memory are available from the threads. The data flow is controlled by CUDA. Initially, space in the GPU device memories is allocated, secondly, data stored in the CPU's memory is transferred to the GPU device read-only memories or the GPU global memory. The calculations are performed on the GPU and the data is stored in the global memory and finally transferred to the host memory (NVIDIA, 2017).

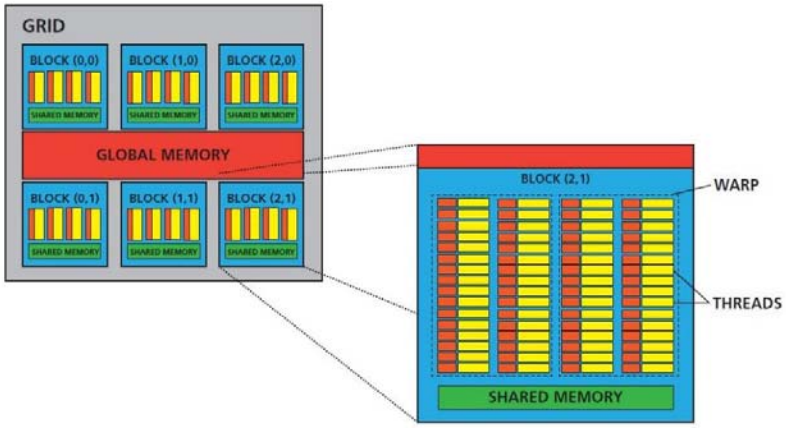

Figure 11: Warps are grouped in Blocks. A warp is a set of 32 threads. Every thread (yellow) has its own local memory (red). All threads within a warp execute the same commands. All threads of the same block have access to a common fast cached shared memory. Independently of their block, all threads have simultaneous access to global memory (NIVIDIA, 2017).

1.4.3 Shared memory for using GPU

As explained by Omlin (2017), memory is distributed on parallelization for problems that can be spatially decomposed into a Cartesian grid of local problems, where each local problem defines the boundary conditions of the common boundary for each adjacent local problem. The size of a local problem, rather than the size of the global problem, is specified in order to make the domain decomposition of the global problem both the simplest possible and always optimal (Figure 12). The size of the global problem is defined implicitly by the dimensions of the grid of local problems, the size of a local problem and the amount the local problems overlap. The amount local problems overlap must be specified. This function sets up MPI and organizes the available processes in a Cartesian grid topology; a local problem is then attributed to each process (in function of the Cartesian coordinates) and the grid of local problems is therefore built. To define a grid of 2 x 2 x 1 processes and therefore a grid of 2 x 2 x 1 local problems, a function must be called with the arguments 2 (x dimension), 2 (y dimension) and 1 (z dimension), i.e. set up grid (2, 2, 1) (Figure 12). The dimensions of the process grid are generally set for each executable.

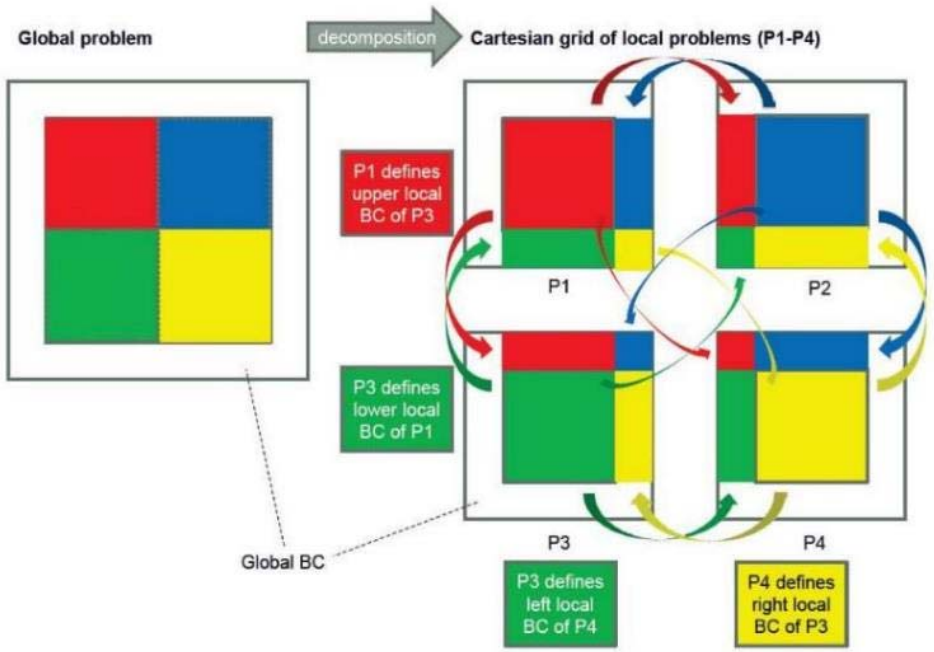

Figure 12: Distributed memory parallelization. A global problem (e.g. 2D) is spatially decomposed into a Cartesian grid of local problem, where each local problem defines the boundary conditions (BC) of the common boundary for each adjacent local problem (Omlin, 2017).

1.5 Related work

1.5.1 High performance development tools

The development of scalable and efficient parallel subsurface simulators is not an easy task. There are not so many computational tools which use multi-CPU or even multi-GPU technology for underground fluid dynamics, but it is of main interest today (Bangerth, 2007; Galvan, 2012; Galvan & Miller, 2013; Kolditz et al., 2012; Hammond et al., 2014; Omlin, 2017). The challenges of developing new algorithms that are well suited for current and future hardware is essential in many ways. One issue would consist in modifying algorithms that are sophisticated and state-of-the-art, but not well suited for current hardware. Going in this direction is very complicated and even practically impossible, because such algorithms are in many cases to a major extent inherently serial. To transform it into a fully parallel algorithm is a huge challenge and may be not feasible. Another issue is that simple algorithms that are well suited for parallelism and have regular data access patterns are typically rather old but mostly don't include state-of-the-art processes. This approach have been successful in several cases (Datte et al., 2009; Gysi et al., 2015; Krothiewski & Dabrowski, 2013; Micikevicius, 2009). The stencil-based methods, which consist in building solvers for partial differential equations (PDE) is perfectly adapted for the current hardware (Strikwerda, 2004). So, building a tool with iterative methods using finite difference (FD) and a regular Cartesian grid would be the solution instead of using direct methods involving complex techniques to compute derivatives and an unstructured grid. The finite difference (FD) method compute local neighboring grid cells (simple and regular data access pattern). The computational domain using a Cartesian grid is perfectly adapted and can be decomposed into several small domains for which iteration and time step can be done independently; it can be solved in parallel.

1.5.2 The Lusi sediment-hosted hydrothermal system in Java, Indonesia

The devastating 2006 mud eruption in the district of Sidoaarjo, Indonesia, caused great damages to the surrounding population. Lusi (Lumpur = « mud » in Indonesia Bahasa ; Sidoarjo = the regency where the eruption occurred) is a geyser system, that's still erupting today and has forced sixty thousands of Indonesians to move (Mazzini et al, 2007). The onset of Lusi has previously been described to be linked to petroleum drilling in the vicinity of Lusi (Davies et al., 2007, 2008, 2010; Tingay et al., 2008, 2015, Tingay et al., 2007) as well as having been triggered by a 6.3 M earthquake that struck the southern part of Java (southwest of Yogyakarta, ~250 km from Lusi) about two days before the eruption (Lupi et al., 2013; Miller and Mazzini, 2018). Lusi has been described as a newborn, tectonic scale, sediment-hosted hydrothermal system linked to the SW adjacent Arjuno-Welirang volcanic complex through the Watukosek fault system (Istadi et al., 2012; Mazzini et al., 2009, 2012, 2018). Hydrogeological, geophysical and geochemical evidence collected over the years showed that the eruption is evolving towards a steady and continuing erupting system (e.g. Fallahi et al., 2017; Karyono et al., 2016, Mauri et al., 2018, Mazzini et al., 2012). Since its inception Lusi has attracted the attention of scientists and numerous dedicated studies have been completed in the framework of the LusiLAB project (ERC grant n°308126, PI A. Mazzini).

This deep hydrothermal system and potentially gigantic geothermal reservoir represent a unique opportunity to understand mechanisms occurring during erupting activity. All studies combined, provide constraints to numerical modelling of multiphysics, and ultimately models of the underlying processes are essential. They are all (e.g. Mazzini, 2018) fundamental in increasing our understanding of this natural system, and exploring possibilities of transforming disaster into development, such as exploiting geothermal energy from this newly formed moderate-to-high enthalpy geothermal system.

2. HULK: Simple and fast generation of structured hexahedral meshes for improved subsurface simulations

"Computers are man's attempt at designing a cat: it does whatever it wants, whenever it wants, and rarely ever at the right time."

EMCIC, Keenspot Elf Life Forum, 2001-Apr-26

This article is published in Computers & Geosciences Journal, February 2017
Gunnar Jansen, Reza Sohrabi, Stephen A. Miller

2.1 Introduction

A geological model should incorporate structural information and rock properties for any kind of subsurface simulation because simulation accuracy strongly depends on the relevant rock properties and their distribution in space. Therefore, reliable results can only be expected when well-constrained geological modelling and subsurface simulation, an integrated approach of modelling the geology and the physics of the subsurface (e.g. flow, deformation, etc.) is in many cases not available. Commercial software exists that provides integrated modelling and simulation, especially in the oil/gas industry, but often requires months of expert training and their usage might be unsuited for academic purposes. Unfortunately most researchers are only expert in a single field. Thus, they might be either experts in geological modelling or very good in simulators, but rarely both. Consequently, this often leads to the situations where very detailed geological models are never used to simulate physics, while simulators with highly sophisticated physics are often only applied to simple and over-simplified geologies. We address this problem for simulators using hexahedral grids by proposing an efficient mesh generation method. The method is based on octree refinement and provides for direct transfer of structural geological information to the numerical simulator of the underlying physics.

2.1.1 Discretization of geological models

Most meshing algorithms focus on aligning the mesh exactly with the boundaries of the structural geological model. This is inevitable in some cases, such as the prototyping of engineering parts. In other cases, such as structural geological models, this requirement of a so-called *conforming* mesh is too strict and not always necessary because of the uncertainties associated with the geological model itself (Bárdossy and Fodor, 2001; Thore et al., 2002; Lindsay et al., 2012; Wellmann et al., 2014). A well-discretized geological model therefore does not necessarily follow the exact boundaries of the geological model, but more importantly enables the simulator to capture the most relevant aspects and to properly model the underlying physics.

Structural geological models can be built using several different methods if the amount of data (e.g. geological, geophysical or seismic surveys) is sufficient and are readily implemented in widely used commercial software packages *Geomodeller (Intrepid-Geophysics), GOCAD (Paradigm)* or *Petrel (Schlumberger)*. In cases where the geological information available is sparse, solely the interpretation of the geologist might be used to build a structural model using a computer aided design (CAD) program. Of course, with less data available, the accuracy of the structural model and thus ultimately of the subsurface simulation is limited.

The type of discretization requested by the wide variety of subsurface simulators varies largely due to the different underlying numerical methods that impose different restrictions on the geological model's discretization. Finite element simulators are often based on triangular or tetrahedral meshes, while many finite volume based tools require quadrilateral or hexahedral meshes (Pruess et al., 1999; Hammond et al., 2012; Jasak et al., 2007; Trefry and Muffels, 2007; Li et al., 2009). Automatic high quality mesh generation software is available for triangular and

tetrahedral elements using Delaunay triangulation (Ho-Le, 1988; Chan and Anastasiou, 1997; Du and Wang, 2006). However, many simulators exist, especially in the field of computational fluid dynamics in general and in high performance computing, that are based on quadrilateral discretizations. Unfortunately, where a quadrilateral/hexahedral mesh is required or beneficial, a general and stable automatic solution method for the generation of a conforming mesh is not available and a field of ongoing research (Botella et al., 2014; Yu et al., 2015; Owen and Shelton). Significant progress was made in recent years and also applied to geological models (e.g. Xing et al., 2009; Zehner et al., 2015; Botella et al., 2016). However, these methods share a certain complexity in terms of automatism and are rather time-consuming (Stupazzini, 2004; Casarotti et al., 2008).

The methods previously described (including most methods from tetrahedral meshing) have their "bottom-up" approach in common. First, two dimensional surfaces based on the vertices on the geological formation boundaries are meshed by quadrilateral elements. The model is then divided into different meshable regions, which are meshed separately by one of the methods in hexahedral meshing such as sweeping or the advancing front technique (Scott et al., 2005; Löhner, 1996). These separated volumes are connected in a last step to a complete discretization.

As outlined previously, a conforming discretization as targeted by these algorithms is not completely necessary. Octree-based meshing algorithms are generally considered very efficient if a good but non-conforming discretization is targeted. Octree methods were introduced in Yerry and Shephard (1984) and further enhanced by various authors (e.g. Schneiders, 1996, 1997; Shephard and Georges, 1991; Maréchal, 2001, 2009; Tu and O'Hallaron, 2004). In general, octree based discretizations have good mesh quality, are adaptive and support automatic generation (Xing et al., 2009). The Los Alamos Grid Tool Box (LaGriT) is specifically designed to generate meshes for geological applications and also supports meshing procedures based on octree refinement. Using the octree refinement method, Miller et al. (2007) used LaGriT to discretize a geological model that demonstrated good performance.

2.1.2 Outline and scope

The purpose of this work is to present a new and simple-to-use tool to reduce the gap between numerical simulators based on structured or octree grids and geological modelling. Short for Hexahedra from Unique Location in (K)convex Polyhedra – HULK is a simple and efficient algorithm to generate hexahedral meshes from geological models. We achieve rapid mesh generation by binary space partitioning and the octree refinement. While the method of octree refinement is not enhanced in this work, we present an alternative approach for handling all geological formations at the same time, classifying their position in space efficiently. We therefore utilize a "top-down" approach in our method, in contrast to most of the meshing procedures mentioned previously.
In the following, we focus on the underlying theory of the implemented algorithm. We first describe the discretization procedure, followed by the theory of binary space partitioning that is essential for method efficiency. We briefly introduce the methods to evaluate its performance

and provide insight into the implementation. The HULK algorithm is then applied to a series of test cases, including an irregularly shaped two component system, a sedimentary basin, and a complex example from the Swiss Jura Mountain range. We then evaluate the method's overall performance (e.g. different input mesh sizes for the same model), and conclude with some perspectives for future research.

2.2 Theory

A fundamental target of geological modelling is to identify the boundaries between geological formations in the subsurface. Consequently, the output of any geological modeller is in most cases a discretized (triangulated) boundary volume representation of the formations. This discretized boundary representation can be used as the input for the meshing preprocessor of the subsurface simulator. We use this representation to generate a binary space partitioning and successively refine a hexahedral background mesh as further described in this section.

2.2.1 Octree-based meshing

The grid generation process in HULK is based on the octree refinement technique (Yerry and Shephard, 1984; Schneiders, 1996, 1997; Shephard and Georges, 1991; Maréchal, 2001, 2009; Tu and O'Hallaron, 2004). Initially, a structured background mesh is generated circumscribing all of the volumes to be discretized. In the next step, each cell is associated with the corresponding geological formation. In HULK this cell-to-formation mapping is performed by binary space partitioning of the input volumes, discussed in detail below. Once the correct position within the input model is determined, cells can be flagged for refinement (or coarsening) based on their affiliation in a third step. Several refinement criteria can be used. Here we chose to flag all cells whose neighbors have non-matching material identifiers for refinement, and cells which have only matching-id neighbors for coarsening (Figure 13). The refinement is then executed according to the flags that were previously set. If these two steps are repeated until a desired accuracy or number of mesh cells has been generated, it forces a cyclic refinement towards the boundaries of the geological formations (Figure 14). The actual implementation in HULK differs slightly from the general approach introduced here and is further explained in Section 3.

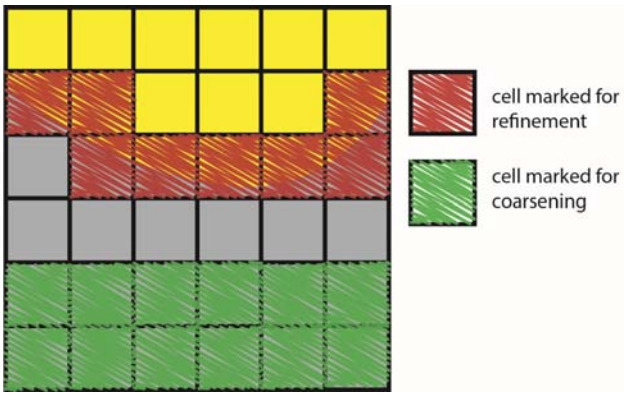

Figure 13: A simple model with two materials. All cells which are at the interface of the two materials are flagged for refinement. In the lower part of the model, where many cells do not have neighbors close to the interface, the cells are marked for coarsening.

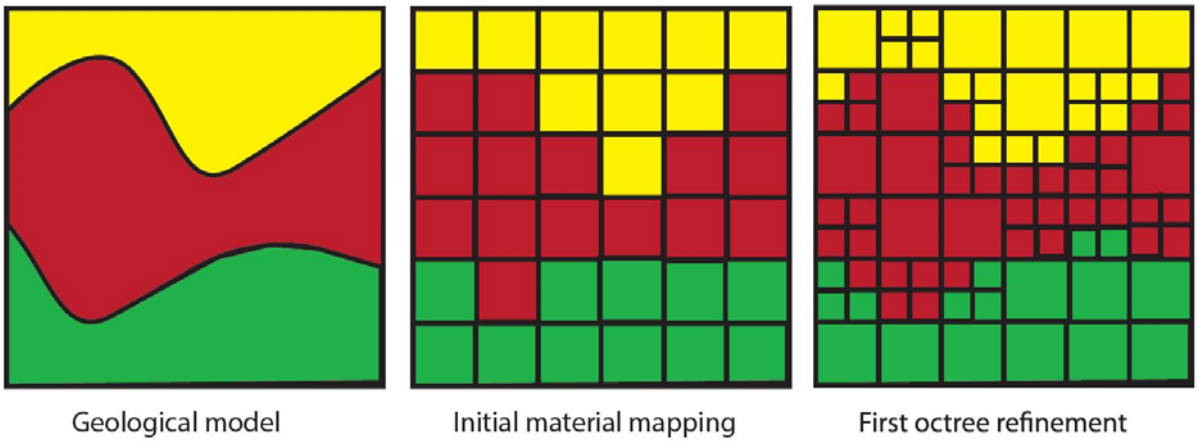

Figure 14: Conceptual model of octree based mesh refinement in the context of geological models. Left: Geological model to be discretized. Middle: In a first step the material properties from the geological model are mapped onto the initial grid. Right: Cells are marked for refinement if any of its neighbors belong to another geological formation. This shows the result after the first cycle of octree refinement, and shows that the initial input are better resolved. With increasing number of refinement cycles, the approximation will become very close to the input geometry.

2.2.2 Binary space partitioning

A key element in the efficiency, and the main novelty of our approach, is the efficient mapping of a cell to the corresponding geological formation. Unlike many other meshing algorithms, all input geometries are treated in a single step. This requires an algorithm that is able to swiftly decide whether or not a point (such as the center of a cell) is contained in a geometry. This test is often called "collision detection" and is a well-studied field in computational geometry (Lin and Gottschalk, 1998; Ericson, 2004). A simple and common technique of collision-detection is ray-tracing, where multiple rays are sent out from the query point in arbitrary directions. Each ray is then tested for its number of intersections with the geometry in order to determine its relative position as "inside" or "outside" of the geometry. Unfortunately, the ray-tracing approach has non-optimal efficiency and is prone to errors due to a number of special cases that need to be treated accordingly (Smits, 2005). Another popular approach is binary space partitioning. Binary space partitioning trees (or BSP trees for short) are structures that can be used to recursively partition *n*-dimensional boundary representations into subspaces with respect to dividing hyperplanes. They are one of many spatial partitioning methods, but considered to be the most versatile and powerful in collision detection algorithms (Ericson, 2004). Originally, BSP trees were developed to address the "hidden surface problem" (Fuchs et al., 1980), but also the computer game engine community takes advantage of the tree structure due to their ability to perform fast collision tests even for a very large number of polygons. If the space to be partitioned is three dimensional, the dividing hyperplanes become regular two dimensional planes. The two partitions or half-spaces generated by a dividing plane are usually called positive and negative half-spaces. We use the convention that the positive half-space lies in front of the dividing plane and the negative half-space behind the dividing plane. In two dimensions the specification of front and back-sides is ambiguous, but as our target geometries are three dimensional the definition is useful. Henceforth, the front side is the side of the geometry's discretized elements whose normal points outward from the geometry.

2.2.2.1 Generation of a binary space partitioning tree

A quick and easy separation of inside and outside the volume ("collision test") is accomplished with BSP trees. Unlike other types of BSP trees, in our method, the dividing planes must be identical with the input geometry's polygons. This selection of the dividing planes is also known as auto-partitioning. Furthermore, all polygons have to be selected exactly once as dividing planes in order to correctly represent the geometry. Note that no actual geometry is stored in the nodes – merely the information pointing to the next nodes in the tree. The end-nodes of a tree partitioning are often called leaves. The leaves store whether the half-space in front/behind the last dividing plane is within the geometry (solid) or outside (empty).

The generation of a BSP tree is illustrated in Figure 15 for a simple dart shaped geometry in 2D. The initial geometry is composed of four vertices (*A*, *B*, *C*, and *D*) connected by four edges (AB^{-}, BC^{-}, CD^{-} and DA^{-}). Now, an edge is arbitrarily chosen to serve as the first dividing plane ①, in this example DA^{-}. All remaining edges are classified according to ①. On the positive side of ①, edge AB^{-} is found and which is going to be the next dividing plane ② and a part of edge BC^{-}. In order to continue the decomposition, edge BC^{-} has to be split into its

parts on the positive sides respectively (③BC^{-}+→③ & ④BC^{-}−→④). The generation of the tree is continued with ②, which will produce a leaf on its positive side (pointing to empty space) and the third dividing plane on the negative side. ③ points to empty space on its positive side. Since all other dividing planes on the negative side of ③have already been considered, it can concluded that it points to solid volume inside the geometry. The tree construction is continued in the same manner until all polygons have been chosen once as dividing plane. With this the BSP tree generation is complete and can be used to query for a location of an arbitrary point with regard to the geometry. Figure 16 shows a graphical representation of such queries for the cases that the query-point is located within and outside of the geometry. Finally note that, although the initial geometry in Figure 15 is concave, the spatial regions corresponding to the leaves are always convex.

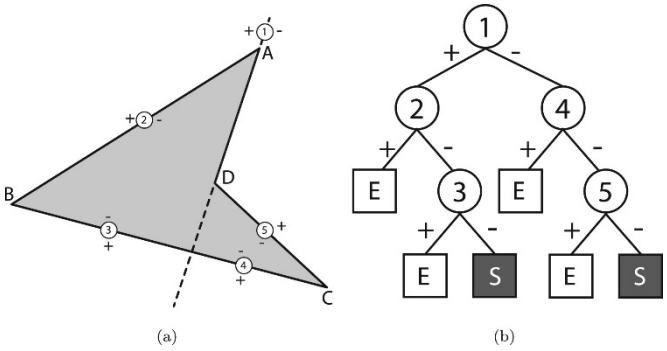

Figure 15: A dart shaped geometry represented by a solid leaf BSP tree. (a) Geometry consisting of 4 vertices and 4 edges resulting in 5 dividing planes as the dividing plane along DA^{-} divides edge BC^{-} into two pieces. (b) The final corresponding BSP tree when all edges are chosen exactly once as dividing plane. Boxes with E signal empty (meaning outside) and dark boxes with S are solid (inside the geometry).

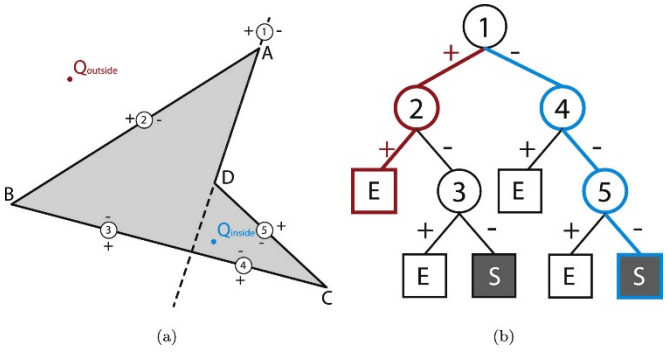

Figure 16: Two query points Q_{inside} and $Q_{outside}$ are tested against a collision of the dart-shaped geometry to obtain a result for the relative position of the query point with respect to the geometry. (a) Geometry with the two query points – the first outside and the second inside the geometry. (b) The corresponding BSP tree query path is visualized for both query points. At each node, the query point is tested against the corresponding plane and sent down in the respective direction. The red path belongs to the outside point, whereas the blue path is

assigned to the inside query point. It is evident that not all nodes of the geometry have to be tested for a collision query. This figure visualizes the optimal complexity of the BSP tree algorithm (cf. Section 2.2.2.2).

2.2.2.2 Complexity of binary space partitioning

Due to the hierarchy formed by a BSP tree with *n* objects in the tree, only on the order of O(log(n)) objects need to be tested by a query (Ericson, 2004). This is due to the fact that typically half of the possibilities can be disregarded with each test. However, in poorly balanced trees the query can cost up to the order of O(n). It is worth noting that the ray-tracing approach is also O(n), yet having higher computational cost per element than the corresponding worst case BSP tree. Auto-partitioning of a square yields in fact a worst case BSP tree and is shown in Figure 17 a. Since none of the dividing planes actually divides the square, no possibilities can be disregarded during queries, leading to an O(n) cost. With this in mind the BSP tree generation of our geological model benefits from complexities in the model as the number of self-intersections is greatly increased. On the other hand, it is clear that we cannot expect to generate perfectly balanced BSP trees from our input geometries with auto-partitioning. Thus a query cost in between O(log(n)) and O(n) can be expected.

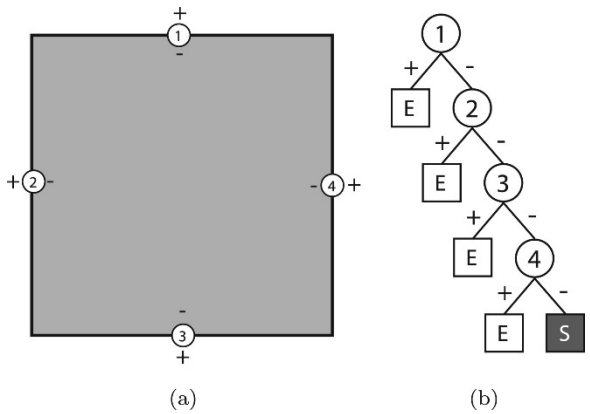

Figure 17: The square geometry. This shows how auto-partitioning can lead to unfavorable BSP tree structures. No part of the tree can be neglected after each test. Real world geometries are not likely to suffer from this problem to the same degree, as irregularities in the domain boundaries will most likely provide suitable dividing planes.

2.3 HULK: Combining octree meshing and space partitioning

The theory is implemented into an efficient and rapid mesh generator. As our primary targets are finite element simulations on adaptively refined grids, we build the mesh generator based on the finite element library *deal.II* (Bangerth et al., 2015, 2007). This library has already previously been used for multiphase flow and transport simulations in the subsurface (Chueh et al., 2010, 2013). Using these subsurface simulators on adequate geological domains is a logical extension of the previous work.
In the following specific parts of the implementation are presented in depth. The pseudo-code for the currently implemented HULK procedure is given in Algorithm 1.

2.3.1 Preparation of the input data

There is currently no standard in the output format of geological modellers or CAD programs. Rather, a set of widely used formats has evolved. A well-known format is the STereoLithography (STL) format, which is available as an export format in almost any of the relevant programs from the geological modelling or CAD environments. The STL format is based on triangulated surfaces describing only the boundaries of the domain. Due to its wide availability, we use the STL output format as input to our mesh generator. STL files contain only an information header, the overall number triangles to be expected, and then a list of all individual triangles. Each triangle is defined by three vertices and a normal vector, and no information is given about the connectivity. While the data format is fairly simple, a number of issues may arise during their creation. Evidently, the input geometry must be an orientable surface for which a system for determining a normal vector can be consistently defined. In other words, it must not contain any holes, self-intersections or multiple shells. Furthermore, any triangle cannot share more than two vertices. This ensures that at least a minimal distance is maintained between all triangles. Fortunately, a number of STL repair methods exist that can detect and often fix these defects automatically (e.g. implemented in the open-source software *MeshLab* and the freeware *netfabb* and recently, Chong et al., 2007). Note that a BSP tree can be generated also if these defects are left unaccounted for, but it is clear that a valid "collision" query on the BSP tree is only possible for orientable geometries. In general, the quality of the input STL does not so much influence the final resulting mesh, but more the generation of the BSP tree structures.

2.3.2 Generation of the BSP trees

The BSP tree generation is performed once at the beginning of the program execution after the corresponding geometry has been read from a file. For each input geometry an individual BSP tree is generated. The pointers to the root nodes of the trees are stored in a shared vector to allow easy queries for all geometries. The current implementation does not cover the selection of a preferable splitting plane to guarantee the generation of a balanced BSP tree. Rather, the first polygon (triangle) from the STL is chosen as a root node of the tree, and generation is performed accordingly until all polygons of the input file are used once as splitting planes.

Clearly, the time to generate the tree structure is directly related to the number of triangles in the geometry. But since it is performed previously to the actual mesh refinement, the overhead is kept small. During refinement the optimal complexity of the BSP tree queries minimizes the dependence on the tree size, largely contributing to the efficiency of *HULK*.

2.3.3 Refinement criteria

Flagging cells for coarsening or refinement is the main control on the cell size and count in the final discretization. A number of different criteria could be used. In HULK relatively basic criteria are implemented at the current state. As the name octree suggests, in the uniform case where all cells are refined, the total number of cells is increased by a factor of 8. Thus, choosing cells to be refined has to be performed cautiously to prevent an unpleasantly large number of cells. On the other hand, cells must be refined enough to resemble the input geometry as close as possible. To this end the following criteria based on each cell's geometric affiliation in terms of a material identifier (*id*) are used:

- Refinement: if id ≠ idi for any *i* neighbors → refine
- Coarsening: if id = idi for all *i* neighbors → coarsen

Additionally, a suitable criterion to cease refinement has to be defined. Here, the generation stops once the distance *d* of the query point *x* is sufficiently close to the BSP tree.

- Evaluate distance: if $d(x) \leq \epsilon \rightarrow$ clear refine flag

Here ϵ is the only actual tuning parameter in HULK. From experience, good results are achieved when $\epsilon \approx 0.005 \cdot \max(Lx,Ly,Lz)$ where L_i are the model extents in the coordinate directions.
In order to assure numerical accuracy, the maximum level difference in refinement between adjacent cells may not be greater than one. This implies that also cells that are not directly associated to the interface might be flagged for refinement in a second internal step. Furthermore, due to the implemented criteria, the number of cells in the initial mesh has to be chosen appropriately to the smallest geometric feature that is to be resolved in the final grid.

Algorithm 1
Pseudo-code for the algorithm used in HULK using octree refinement to resolve complex geometries in hexahedral cells.

```
for all input geometries do
    read input data from file;
    generate BSP tree;
end
while cycle < maxCycles and number of cells < MaxCells do
    for all cells do
        for all BSP trees do
            if is inside current BSP tree then
                set id = corresponding material identifier;
                break loop;
            else
                continue with BSP tree for next input geometry;
            end
        end
        if (neighbor's id ≠ cell's id ) for any neighbor then
            flag cell for refinement;
        end
        if (neighbor's ID = cell's ID) for all neighbors then
            flag cell for coarsening;
        end
        if cell's distance to cell's corresponding BSP tree
        ≤ ε · max(L_x, L_y, L_z) then
            remove cell's flag for refinement;
        end
    end
    execute refinement;
end
```

2.4 Methods for mesh quality analysis

Measuring the quality of the generated discretized domain is an important part of a meshing algorithm. Standard procedures include the measurement of element skewness, aspect ratio and distortion. These quantities are mainly used to determine the quality based on the degree of conformity and to identify degenerate elements. Since we do not seek a conforming discretization of the input geometries and the discretization is based on regular octree meshes, some techniques of defining mesh quality no longer apply; for example element skewness and aspect ratio become constant and attack optimal value in this case. In order to give a measure of the degree of conformity nonetheless, we compute the "mean distance" between the triangulated input and our hexahedral approximation as well as the volumetric space filling.

Measuring the distance or similarity of two discretized surfaces is not straightforward. Many of the more sophisticated theories developed are used in the field of automatic face recognition (Abate et al., 2007). A simpler approach is used here which computes the minimum distance between the cell centers of cells at the interfaces and the BSP tree of the corresponding geological formation. From this, the mean distance is calculated. Ideally, the BSP tree – cell center distance distribution should have its maximum at zero. However, since we compare the cell centers we expect a shift of the mean distance towards the half the size of the largest element on the boundary. In any case, with progressing refinement of the mesh the mean distance is expected to decrease continuously.
Further, the accuracy in volume of the mesh is considered. To this end, the percentage deviation between the volume of the input V_0 and the final discretized mesh V is calculated:

$$\text{Deviation}_{\text{vol}}\,(\%) = \frac{V}{V_0} \cdot 100\% - 100\% \tag{2.1}$$

The deviation by itself is not a good indicator for the mesh quality, as no information about the shape of the geometries is incorporated and in fact could lead to very poor discretizations. However, in combination with the mean distance it becomes a viable indicator for mesh accuracy.
The quality of octree-based discretization in general is known to be good (e.g. Xing et al., 2009), but the accuracy of the numerical method depends on the overall distribution of the cell sizes. Assuming the numerical accuracy is ideal if all cells are of the same size, the utilization of octree refinement can increase computational efficiency while maintaining the same numerical accuracy only if the cell size distribution is only mildly altered. In other words, smooth cell size distributions with a single peak should always be preferred. Again, this is not a direct measurement of mesh quality, but serves as an important indicator for the expectable accuracy of the applied numerical simulators.

2.5 Results

The implemented algorithm is validated against three test geological scenarios. The first is a 3D model of an artificial dike intrusion into a single constituent host rock to demonstrate the general performance of the algorithm. We then present an example of a simplified three-dimensional model of the newly born hydrothermal system called "LUSI" in Indonesia (Mazzini et al., 2012; Lupi et al., 2013). This model already consists of multiple geological layers of a sedimentary basin. A third example is a full scale geological model of a part of the Swiss Jura Mountains. The models vary in size and complexity. Table 1 shows detailed information on the test geometries used.

Table 1: Three model types from different settings are used to evaluate HULK*'s performance. They vary in size, amount of shells and their underlying complexity.*

Model name	Setting	Volumes	Input size (triangles)	Complexities
Dike intrusion	Volcanic	1	$1.9 \cdot 10^5$	Locally steep gradients
LUSI	Sedimentary basin	5/7	$4.5\text{-}7.5 \cdot 10^5$	None/large scale faults zones
GeoNE	Swiss Jura	25	$1.5\text{-}11.9 \cdot 10^6$	Folding and faulting including offset

2.5.1 Dike intrusion

Figure 18 shows the initial model for the first example. As the model consists only of two geological formations, the volcanic intrusion at the bottom and a host rock on top, only the resulting hexahedral mesh for the volcanic intrusion layer is shown. Note that the input consists only of one shell which describes the geometry of the dike. We assume that the region of interest is a rectangular box around the dike, thus making a second input geometry for the host rock unnecessary.

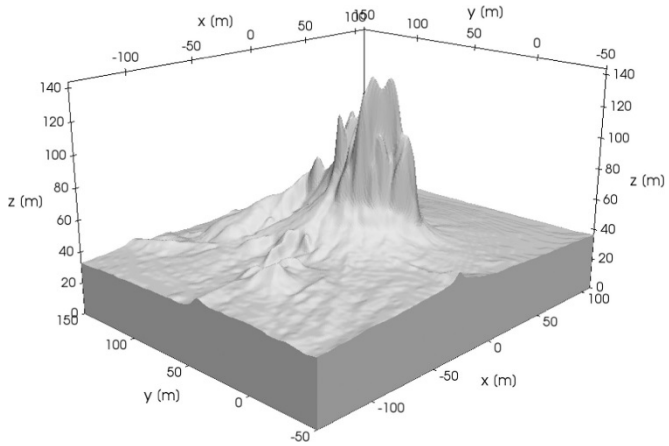

Figure 18: The geological model and input for the dike model. The dike has a non-trivial shape with steep gradients to evaluate the implemented algorithm.

The geometry was discretized using four refinement cycles. In Table 2 the resulting number of cells in the whole (both volcanic intrusion and host rock) are shown for all cycles. Furthermore we evaluated the performance of volumetric filling for the dike intrusion model. To this end we compared the meshed volume against the computed volume of the input STL file. The resulting deviation in volume as well as the distance (measured to the BSP tree) from the input geometry is also presented in Table 2. The accuracy of the upper layer can easily be computed by $(\delta\%)^1=1-(\delta\%)^0$.

Table 2: Mesh statistics for the dike model. The number of cells, volumetric filling accuracy as well as the distance to the corresponding BSP tree were analyzed for all performed refinement cycles on the dike intrusion model. The volumetric deviation alone is not a sufficient indicator but shows in combination with the BSP distance an overall increase in mesh accuracy with refinement cycles.

Cycles	Cells	Deviation (%)	BSP distance (–) $\cdot 10^{-3}$
0	32’768	0.04	23.8
1	21’715	1.33	52.6
2	77’708	0.47	34.3
3	269’746	0.13	22.6
4	861’617	0.19	13.8

As mentioned in Section 2.4 the volumetric filling is not a sufficiently good indicator by itself. This is clearly visible as it is already very high even when the visual accuracy of the mesh is still unsatisfying. Regardless, a clear trend towards the correct theoretical volume is visible. In combination with the measured distance to the BSP tree we can conclude that the mesh accuracy increases with the number of refinement cycles.

Figure 19a and b show the mesh after different cycles. Clearly the refinement towards the boundaries is visible. The final model is shown in Figure 20, which shows that all important features of the initial model were captured by the algorithm. Note that due to the selection of refinement criteria the cell size distribution is not uniform at the interface. Rather flat regions of the model are less refined, whereas areas with steeper geological features exhibit a stronger refinement to capture the curvature of the geometry correctly. After the last cycle the mesh contains roughly 1 million cells which might be too big for initial simulations. However, the accuracy of the preceding cycles is also good and yield a cell count of maximum a few hundred-thousand cells, which can be handled by modern parallel computing systems (Hammond et al., 2014).

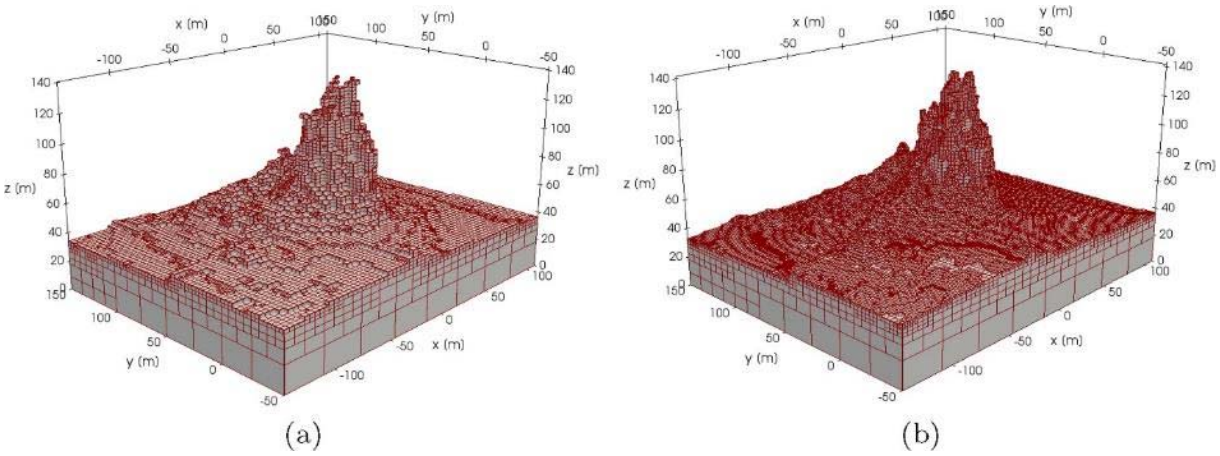

Figure 19: The generated mesh for the dike model after different refinement cycles. (a) After the 2nd cycle. The general shape of the dike is already captured but its extends are slightly overestimated and smaller features not yet captured. (b) Mesh after the 3rd cycle of refinement. The peak shape is still not matching the input model completely. Yet on the rather flat zones of the interface refinement towards smaller features is visible.

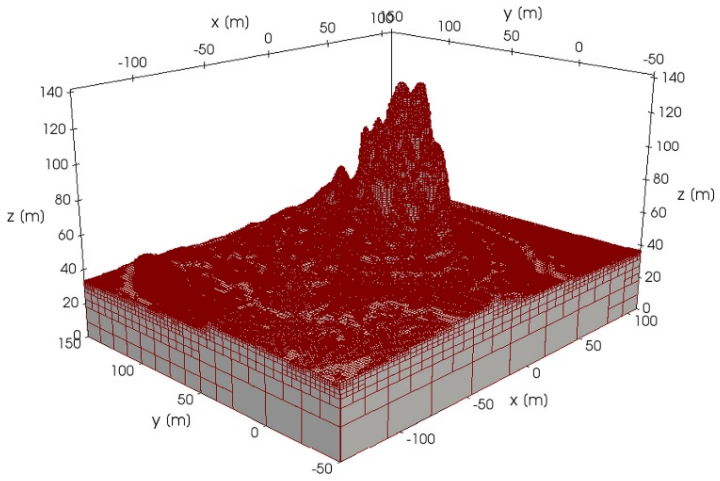

Figure 20: The final mesh of the dike model after 4 cycles of refinement by HULK. All important geometric features of the input geometry are captured and provide a good hexahedral approximation to the initial geometry (cf. also Table 2 for detailed accuracy evaluation). Different levels of refinement are visible depending on the curvature of the dike's shape. Flat regions are slightly less refined than the peak for which cells are highly refined to capture its extends.

2.5.2 LUSI

The second example is a simplified model of the LUSI mud eruption in Eastern Java, which appeared in 2006 and continues today as a geyser system (Mazzini et al., 2012; Lupi et al., 2013; Sawolo et al., 2009). LUSI is located in a back-arc sedimentary basin that is likely influenced by nearby active volcanism. The eruption is located at the intersection of two major regional faults which were included in the geological model as finite width faults. In the following we present the model with and without the faults to increase the clarity in analyses. In general, the model does not show many complexities, as the sedimentary basin is mostly undisturbed except for the intersecting strike-slip faults. We generated a model based on seismic and borehole data obtained in the framework of the LUSI Lab project and computed with *Geomodeller* (Lajaunie et al., 1997; Calcagno et al., 2008). The number of input geometries range from 5 formations up to 7 formations if the two major faults are included. The initial model is shown in Figure 21.

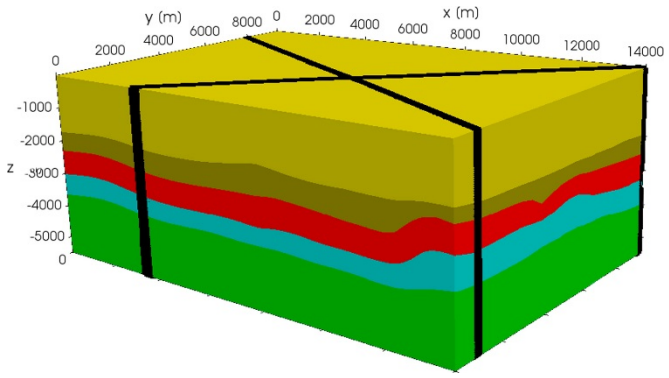

Figure 21: The geological model for LUSI used to generate a hexahedral mesh with HULK. Note that the two faults are implemented a posteriori into the model which makes certain analysis unavailable for this model.

The final discretizations of the LUSI model consist of 346,991 hexahedral cells without and 513,409 cells including the faults. The final meshes without and including the faults are shown in Figure 22. A visual comparison of the input geometry and the final discretization shows that all important geological features of the sedimentary basin are preserved. The LUSI geological model was discretized using five refinement cycles in HULK. For each cycle all volumes are compared to the reference volume of the input geometry. Unlike the dike model, the accuracy of the volumetric filling is not as high during the first refinement cycles. This is mostly due to a different refinement strategy chosen in this example. For this model we decided to change the refinement strategy to a uniform refinement without coarsening or removal of refinement flags in order to show the excellent refinement towards the models boundaries. However, as shown in Figure 23 the accuracy is greatly increased in later refinement cycles. The final accuracy can also be seen in the *y*-slice view of the model which is shown in Figure 24 for the final mesh where the boundary cells for each layer and the outline of the corresponding input geometry are shown. Here it is very well visible that the boundary cells coincide very well with the input geometry after the last refinement step.

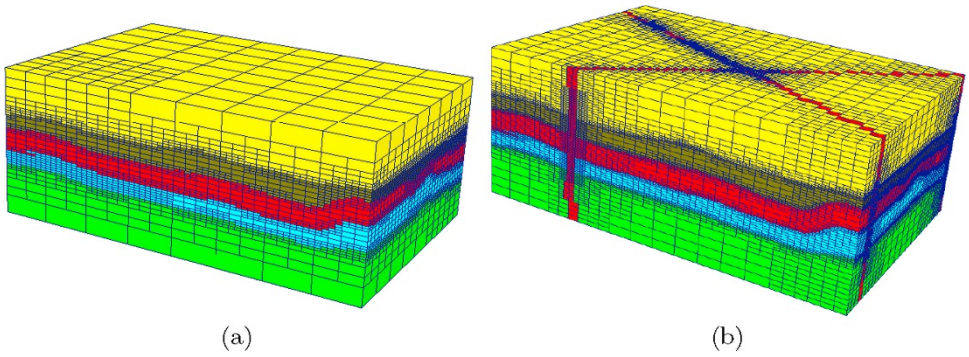

Figure 22: The final LUSI model based only on the geological layers of the sedimentary basin with and without big scale faults. The successive refinement into the boundaries of the geological formations is visible and working well. Yellow – sandstone formation, brown – clay formation, red – volcanoclastic formation, blue – carbonate formation and green – mudstone formation. (a) Without faults and (b) with faults.

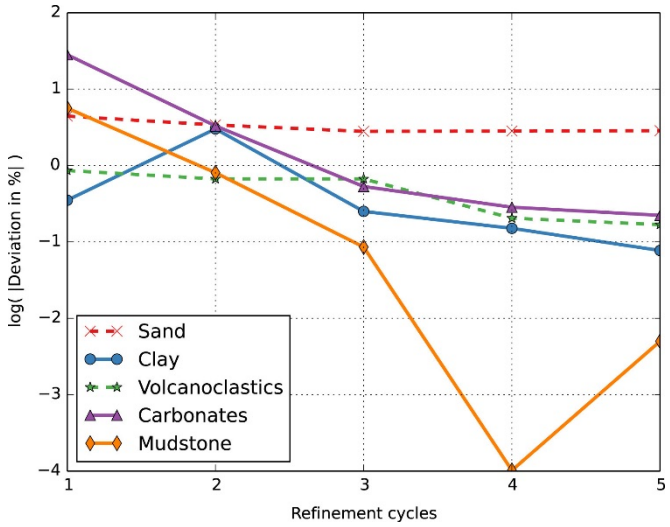

Figure 23: The deviation of volumetric filling for the LUSI model is shown for the refinement cycles used. The accuracy is increased by one or two order of magnitude for all formations.

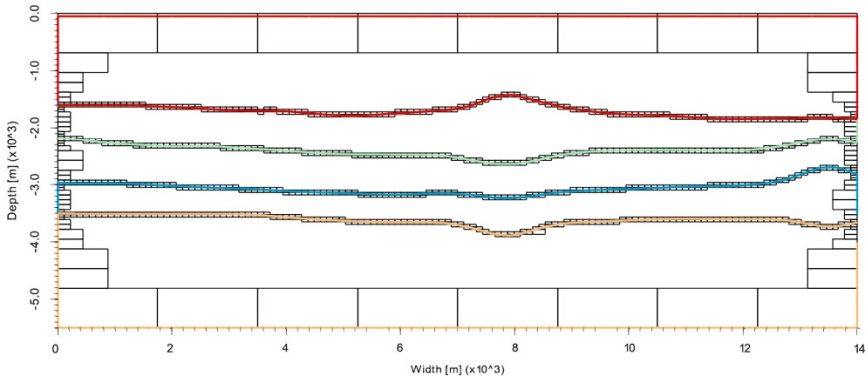

Figure 24: The accuracy around the formation boundaries after the 5th and final cycle of refinement is greatly increased as visible in this slice through the model. The achieved accuracy is sufficient for a structured hexahedral approximation of the input geometries.

2.5.3 GeoNE

The GeoNE model is by far the most complex model that we use to evaluate the performance of HULK. Between May 2010 and July 2012, the Laboratory of Geothermics at the University of Neuchâtel studied the potential of deep geothermal resources in the Canton of Neuchâtel in Switzerland (CREGE, 2014). As part of the project a detailed 3D geological model was built. We present a part of this geological model here to generate a hexahedral mesh. This model is going to be used also for the input mesh scaling in the next section. In this section the GeoNE50 model containing a total of 5.9 million triangles is used. The geological model as we use it here is shown in Figure 25 a. The model features geological formations of different sizes as well as folds and faults including offset. Figure 25 b shows a cross section through the model, where the intersection of multiple faults in a fold is visible. This provides an excellent opportunity to investigate the algorithm's performance in complex settings. The model consists of overall 25 parts which are all included in the meshing procedure.

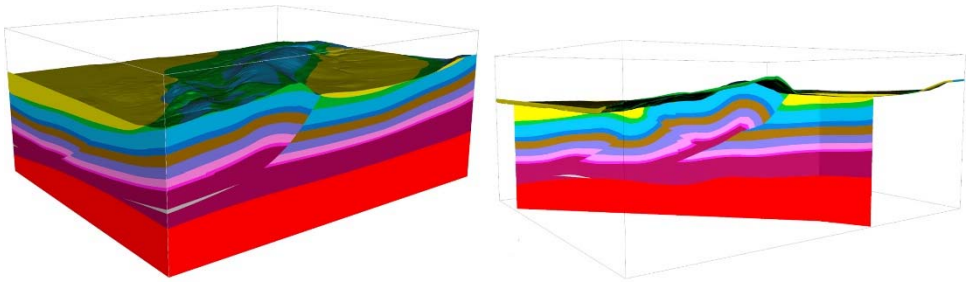

Figure 25: The GeoNE model containing 11 formations in a total of 25 parts. (a) An outside view of the complete model. (b) Cross section through the model showing the complex interior including multiple faults including offset.

Due to the high complexity of this model the final discretization includes 1.4 million hexahedral cells. The final result for the whole model and the cross section through the model are shown in Figure 26 and Figure 27 respectively. A visual comparison of the input geometry and the final discretization shows very good agreement. The GeoNE50 geological model was discretized using 4 refinement cycles in HULK. The high complexity of the model prohibits a meaningful volume analysis as performed in the other examples. However, the mean distance to the BSP tree of the corresponding geological formation could be calculated and is shown in Table 3. The overall decrease in the distance indicates a distinct increase in accuracy with later refinement cycles. This further supports the conclusion of the visual analysis of the final discretization. A detailed comparison on the cross section through the geological model (Figure 25) and the discretization (Figure 27) shows how detailed the hexahedral approximation by HULK really is. Although the faults in the model could not be included in the meshing process as they were modeled as 2D surfaces instead of finite width faults, their resulting offset is clearly visible. Overall, all 11 formations were resolved with very good accuracy, capturing also the complex interior with intersecting fault offsets in a folding environment.

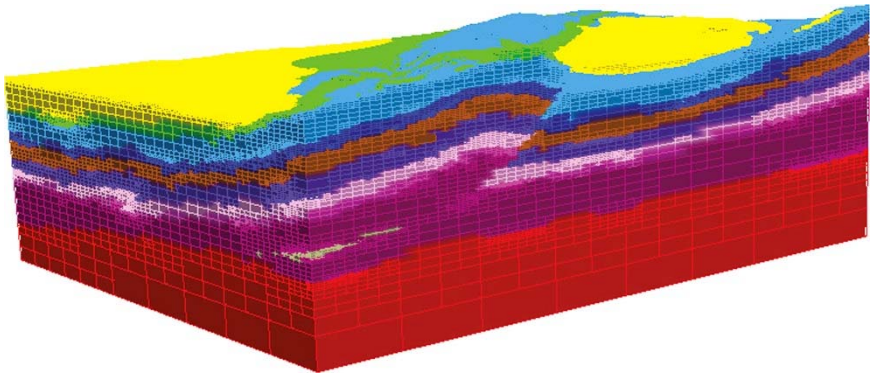

Figure 26: The final mesh of the GeoNE50 model after 4 cycles of refinement by HULK and contains 1.4 million cells. All important geometric features of the input geometries are captured and provide a good hexahedral approximation to the initial geometry. Even smaller features such as a small intrusion (shown in gray at the front corner) as well as the very fine quaternary deposits at the top of the model are well-resolved. Dynamic cell size changes are visible especially in vicinity of the large offset fault visible on the right face of the model.

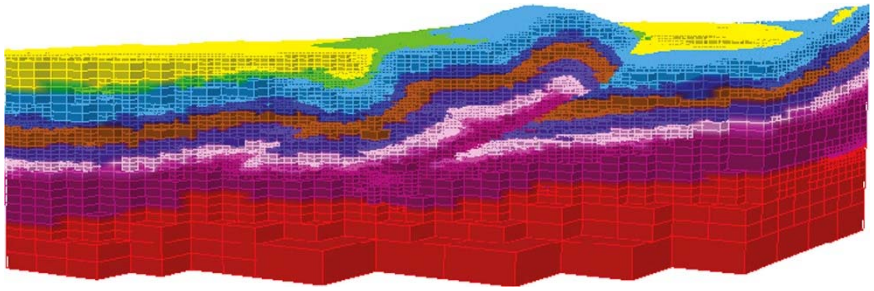

Figure 27: Cross section through the complex interior of the final mesh of the GeoNE50 model after 4 cycles of refinement by HULK. The whole model contains roughly 1.4 million hexahedral cells. In comparison with Figure 25b the accuracy is very good. All three main offset faults visible in the cross section are resolved by the mesh. Solely, a small intrusion (shown in gray in Figure 25b) is not resolved by the hexahedral approximation. Note that the adaptivity of the octree mesh is not as clearly visible in this section through the mesh as many complexities have to be resolved, leaving little room for cell number optimization through mesh coarsening.

Table 3: Simple mesh statistics for the GeoNE50 model. The number of cells as well as the distance to the corresponding BSP tree was analyzed for all performed refinement cycles on the complex geological model. The BSP distance indicates an overall increase in mesh accuracy with refinement cycles.

Cycles	Cells	BSP distance (–)
0	32’768	1.91
1	40’489	2.84
2	135’290	2.74
3	459’040	1.91
4	1’408’975	1.20

2.6 Discussion

In the previous section, three models with varying degree of complexity were used. However, in order to evaluate execution timings as well as scalability a more reliable basis needs to be created. To this end the GeoNE model is used. We use the quadric edge collapse decimation technique to reduce and increase the number of triangles in the input geometries while conserving all formations and faults in the model (Hoppe, 1999). The initial model is the GeoNE50 model consisted of roughly 6 million triangles. In the following we will consider two down-sized models (GeoNE25 ∼3 million and GeoNE13 ∼1.5 million triangles) as well as one up-sized model GeoNE100 with a total of ∼12 million triangles in the input geometries in addition to the initial GeoNE50 (∼6 million), LUSI (∼0.5−0.8million) and Dike (∼0.2 million triangle models).

2.6.1 Mesh quality

As discussed in Section 2.4 the quality of octree based meshes is in general quite good. However, for accurate simulation results the cell size distribution within the model might be important. In order to guarantee high accuracy the maximum level difference between neighboring cells is set to 1. Here we present the distribution of refinement levels for the cells in the different models. Figure 28 shows the distributions for all three models presented in the previous section and additionally the largest version of the GeoNE model. In general, smooth distributions are visible for all models, which indicates good quality with respect to the expected numerical accuracy. The dike model's distribution has its peak at the highest level of refinement, which is due to the high curvatures in the input geometry. The effect of the curvature of the input geometries is also visible in the LUSI model that contains only moderate curvatures and which leads to a more widened distribution of the cell sizes within the model. Both GeoNE models show a similar distribution of cell sizes indicating that the resolution of the input geometries – given that it is reasonably good – does not significantly influence the distribution of cell sizes in the final discretization.

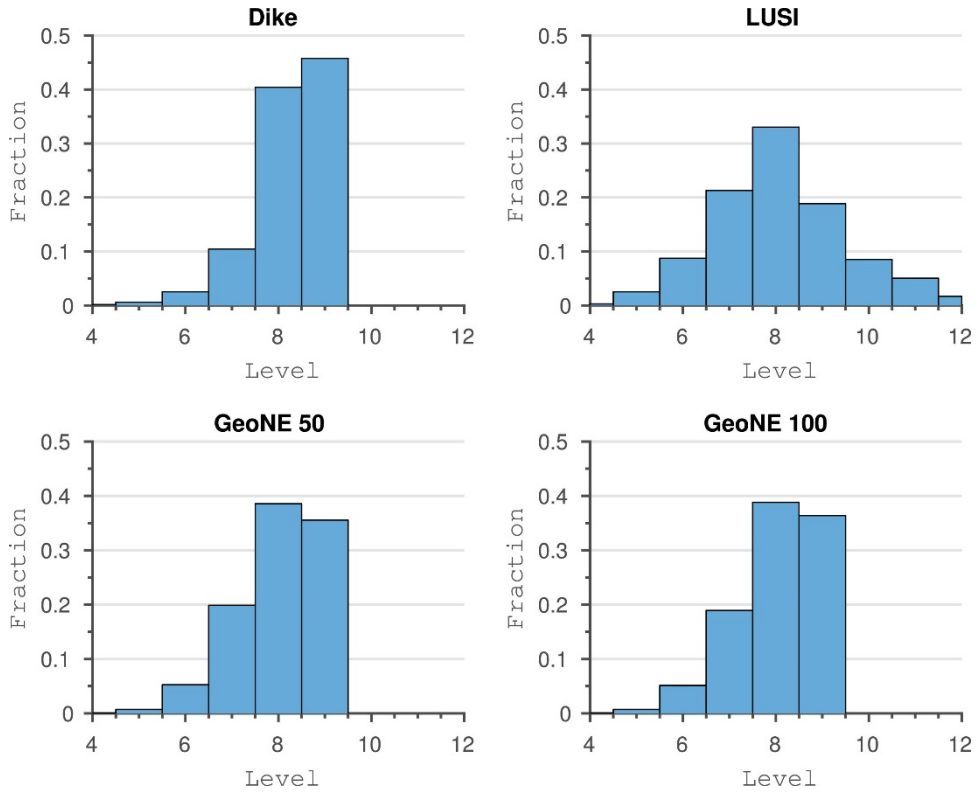

Figure 28: Mesh quality analysis based on the refinement level distribution of the cells in four different models. Sharp distributions are likely due to sharp gradients in the input geometries, as for example the dike model. Rather smooth distributions as seen for the LUSI model also indicate rather smooth input geometries.

The distance to the BSP tree is also an indicator for the accuracy of the discretizations. Figure 29 shows the calculated mean distances to the corresponding BSP tree structures for all cells in each refinement step for the dike and GeoNE models. The mean distance is decreasing continuously after the first cycle for the GeoNE models. This is due to the fact that indeed within the first refinement cycle more cells are coarsened than refined, leading to an initial shift in the medium distance towards bigger distances. For the final models the distances are well below the initial distances, indicating the overall increase in accuracy as already indicated by the volumetric deviation and the visible confirmation.

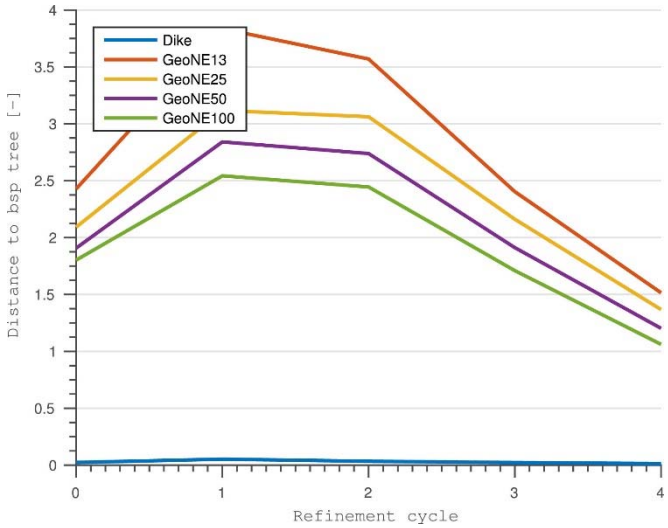

Figure 29: The mean distance to the BSP tree is shown for the dike and GeoNE models. The initial increase in distance is caused by a dominating cell coarsening in the first refinement cycle of the GeoNE models. The final discretizations exhibit distances well below the initial value.

2.6.2 Computing time

We show the performance and efficiency of the proposed method by a series of execution timings. All simulations were run in serial, single threaded on an Intel Xeon E5-2650 CPU with 2.3 GHz clock speed. Figure 30 shows the time needed to generate the BSP trees for all models used in this paper. The generation of the BSP tree shows a linear scaling with size of the input geometry. Solely for small inputs small deviations from the linear behavior are visible. This in however not related to the BSP tree construction but due to a small computational overhead when generating multiple BSP trees from different geological formations. With increasing size of each formation this overhead is relatively reduced, showing better linear scaling.

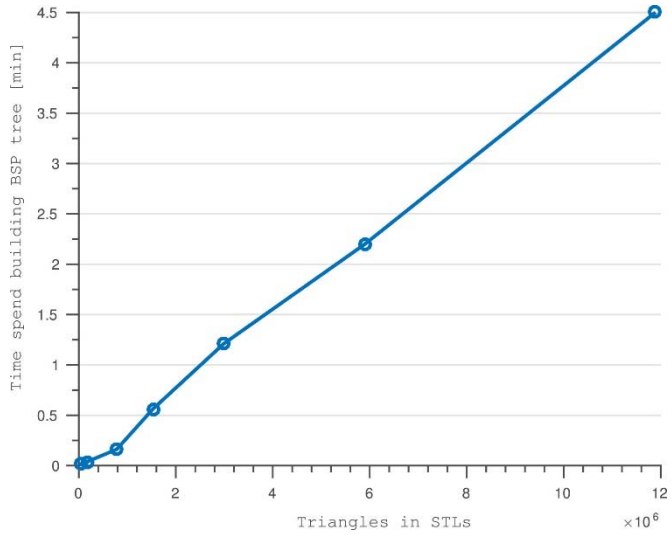

Figure 30: The BSP generation shows excellent linear scaling for moderate to large input files. Small input files suffer from a slight computational overhead if multiple BSP trees are generated for a series of geological formations such as the smallest GeoNE model.

The overall timings for the generation of the final discretization for all models is shown in Figure 31. Output of the final discretization as well as the actual refinement are the main contributors to the overall runtime of the execution. Again, the near-linear scaling of the generation of the BSP trees is visible, particularly for the four GeoNE models. We observe that the time consumed by the refinement procedure does not appear to strongly depend on the size of the BSP tree, and also not strongly dependent on the number of triangles in the input. The figure further shows that the main contributor to overall execution time is the output. This time is shared also with other mesh generators and needs to be taken into account when comparing execution timings. In general, the execution times range from less than 1 min for the simple LUSI model without faults up to about 12 min for the largest of the GeoNE models with an overall input size of roughly 12 million triangles. It becomes evident that the execution time strongly depends on the complexities in the model. Better refinement criteria might mitigate this effect in the future.

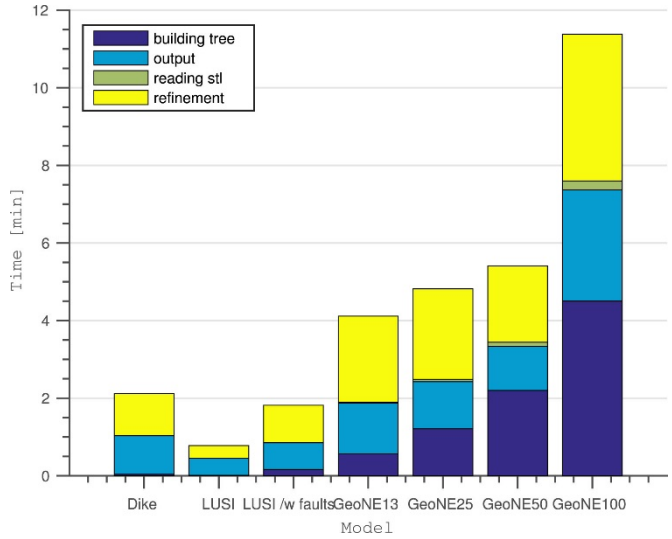

Figure 31: Comparison of the execution times of the different models discretized by HULK. *All models were executed in a single threaded on an Intel Xeon E5-2650 CPU with 2.3 GHz clock speed. The execution time strongly depends on the complexities in the geological model (cf. Table 1).*

2.6.3 Comparison with uniform refinement

We can further evaluate the efficiency of our refinement technique by comparing the refinement behavior of all models compared to uniform global refinement. The refinement curves in Figure 32 show the number of cells depending on the refinement cycle. Two theoretical curves for uniform global refinement with different number of initial cells are also shown. It can be seen that the proposed method is effective in terms of refinement cost as both models have a refinement factor much less than the uniform refinement. Nevertheless, the possibility to utilize the algorithm also on a structured grid with uniform refinement is very useful because many reservoir simulators still utilize this type of grid, and where our algorithm can simplify and speed up the grid generation process. In cases where the structured grid is coarse, our algorithm can be interpreted as a very simple upscaling technique mapping the geological domains and properties on the structured grid.

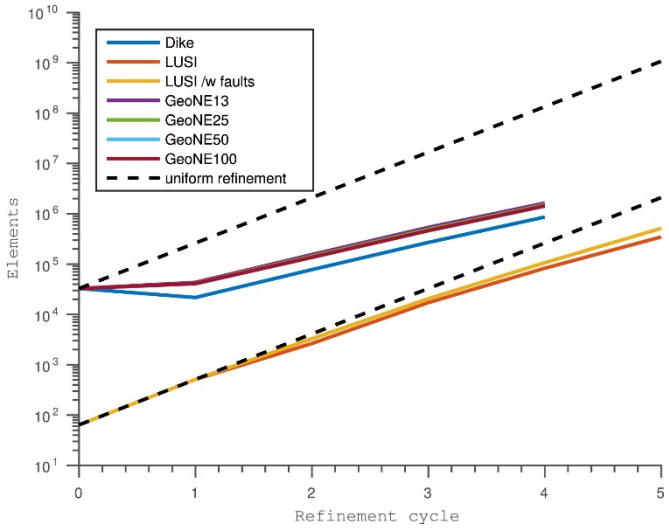

Figure 32: Comparing the refinement factor for the models under consideration. The dashed lines represent uniform global refinement. All models show a slope much lower than the unfavorable uniform refinement curve, showing the efficiency of the chosen octree refinement in the algorithm. (Note the logarithmic scale on the y*-axis).*

2.7 Conclusions

All three examples demonstrate that the implemented algorithm works very well. The input geometries are reasonably well represented in the hexahedral discretizations. In general the number of cells needed for a satisfying model is on the order of a few hundred thousand to roughly 1.5 million cells. This is quite a large number, but compared to the grid resolution used in classical benchmark models (e.g. Johannsen formation with 149 × 189 × 16 = 450,576 cells and SPE10 with 60 × 20 × 85 = 1,122,000 cells) it is competitive (Eigestad et al., 2009; Christie et al., 2001).

A common solution strategy for these large full field models is the division into smaller sections and a successive solution of each section. This procedure could also be applied to the mesh constructed by our algorithm if the required number of cells is too big for a full field solution. Nonetheless, state-of-the-art parallel subsurface simulators such as *pflotran* are able to handle large number of elements (Hammond et al., 2014). With the utilization of new programming techniques and the advances in hardware accelerators will enable and promote simulations with multi-million cells. The number of hexahedral cells necessary for the models is also comparable to the number of cells in a corresponding tetrahedral triangulation. To compare against a tetrahedral discretization, we used the open source software *gmsh* and computed a conforming tetrahedral triangulation on each formation of the LUSI model (Geuzaine and Remacle, 2009). We find that in this case the number of tetrahedral cells (gmsh: 421,392) needed is even greater than the hexahedral approximation by HULK (346,991). It is important to note that the tetrahedral discretization algorithm builds a conforming mesh which coincides exactly with the

input geometry. Thus the quality, namely the number of elements of the input geometries' discretization, is directly linked to the number of cells in the final mesh. In *HULK* however, the accuracy of the initial boundary description is not directly linked to the number of cells as we are only interested in a good quality non-conforming approximation.
The implemented algorithm could be improved by a technique called *edge-snipping*, which would result in a conforming mesh by moving the outer boundary vertices to the exact position of the input geometry surface. This procedure, however, comes at a high computational effort, and even prohibits some parallelization techniques such as scalable adaptive mesh refinement that performs better on structured octree grids (Burstedde et al., 2011). Therefore it has been omitted in the current work but yields a possible extension of the algorithm for the future.

Accounting for structures in the subsurface using a geological model efficiently helps increase the accuracy of any kind of numerical subsurface simulation. We developed and implemented a fast and efficient hexahedral mesh generator for subsurface simulations. The underlying theory and the simple structure of the algorithm makes it also possible to implement the algorithm directly in the discretization part of other simulation software. However, it can also be used as a stand-alone preprocessing unit. Simulators that use adaptive mesh refinement based on the physics can utilize our method within their simulations to dynamically resolve only those parts of the input geometry that are of interest in the current state of the simulation.

3. GEYSER: 3D Thermo-hydrodynamic reactive transport numerical simulator including porosity and permeability evolution using multi-GPU clusters

"Numerical modelling is simple and is based on simple mathematics. All you need to know is: linear algebra and derivatives."
"Most of the complicated mathematical knowledge is learned in school before we even start to study at university! All you need is: strong motivation, usual maths, clear explanations, and regular exercises… motivation is most important, indeed…"

Prof. Dr. Taras Gerya

This article is in preparation for submission to Computational Geosciences Journal, April 2018
Reza Sohrabi, Samuel Omlin, Stephen A. Miller

3.1 Introduction

The purpose of this paper is to develop a high resolution 3D heat and mass transport model using multi-GPU parallel processing incorporating dehydration reactions and porosity changes in response to input of a substantial heat source, and to determine its scalability on multiple GPU's. The application of this work is to investigate a generic case of the consequences of a magmatic intrusion within a sedimentary basin. The most relevant system where this applies is the Lusi geyser system in Java, Indonesia (Mazzini et al., 2012), but the model applies to any situation where heat input results in dehydration of hydrous minerals.

The use of supercomputing in Earth sciences, in both research and industrial applications, has increased dramatically over the last decade. "Software scalability is the most significant limiting factor in achieving the next 10x improvements in performance, and it remains one of the most significant factors in reaching 1000x" is one of the key findings of the recent High Performance Computing (HPC) market study by the U.S. Council on Competitiveness (Stefano and Hailu, 2014).

Since the beginning of the 21st century, academia and industry have been limited in adapting 3D software and numerical algorithms to the changes in hardware evolution. As a result, many 3D applications and algorithms are not well suited for the available hardware, limiting performance far below the hardware's peak. In this article, we describe and present a simulator designed for multi-GPU workstations, clusters, or supercomputers. The algorithm solves systems of strongly non-linear partial differential equations (PDEs) at very high spatial and temporal resolutions, and it's thus capable of resolving many scales in both space and time. Non-linear couplings arise in many natural and engineered systems, including those described here involving fluid flow, mass and heat transport in fractured porous media. We also consider porosity and permeability changes due to dehydration reactions, where the porosity created from the reaction is less than the fluid mass generated, thus resulting in local fluid overpressures at the dehydration nucleation site.

The development of scalable and efficient parallel subsurface simulators is not trivial. There are only few computational tools which used multi-CPU or even multi-GPU technology for underground fluid dynamics, but it is of main interest today (Bangerth, 2007; Galvan & Miller, 2013; Kolditz et al., 2012; Hammond et al., 2014). The development of new algorithms that are well suited for current and future hardware is essential in many ways. One challenge consists of modifying algorithms that are sophisticated and state-of-the-art, but not well suited for current hardware. Another issue is that simple algorithms that are well suited for parallelism and have regular data access patterns are typically rather old but mostly don't include state-of-the-art processes. This approach have been successful in several cases (Datte et al., 2009; Gysi et al., 2015; Krothiewski & Dabrowski, 2013; Micikevicius, 2009). The stencil-based methods, which permit building solvers for partial differential equations (PDEs) is perfectly adapted for the current hardware (Strikwerda, 2004). So the idea is to design a tool with iterative methods using Finite Difference (FD) and a regular Cartesian grid avoiding any direct methods using complex techniques to compute derivatives and unstructured grids.

Many numerical models have been developed for reactive transport considering heat and mass transport through porous media with even more complex multiphysics (Kolditz et al., 2012; Hammond et al., 2014). The need for predictive tools led to the development of reactive models considering reaction kinetics and reaction induced changes in porosity (Lichtner & Carey, 2006; Lichtner & Kang, 2007; Steefel et al., 2005; Xu et al., 2006). However, none of them used multi-GPU computing.

Our workflow incorporates complex 3D geological structures using a grid generator (Jansen et al. 2017) with parallel scaling to simulate the physical processes under consideration (Figure 33). We solved the equations governing fluid flow and mass transport in a system undergoing thermally induced dehydration reaction/porosity creation on a multi-GPU (Graphics Processing Unit) parallel processing platform to efficiently calculate the 3D time evolution of fluid flow with mass and heat transport generating porosity and permeability evolution in a reactive system at high resolution. Post processing data analysis and visualization are performed with open source platform Paraview (Henderson et al., 2004).

Figure 33: Our workflow for 3D numerical modelling based on "High Performance Computing" algorithms using CPU, GPU or MIC clusters.

Understanding these processes using High Performance Computing (HPC) is fundamental for geo-resource development or CO_2 sequestration where the reaction rate of minerals regarding CO_2-water also depends on porosity volume change by temperature and pressure decarbonization. We conclude the article with an outlook for future development of our multi-GPU simulator.

3.2 Methodology and implementation

3.2.1 Conceptual model

We consider the case of a heat and fluid flow in a hydrothermal system where a magmatic intrusion at depth induces large-scale dehydration of hydrous bearing rocks or clays (Figure 34). The addition of substantial water to the system will increase fluid pressure, and if the fluid pressure is greater than the minimum principle stress, this induces local hydro-fractures. This sudden volume expansion similar to corn popping, produces fluids which will rise to the surface in different manifestations of hydrothermal systems such as hot springs, mud volcanoes or geysers systems. Many studies have shown that the dehydration of different rock types should be considered in deep hydrogeological or geothermal processes, and different models have been proposed (Miller et al., 2003, Malvoisin et al. 2015, Omlin et al., 2017).

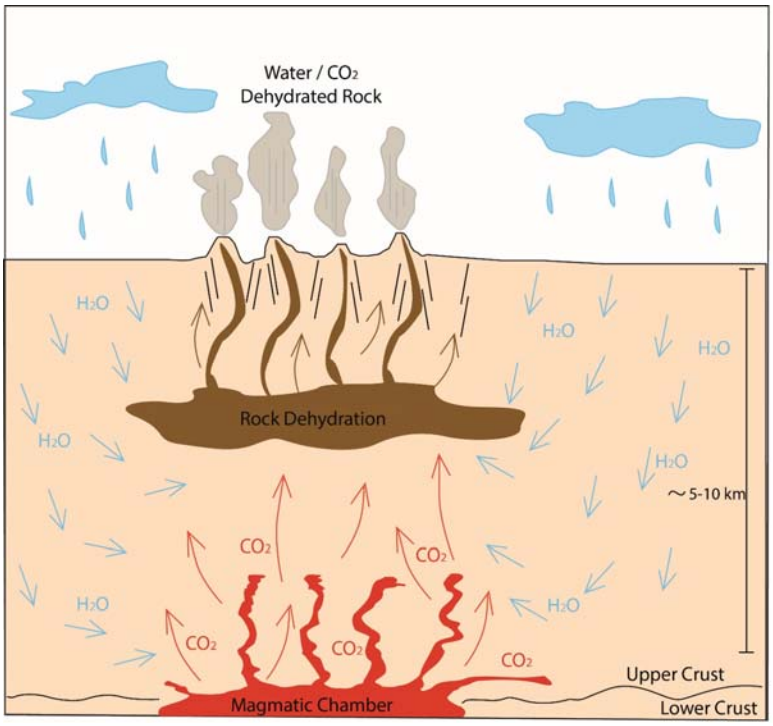

Figure 34: General conceptual model for a fluid pressure-controlled by dehydration in deep hydrothermal system or geothermal reservoir. Under conditions of increasing temperature and pressure, dehydration reactions begin for minerals (e.g. clay minerals).

The large-scale geology considers all the structural complexities and heterogeneity introduced into the model. We include a model for fluid generation from metamorphic reactions, in this case dehydration of hydrous clays, but can easily be adapted to other dehydration or decarbonization reactions that produce either water or CO_2. Metamorphic reactions result in fluid pressure changes between fluid phase and solid matrix phase, thus modifying porosity and permeability through time. Conceptually, reactions can also induce hydro-fractures (Connolly et al. 1997; Miller et. al., 2003) further enhancing the permeability network. Fluids move relative to the solid matrix in response to fluid pressure gradients.

3.2.2 Mathematic model

3.2.2.1 Large-scale hydrothermal systems or geothermal reservoirs

The physical behavior of large-scale hydrothermal systems or geothermal reservoirs entails coupled and nonlinear flow, mass and heat transport, and deformation in highly heterogeneous geological media. Simulating these complex systems relies on numerical solutions to coupled partial differential equations (PDEs) and complementary equations of state (EOS). For decades, natural and engineering sciences have seen a growth in computational power for numerical models that has eliminated or minimized various simplifications like physical processes, three-dimensional structures of conceptual models or time scale assumption. Hydrothermal systems

have immense scientific and engineering significance and have been studied though many disciplines to understand their geothermal potential (Bowen, 1979; Ingebritsen et Sanford, 1999; Ingebristen et al., 2010; Jeanne et al., 2014; Karyono et al., 2017; Lizarralde et al., 2010; Mazzini et al., 2012; Svensen et al. 2009; White, 1957). The physical understanding of these deep complex systems is challenging where data acquisition is difficult or sometime impossible and where numerical modelling is the only "*cheapest*" and "*fastest*" way, compared to deep borehole campaigns, to understand what occurs at depth.

3.2.2.2 Permeability and porosity model for clay dehydration reaction

Clay dehydration is a step function that involves large and sudden volume changes related to release of water with loss of water layers. The sudden volume changes and the release of water are possibly not restricted to the conditions of diagenesis, but also due to metamorphism with an increase of pressure and temperature. Thermodynamic data can be used to quantify these processes. Vidal and Dubacq (2009) showed that the volume and water content of a rock with a bulk composition corresponding to 50% Na-beidellite and 50% Na-saponite metamorphosed along a hypothetical P-T path from 25°C at 1 MPa up to 400°C and 500 MPa (Figure 35). These results show that the rock volume and the water-content variation associated to clay dehydration are far from negligible, and a similar evolution in natural conditions should have a strong impact on the rheology and hydrogeology of clay-rich rocks.

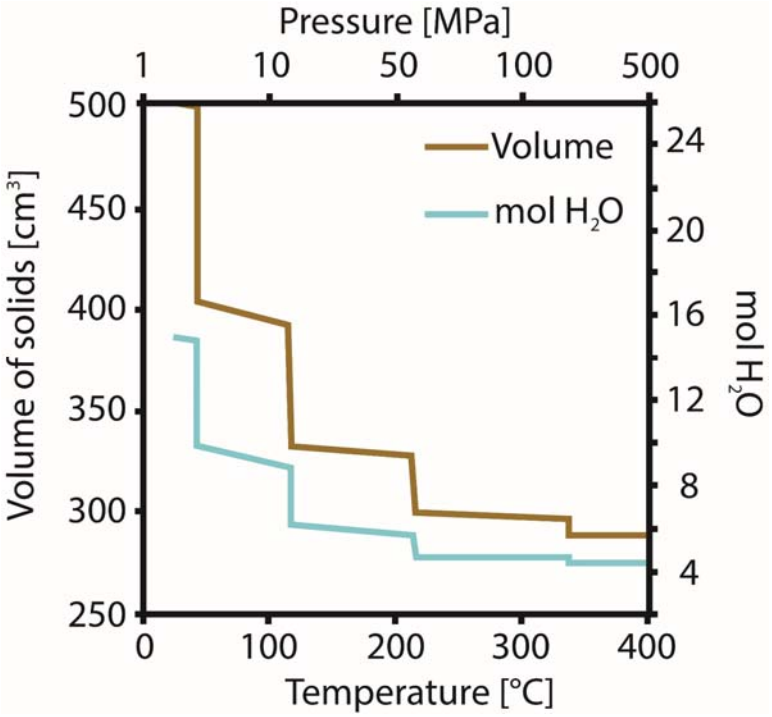

Figure 35: Evolution of the water content of clay (blue line) and total volume of solids (brown line) as a function of pressure and temperature (modified after, Vidal and Dubacq, 2009).

The measurements in Figure 35 are implemented into the model. These processes may control some over-pressure behavior at hot springs, geysers, or sedimentary-hosted hydrothermal systems (Mazzini et al., 2012).

3.2.3 Governing equations

Natural convection is the phenomenon of fluid flow driven by density variations in a fluid subject to body forces. Density is a function of pressure, temperature or solute concentration (in the case of a binary mixture) and its variation with respect to pressure is much smaller than that with respect to temperature or concentration. Hence, the convection can be driven either by temperature variations or by variations in solute concentration or by both. The solute or heat transport equation should be included in the model and should be extended as well to account for the solute effect on density. We formulate the governing transport equation in terms of fluid pressure, temperature or concentration. We assume that the system is in thermodynamic equilibrium, heat conduction is predominant in the rock and can be described by a bulk thermal conductivity and that capillary pressure effects are negligible (Bear, 1972). The subscripts *'s'* and *'f'* refer to the solid and the fluid phase.

3.2.3.1 Mass conservation

The basic equation describing filtration of a fluid though a porous and reacting medium is the continuity equation, which states that mass is conserved:

$$\frac{\partial(\rho_f\phi + \rho_s(1-\phi))}{\partial t} + \nabla\cdot\left(\rho_f\phi v_f + \rho_s(1-\phi)v_s\right) = 0 \tag{3.1}$$

where ϕ, ρ, v are the porosity (volume fraction of fluid), the densities and the velocities, respectively. The subscripts *f* and *s* denote the properties of the fluid and the solid, respectively.

Mass of nonvolatile species is conserved as well (Malvoisin et al., 2015):

$$\frac{\partial(\rho_s(1-X_s)(1-\phi))}{\partial t} + \nabla\cdot(\rho_s(1-X_s)(1-\phi)v_s) = 0 \tag{3.2}$$

3.2.3.2 Conservation of momentum

The conservation of fluid momentum is expressed by the Darcy's law:

$$\phi(v_f - v_s) = -\frac{k_0\phi^3}{\mu_f}(\nabla P_f - \rho_f g) \tag{3.3}$$

where the permeability is related to the porosity through the Kozeny-Carman relationship with an exponent 3 and a constant background permeability k_0 (Carmen, 1937, 1956; Kozeny, 1927). μ_f is the fluid viscosity, g is the gravitational constant and P_f is the fluid pressure

The fluid pressure considering the impact of rock dehydration on volume change (rock density ρ_s constant without viscous deformation) can be expressed as (Malvoisin et al., 2015):

$$\nabla\frac{k_0\phi^3}{\mu_f}\left(\nabla P_f - \rho_f g\right) = \beta_{eff}\frac{dP_f}{dt} + \left(1 - \frac{\rho_s}{\rho_f}\right)\cdot\frac{1-\phi}{1-X_s}\cdot\frac{dX_s}{dt} \tag{3.4}$$

where the amount of fluid into the solid X_s is calculated at the equilibrium with a fit of the data of Vidal and Dubacq (2009) giving X_s as a function of temperature in the smectite/illite system. β_f and β_s are the fluid and pore (crack) compressibility, The effective compressibility β_{eff} is described by:

$$\beta_{eff} = \beta_f + \frac{\beta_s}{1-\phi} \tag{3.5}$$

The porosity change due to fluids extraction from the rock by metamorphism can be expressed by (Malvoisin et al., 2015):

$$\frac{d\phi}{dt} = \beta_s \frac{dP_f}{dt} - \frac{(1-\phi)}{(1-X_s)} \cdot \frac{dX_s}{dt} \tag{3.6}$$

3.2.3.3 Energy conservation

The energy heat conservation over an elemental volume of medium for a solid and a fluid phase and considering thermal equilibrium so that $T = T_s = T_f$ (Nield et al. 2006):

$$\Big((1-\phi)\rho_s c_s + \phi\big(\rho_f c_f\big)\Big)\frac{\partial T}{\partial t} + \big(\rho_f c_f\big) v_f \cdot \nabla T = \nabla \cdot \Big(\big((1-\phi)\lambda_s + \phi\lambda_f\big)\nabla T\Big) + \Big((1-\phi)q_s + \emptyset q_f\Big) \tag{3.7}$$

where c is the specific heat of the phase, λ is the thermal conductivity and q is the heat production per unit volume. Equations 3.1 to 3.7 results in a highly nonlinear system of differential equations solved here by using a Finite Difference (FD) method (Patankar, 1980).

3.2.4 Numerical model

The theory is implemented into the simulator that solves the coupled equations (3.1) to (3.7) with a finite difference scheme (Figure 36).

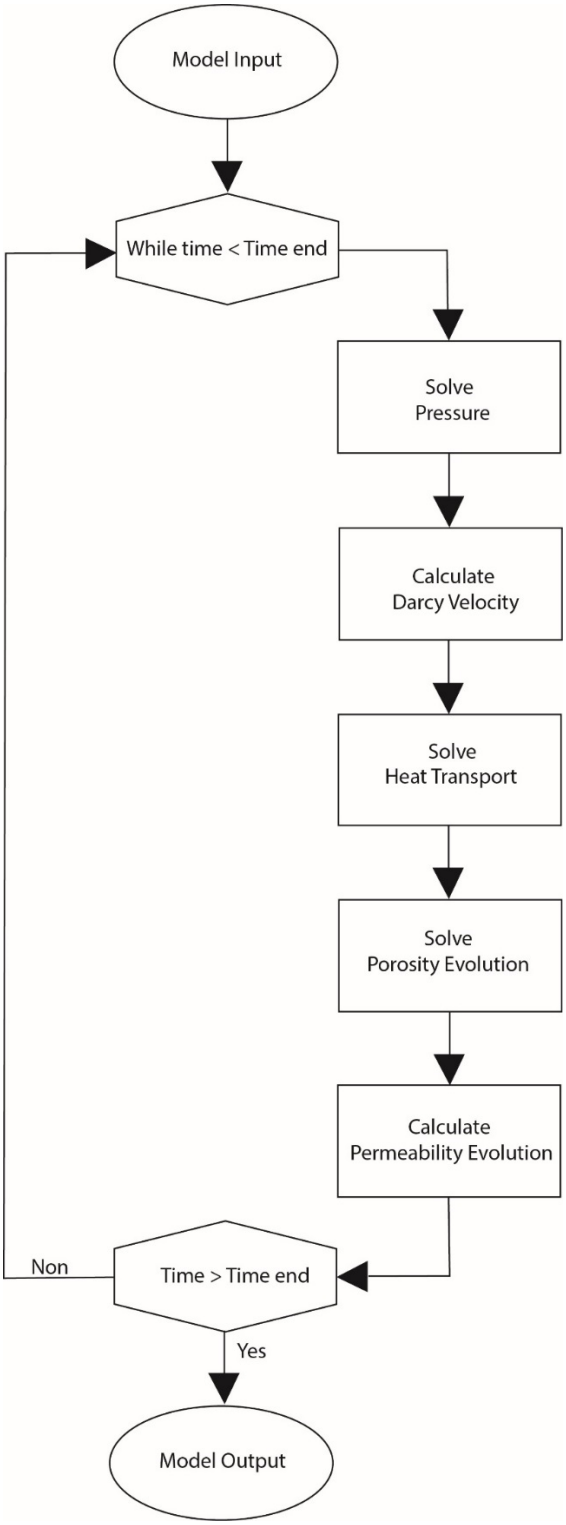

Figure 36 : A simplified flowchart of the implementation solution strategy for coupled flow and reactive transport problems including porosity and permeability evolution.

We use an explicit finite difference discretization on a staggered grid. The temperature equation is solved by applying an Eulerian upwind approach. The intensity of the numerical diffusion depends on the number of numerical steps performed and not on the absolute time of advection. Time steps are sufficiently small to satisfy the time limitation condition. The 3D geometry input is constructed using an automatic mesh generator that uses binary space partitioning (BSP) called *HULK* (Jansen et al., 2017), which can deal with any 3D complex geological structures. Here, we use a simplified 3D geological model that includes four geological layers and two fault/shear zones. The geometry is incorporated into *GEYSER* via *HULK* to be correctly redistributed on multiple GPUs and calculated the necessary multiphysics of interest.

A no-flow boundary condition is imposed on all boundaries except the upper surface, where a constant head (hydrostatic pore pressure) boundary condition is imposed. The surface temperature is set to 27°C. A geothermal gradient of 45°C/km is apply in the model. A magmatic intrusion is imposed at 6km depth on the bottom at 500°C as a source of deep fluids (water/CO_2) as proposed in the conceptual model (Figure 37).

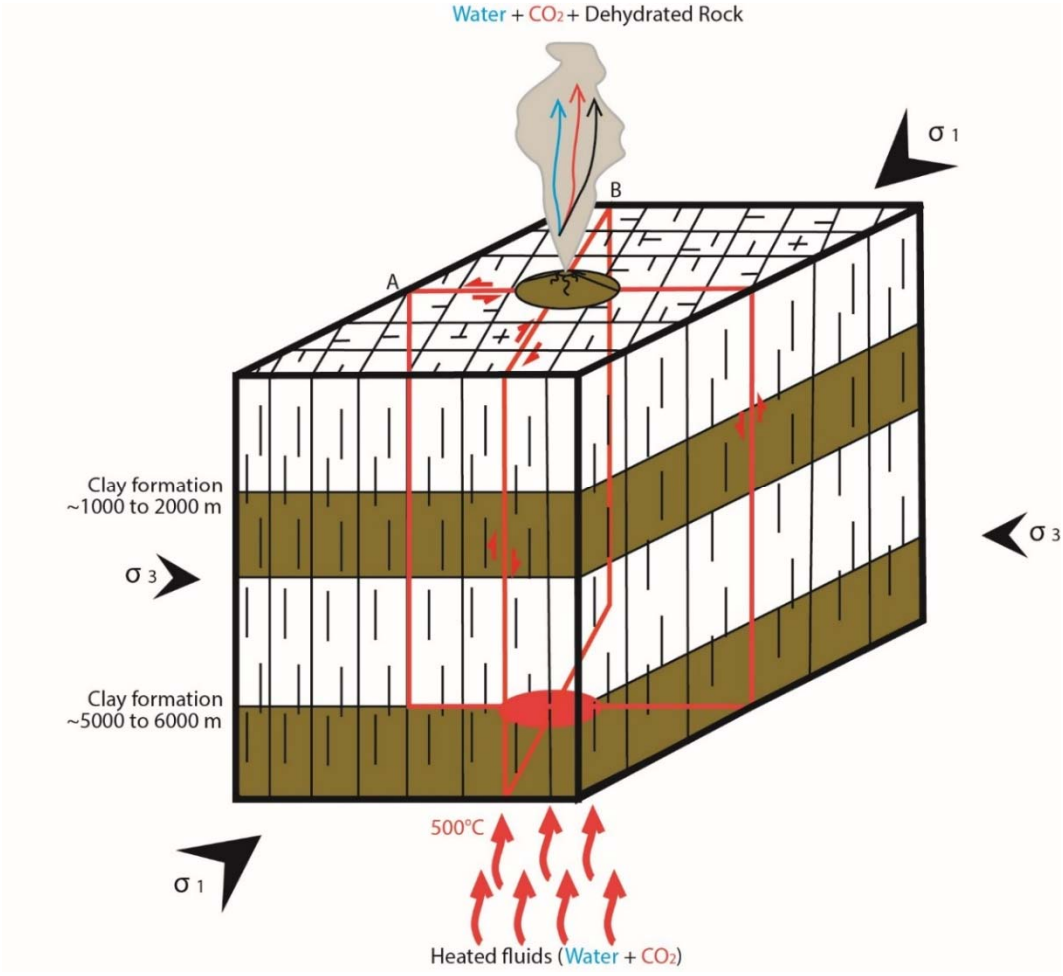

Figure 37: 3D structural fractured model considering two clay formations at different depths where dehydration may occur considering two fault/shear zone due to geodynamics constrains. A magmatic intrusion would be the process which will rise the pressure and temperature in the clay formations and induce fluids liberation at the surface due to fluid migration caused by porosity evolution in time, which would induce seismicity by permeability progression.

We assume that flow properties of supercritical CO_2 at the pressure and temperature conditions is ten times more compressible than water, but it is of the same order less viscous, resulting in similar flow properties. The numerical implementation of the density and the viscosity time dependence of the fluid is following the work of Sun et al. (2008). When the supercritical point is reached we assume Oberbeck-Boussinesq approximation (Joseph, 1976) for the fluids mass and heat transport. General parameters are shown in Table 4.

Table 4: Fully coupled modelling parameters

Symbol	Definition	Units
P_f	Fluid pressure	Pa
ρ_f	Density of fluid	$kg \cdot m^{-3}$
ρ_s	Density of solid	$kg \cdot m^{-3}$
v_f	Velocity of fluid	$m \cdot s^{-1}$
β_f	Compressibility of fluid	Pa^{-1}
β_s	Compressibility of solid	Pa^{-1}
β_{eff}	Effective Compressibility	Pa^{-1}
∅	Porosity	-
k	Permeability	m^2
X_s	Mass fraction of fluid in solid	wt %
T	Temperature	°C
c_f	Fluid specific heat	J/kg·K
c_s	Solid specific heat	J/kg·K
λ_f	Fluid thermal conductivity	W/ m·K
λ_s	Solid thermal conductivity	W/ m·K
q_f	Fluid heat production	$J/ m^3/ s$
q_s	Solid heat production	$J/ m^3/ s$
g	Gravity acceleration	$m^2 s^{-1}$

The post processing data analysis and visualization is done with an integral open-source tool related to high performance computation called Paraview (Henderson et al., 2004).

3.2.5 Solver

The solver uses a regular Cartesian 3D grid, and spatial derivatives are computed with the smallest possible finite difference stencil. This simple method is highly data-local, which allows for the construction of 3D solvers that achieve performances near hardware's peak (Krotkiewski and Dabrowski, 2013; Micikevicius, 2009; Omlin et al., 2017), and that scale close to ideally on thousands of GPUs (Omlin et al., 2015).

The solver features intra-GPU parallelization with CUDA and inter-GPU parallelization with CUDA-Aware MPI. Multiple performance optimizations were applied. The solver features in particular the on-the-fly computation of fields that do not depend on their own history, for example fluid or heat fluxes. These fields are never stored in main memory but instead recomputed whenever needed. Thus, we avoid the creation and access of many large arrays in the main memory. The access of main memory is the bottleneck of our stencil applications.

3.2.6 Performance evaluation

P_f,T, $\emptyset$ and X_s are the only fields storages that need to be stored in the main memory. As it is presented in equations (3.1) to (3.7), these unknowns have a time derivative dependence. Thus, to compute their state at time $+dt$, their previous state at time t must be read from the main memory. Additionally, the state at time $t + dt$ must be written back to main memory, once it is computed, in order to permit in the next iteration to compute the state at time $t + 2dt$. Fields P_f, T, $\emptyset$ and X_s must therefore be updated every iteration in the main memory, i.e. read and written. Ideally, each field must be read and written only once per iteration. The "*minimally required main memory access per iteration"* of our solver, which we call "*effective main memory access per iteration"* in the remainder, is:

$$A_{eff} = 2 * 4 * N * p * 10^{-9} ,$$

where N is the number of grid points, i.e. the number of floating point numbers per field, and p is the precision in bytes (2 memory accesses for each of the 4 fields of N grid points of precision p) with units in Gigabytes (GB).

A simple "*effective throughput metric"* (GB/s) is defined in a straightforward manner as:

$$T_{eff} = \frac{A_{eff}}{t_{it}} ,$$

where t_{it} is the execution time per iteration in seconds.

We always have:

$$T_{eff} \leq T_{peak} ,$$

T_{peak} is the maximum speed at which the hardware can copy data from main memory (i.e. access it).

The ratio T_{peak}/T_{eff} gives the absolute maximum possible speedup for an iteration that any improvements in the solver's numerical algorithm or the implementation may potentially bring. The amount of on-chip memory on current hardware does however not allow to obtain T_{eff} very close to T_{peak}. We report in the section results (cf. Figure 38 and Figure 39) the achieved T_{eff} of our solver on two different multi-GPU architectures in comparison to their T_{peak}.

A great property of T_{eff} is that it fully reflects runtime across changes of the numerical algorithm or its implementation. Only the implemented system of equations matters for the metric (A_{eff} is determined based on it). The effective throughput metric is therefore highly useful for both performance optimization and evaluation.

3.3 Results

3.3.1 Performance

Our test systems are the "Thor" cluster hosted by the Centre of Hydrogeology and Geothermics (CHYN), Laboratory of Geothermics and Geodynamics at the University of Neuchâtel (Neuchâtel, Switzerland) and the "Octopus" cluster hosted by the Faculty of Geosciences and Environment, Swiss Geocomputing Centre at the University of Lausanne (Lausanne, Switzerland). Thor consists of 4 compute nodes connected via a fast, low-latency InfiniBand interconnect. Each compute node contains 2 Intel Xeon E5-2650v3 (10 cores), at 2.3GHz, 2 NVIDIA Tesla K40c (2880 CUDA cores) and one Intel Xeon Phi coprocessor. Furthermore, each node is equipped with 500 GB Ram and a local 1TB SSD hard disk. It has an additional HDD storage capacity of 20 TB. Octopus consists of 34 compute nodes, each containing 4 NVIDIA GeForce GTX TITAN X GPUs (Maxwell GM200 architecture; 3072 CUDA cores), 2 Intel Xeon E5-2620v3 (6 cores) and 128 GB system memory. The nodes are interconnected with dual rail FDR InfiniBand. To sum up, Thor cumulates 8 GPUs (23'040 CUDA cores) and Octopus 128 GPUs (393'216 CUDA cores).

Our multi-GPU simulator *GEYSER* reaches a performance near to the hardware's peak and scales close to ideally on Thor (Figure 38) and Octopus (Figure 39).

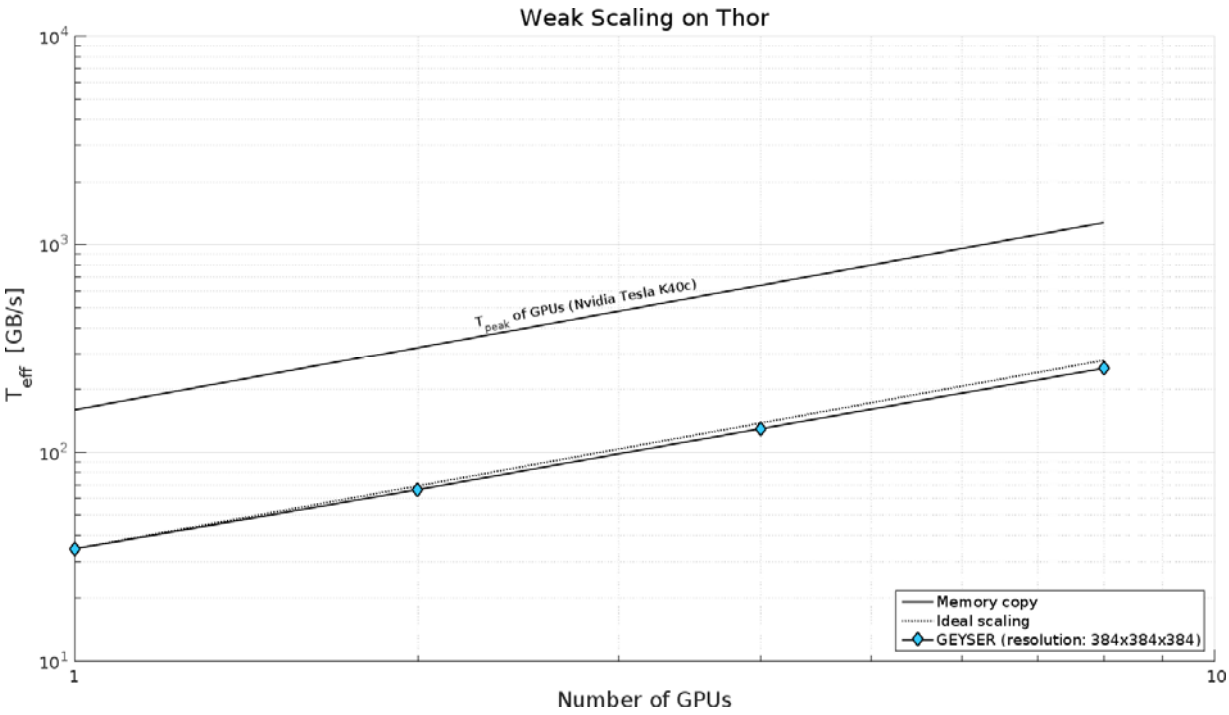

Figure 38: Performance and scaling of our simulator "GEYSER" allowing for the simulation on the Thor cluster. The effective memory throughput T_{eff} [GB/s] (left axis). T_{eff} is computed as the effective main memory access per iteration, i.e. the minimally required main memory access per iteration [GB], divided by the execution time per iteration t_{it} [s].

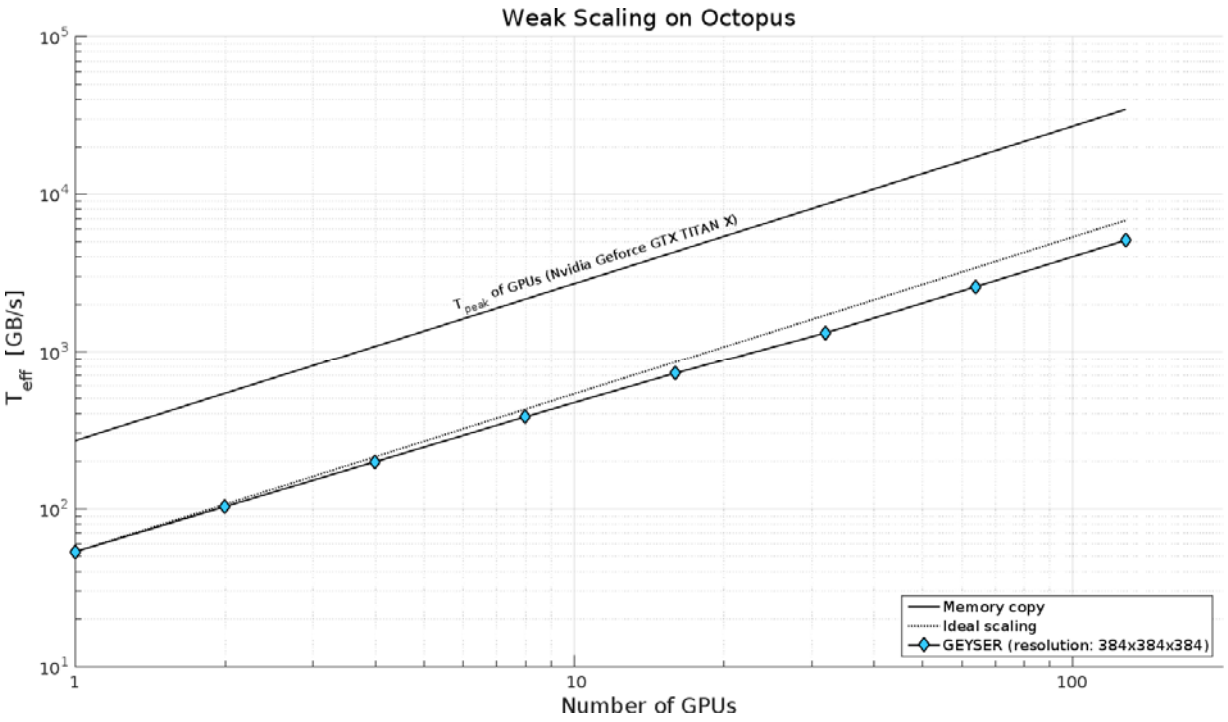

Figure 39: Performance and scaling of our simulator "GEYSER" allowing for the simulation on the Octopus cluster. The effective memory throughput T_{eff} [GB/s] (left axis). T_{eff} is computed as the effective main memory access per iteration, i.e. the minimally required main memory access per iteration [GB], divided by the execution time per iteration t_{it} [s].

3.3.2 Numerical simulations

We adopt a numerical model for porosity and permeability evolution as a highly non-linear function. The simple structural geology implemented in the simulator is shown on Figure 37. In our model we implemented four different layers crossing by two fault/shear zones for a simple large-scale hydrothermal system (Figure 40). We used this simple geometry because it can be relatively and easily correspond to general sediment-hosted hydrothermal systems (Mazzini et al. 2012), however any complex 3D geological model can be used via *HULK* (Jansen et al. 2017). We made an artificial "test case" but feasible initial condition of a 3D structural geology with a heterogeneous permeability distribution from 1 to $5 \cdot 10^{-17}$ m^2 for the geological layers and values from 1 to $5 \cdot 10^{-15}$ m^2 for the two fault/shear zones. The initial porosity distribution for the geological layers has a value of 0.1 considering a large-scale thermo-hydrodynamic system and the two fault/shear zones has a value of 0.15. The initial parameters used in the simulation are shown Table 5, they are representative of a sediment-hosted hydrothermal system in a volcanic arc where hot springs, mud volcanoes or geysers are common (Pollack, 1993; White, 1957).

Table 5: Initial parameters used for simulations presented on Figure 41 to Figure 45.

Parameters	Values
Surface temperature	27°C
Geothermal gradient	0.045°C/m
Rock density	2650 kg/m^3
Thermal conductivity (fluid)	0.6 W/m·K
Thermal conductivity (rock)	2.1 W/m·K
Specific heat capacity (fluid)	4190 J/kg·K
Specific heat capacity (rock)	1000 J/kg·K
Compressibility (fluid)	$1\cdot^{-10}$ Pa^{-1}
Compressibility (rock)	$1\cdot^{-9}$ Pa^{-1}

The numerical simulator resolves 3D time dependent evolution of pressure (P_f), temperature (T), porosity ($\emptyset$), permeability (k) and quantity of fluid (X_s) filing the porous media in large-scale hydrothermal systems or geothermal reservoirs. We present here results of high-resolution simulations for a special "test" case. All simulations were run on multi-GPU on Thor cluster (8 GPUs) or on multi-GPU on Octopus cluster (128 GPUs). On Figure 40, we show the 3D simple geological grid transferred on multi-GPU. We performed a series of 3D simulations with this structural geology for fluid density driven by pressure, temperature, water content, porosity and permeability evolution.

Figure 41 to Figure 45 show the state of the system for different time during the simulation generated by fluids dehydration. Figure 41 show the pressure evolution in time for different time steps through the two fault/shear zones. Figure 42 show the temperature evolution from the heated fluids coming from 6km depth through the two fault/shear zones. The thermal structure with higher permeability in the fault/shear zones of the system undergoes significant changes from incipient to the simulation. The temperature reached ~350°C, through the two fault/shear zones, at 3km depth after 50 years of simulation. Considering high pressure and temperature Figure 43 show the water liberation through the two clay layers. The consequence on the porosity and the permeability is shown on Figure 44 and Figure 45 with an increasing change of the rock properties in the two different clay layer depth through the two fault/shear zones.

The structural geology considering two fault/shear zones and the multiphysics involved in such system were successfully implemented and resolved in 3D with our multi-GPU tool *GEYSER* reaching a performance close to hardware limit (Figure 38 and Figure 39).

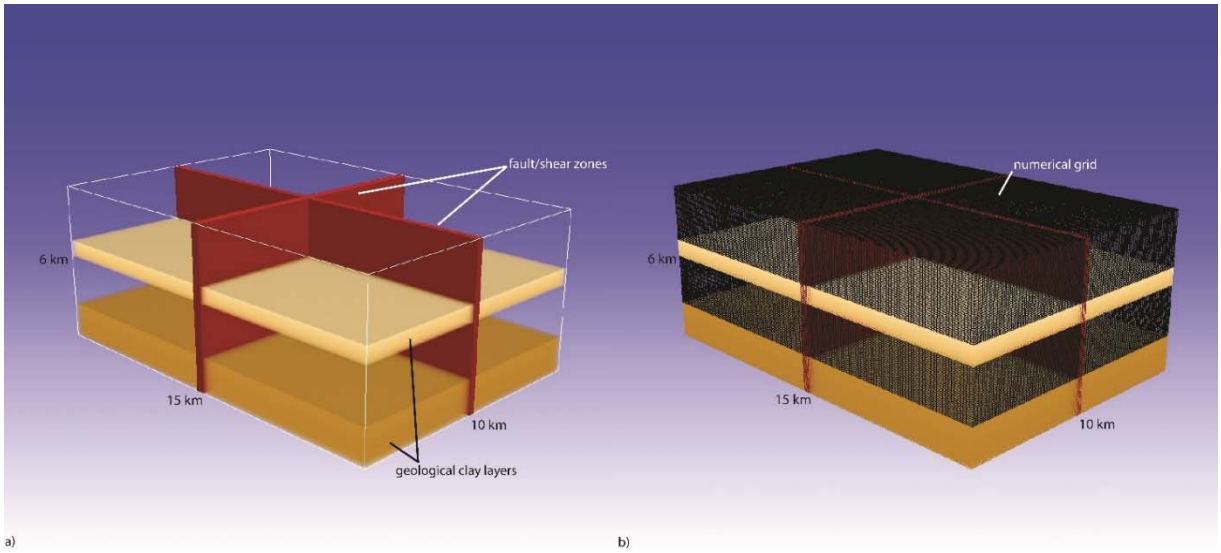

Figure 40: 3D structural volume information a) from our grid generator b) implemented for multi-GPU distribution on GEYSER.

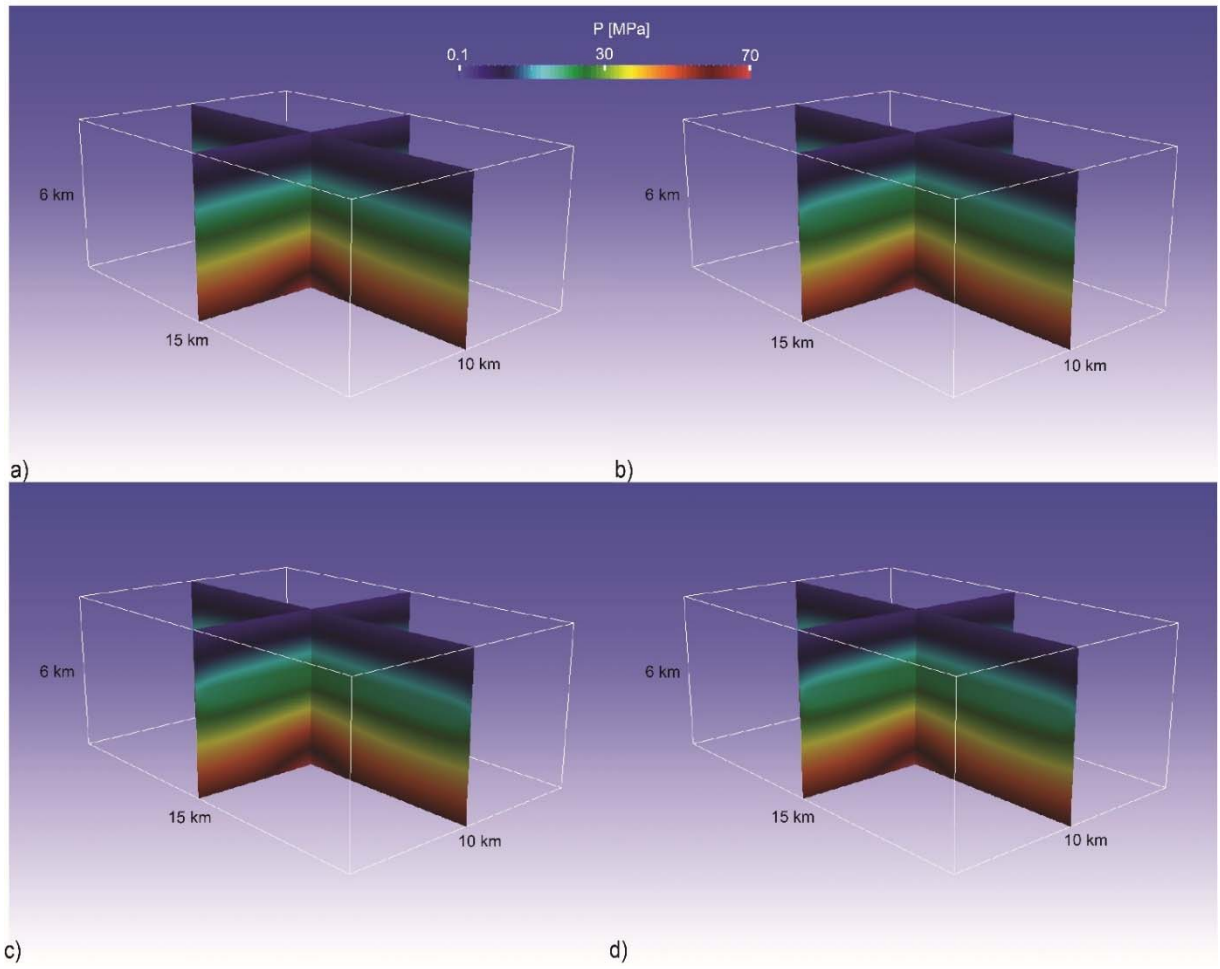

Figure 41: Evolution of the pressure field over different time a) 5 years, b) 25 years, c) 50 years and d) 100 years through the two fault/shear zones.

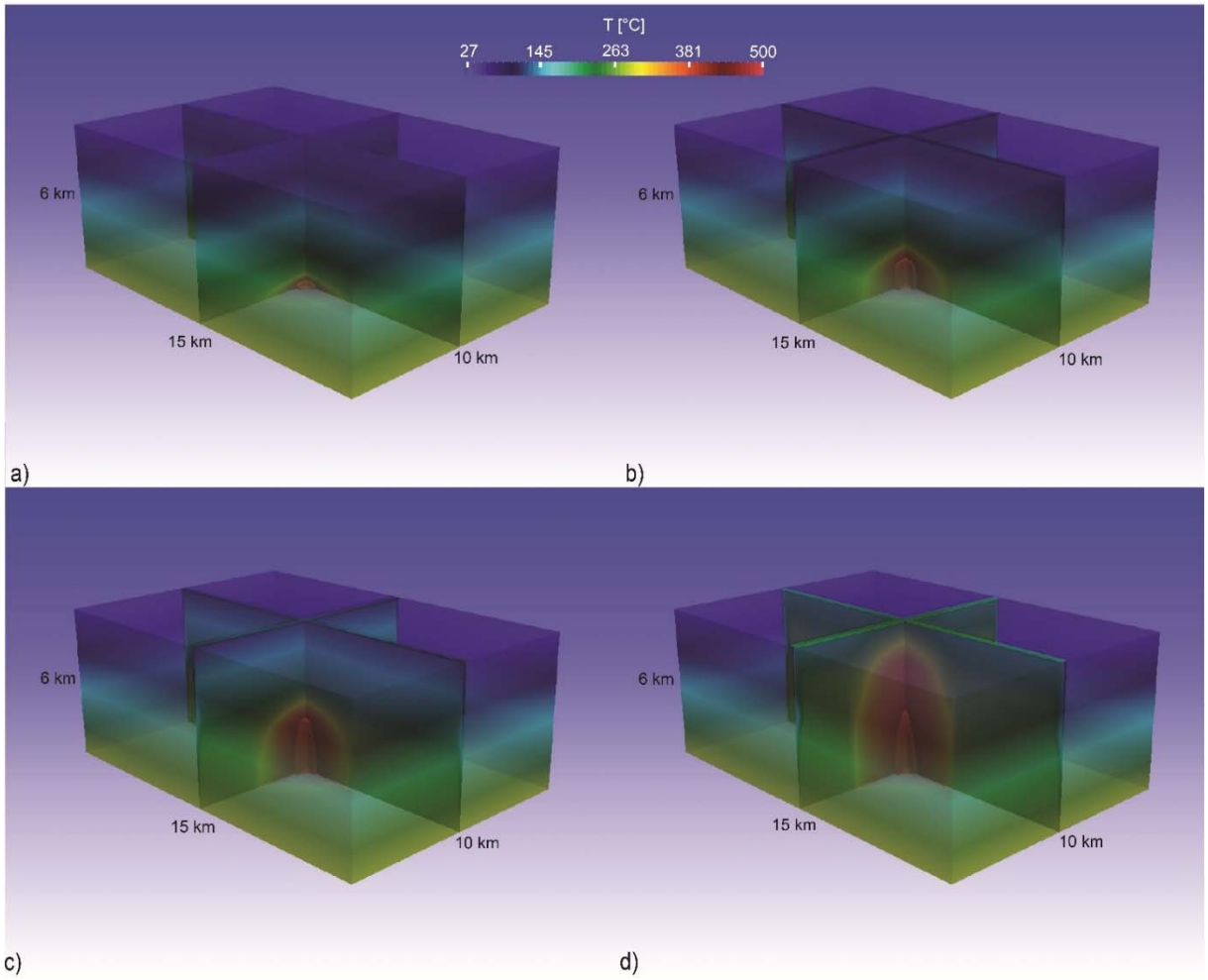

Figure 42: Evolution of the temperature field over different time a) 5 years, b) 25 years, c) 50 years and d) 100 years through the four different geological layers and two fault/shear zones. The temperature field colour opacity over the entire 3D system was reduce to highlight the temperature evolution in the two fault/shear zones.

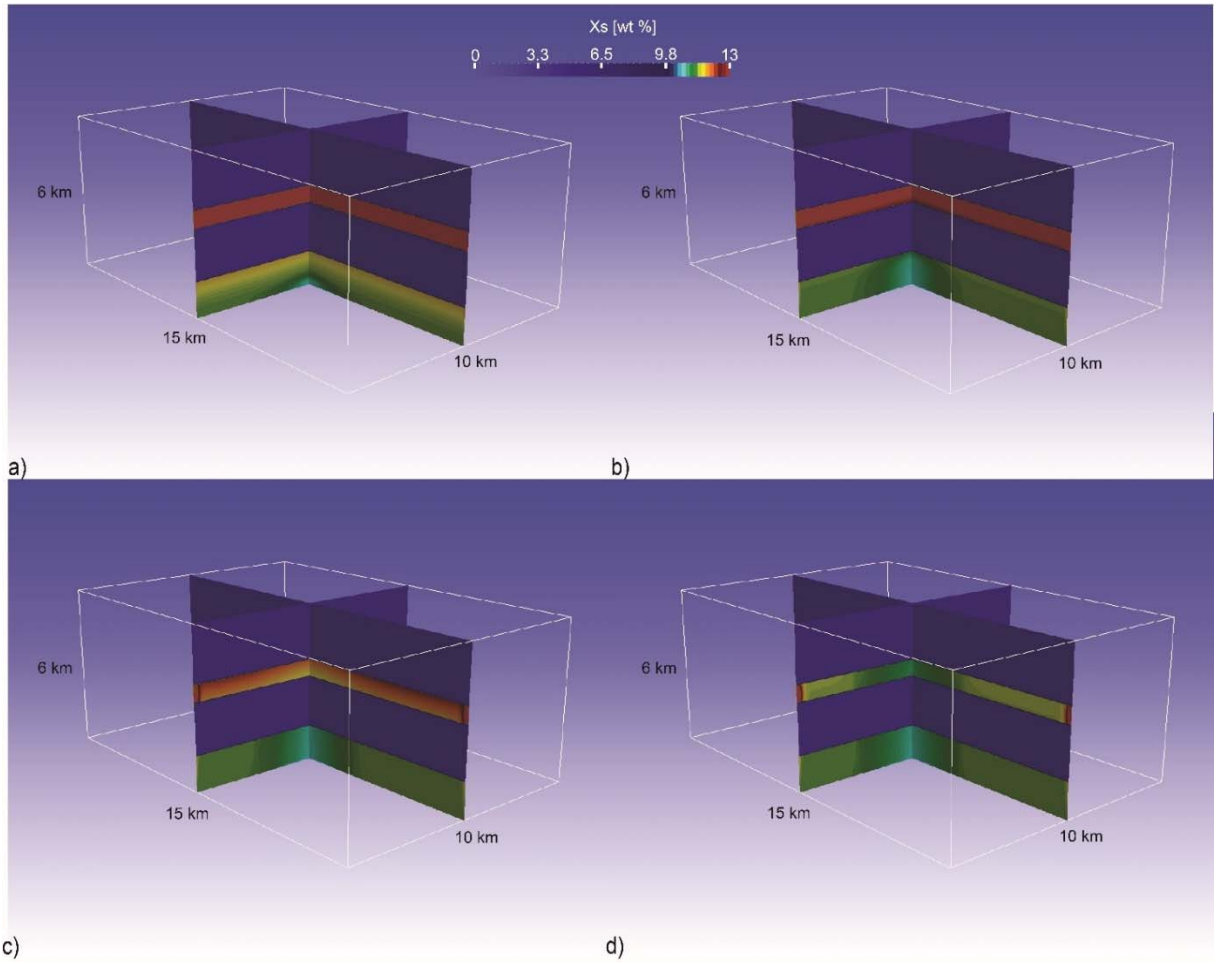

Figure 43: Evolution of the mass water contented in the clay layers over different time a) 5 years, b) 25 years, c) 50 years and d) 100 years through the two fault/shear zones.

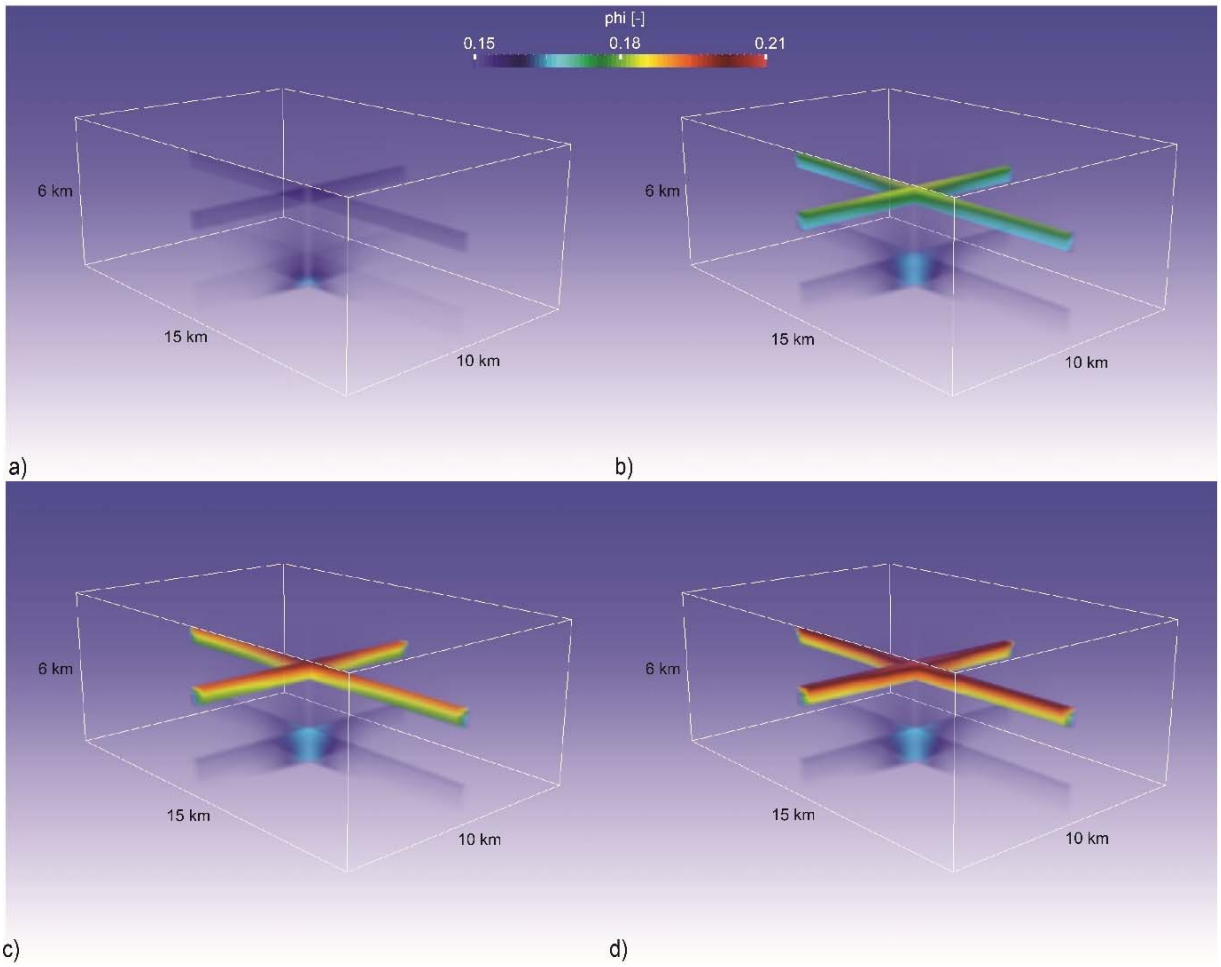

Figure 44: Evolution of the porosity in the clay layers over different time a) 5 years, b) 25 years, c) 50 years and d) 100 years through the two fault/shear zones.

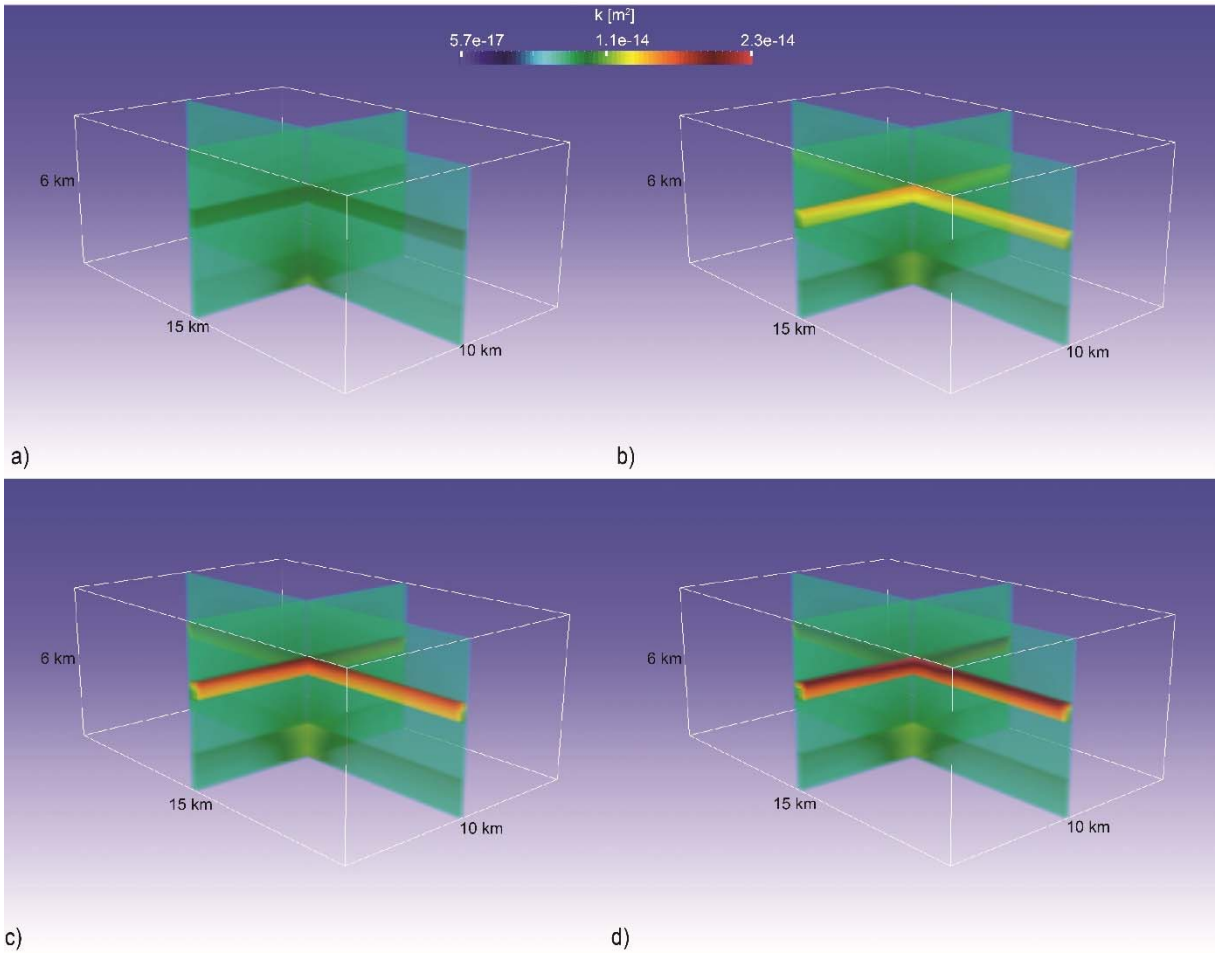

Figure 45: Evolution of the permeability in the clay layers over different time a) 5 years, b) 25 years, c) 50 years and d) 100 years through the two fault/shear zones.

With results presented, we can observe that the evolution of the pressure and the temperature (Figure 41 and Figure 42) has an important effect on the dehydration of the clay rock layer (Figure 43) as observed in laboratory by Vidal and Dubacq (2009). The dehydration effect is clearly impacting on the two different depth of the 3D model (Figure 44 and Figure 45). The effect is more important, as expected, in the fault/shear zones (considered 100x more permeable than the rest of the model), but the liberation of water content in the clay rock is liberated at both levels (Figure 43). As we can see on Figure 44, the porosity evolution is more important in the lowest layer (~1000 to 2000m), which demonstrate that more fluids is liberated and can reach the surface from this specific geological layer. The initial natural condition (hydrostatic pressure and geothermal gradient) has a major impact on the dehydration of the entire system. But after a certain time the fluids coming from the deepest layer (~5000 to 6000m) will also reach the surface. We observed that the permeability of the clays is what drives the fluids to the surface is clearly flowing through the channel which combine the geological layers together. The dehydration of the clay can have important effect on induced seismicity. As it is shown on Figure 45 the permeability is increasing through time slowly put on a long time period the liberation of water at different level would liberate a quantity of fluids not negligible and the fault/shear zones would be a perfect path for driving these quantities of fluids to the surface and cause many different kind of natural hydrothermal eruptions. This simple conceptual model is physically and numerically presented here with a powerful multi-GPU tool, but would be of interest to apply this model to a real world case study.

3.4 Discussion and conclusions

We developed and implemented a fast and efficient methodology using high resolution technology to simulate physical processes for large-scale hydrothermal system or geothermal reservoirs. The goal of this work was to present a conceptual model for rock (e.g. clay) dehydration in hydrothermal environment and use a multi-GPU programming cluster to model the space and time evolution in 3D in order to handle the complexity of deep hydrothermal systems or geothermal reservoirs. Our conceptual model can easily explain complex physical behaviors of such hydrogeological systems. Our algorithm *GEYSER* shows that it simulates such complexity at high resolution very quickly. The computational power of *GEYSER* almost reaches the peak performance of the multi-GPU used. It can be run on a single work station, a cluster or even a supercomputer.

The simulations showed that the combination of high pressure fluids with high temperature can substantially increase porosity and permeability evolution over time when water is liberated from clay rocks due to pressure and temperature increases. Our state-of-the-art tool correctly simulate the physics of fluid flow and heat transport through complex geological media considering liberation of water, based on thermodynamic calculation. Rock dehydration can liberate a no-negligible amount of fluids and may induce seismicity at different hydrogeological scales.

Although we assumed a single phase fluid (water and CO_2) and no rock density changes, it would be interesting to observe how the simulator would perform by implementing multicomponent, multiphase changes, stress dependency or poro-elasticity processes. The strong non-linearity of these processes would probably influence the performances.

We should also add an in-situ visualization with Paraview (Ayachit et al. 2015) or VisIt (VisItusers). In-situ visualization software enables connecting directly to a running simulation and allows the visualization of intermediate or final simulation results continually, direcly accessing the data in the memory. Testing *GEYSER* on the supercomputer “Pitz Daint” (5000 GPUs) at the Swiss National Supercomputing Centre would be of interest to get the highest performance from our simulator and the highest resolution of future simulations.

To conclude *GEYSER* is a powerful tool for simulating large-scale hydrothermal system or geothermal reservoirs with high resolution. Our future goal is to use it for a real world case study involving a large-scale natural hydrothermal system and add a real case geological structure of such systems and comparing it with data field measurement. This approach would be important to predict any driven fluids to surface acting like hot springs, mud volcanoes or geyser eruptions. Using this simple conceptual model and using our High Performance Computing (HPC) tool would be very beneficial in forecasting any potential evolution of hydrothermal eruptions or predicting long term geothermal reservoir production.

4. Numerical modelling of the Lusi hydrothermal system: Initial results and future challenges

"Lusi is the most powerful and interesting disaster I have ever seen!
Since the beginning, for me, Lusi has been a geyser system."

Trying to understand my natural conceptual perception of Lusi.

This article is published in Marine and Petroleum Geology Journal, February 2018
Reza Sohrabi, Gunnar Jansen, Benjamin Malvoisin, Adriano Mazzini, Stephen A. Miller

4.1 Introduction

4.1.1 Hydrothermal system

Geysers and hydrothermal eruptions (e.g. hot springs) show a wide range of eruptive styles that are driven by large-scale complex geodynamic processes and groundwater recharge. The convection of fluids in the subsurface plays a leading role in many geological and hydrogeological processes. These deep hydrothermal systems can be of significant importance for geo-resources such as geothermal energy.

Since May 2006, the Lusi mud eruption in East Java, Indonesia, (one of the largest natural disasters in East Java (Van Noorden, 2006)) behaves as a geyser and has led to wide interest across the scientific community (Karyono et al. 2017; Lupi et al., 2013; Mazzini et al., 2007; Mazzini et al. 2012; Zoporowski and Miller, 2009). The onset of the Lusi eruption has previously been described to be linked to petroleum drilling in the vicinity of Lusi (Davies et al., 2007, 2008, 2010; Tingay et al., 2008, 2015) as well as have been triggered by a 6.3 M earthquake that struck the southern part of Java (southwest of Yogyakarta, ~250 km from Lusi) about two days before the eruption (Lupi et al., 2013). Lusi has continuously discharged mud-breccia, liquid water, and released to the atmosphere aqueous vapor containing a small percentage of CH_4 and primarily CO_2 (Mazzini et al., 2012; Vanderkluysem et al., 2014). Lusi has been described as a newborn, tectonic scale, sediment-hosted hydrothermal system linked to the SW adjacent Arjuno-Welirang volcanic complex through the Watukosek fault system (Istadi et al., 2012; Mazzini et al., 2009, 2012, 2018). Numerical modelling of such complex systems is a challenge because it must take into account a variety of coupled thermal, hydraulic, mechanical and chemical (THMC) processes. To provide first estimates of the behaviour of this deep hydrothermal complex, geological structures of the sedimentary basin in East Java must be constrained, and the fluid dynamics, mechanics and the heat transport need to be investigated in three dimensions. Modelling these processes numerically at adequate resolution and reasonable computation times requires a suite of tools (cf. Figure 46) that we are developing and/or utilizing to investigate the Lusi system.

Figure 46: Ideal workflow for 3D numerical modelling based on AMR algorithm, C++ libraries and MPI architecture CPU/GPU.

In this paper, we discuss the geological background of the Lusi system and its context within a sediment - hosted fractured hydrothermal system. We then construct a geological model based on data gathered from previous studies prior to the initial eruption including seismic lines and borehole information. From the geological model we construct a numerical grid using our mesh generator "HULK" (Jansen et al., 2017) that provides the numerical domain. The governing equations relevant to this system are discussed, and we present simulation results for a two-

phase system (Water/CO_2) coupled to a simplified model of mechanics to help understand the birth of Lusi from a hydrogeological perspective. We conclude with an outlook for future simulations using additional geophysical observations, and discuss the requirements for implanting our algorithms on High Performance Computing (HPC) platforms.

4.1.2 Geological background

Lusi is situated in an inverted back arc basin in East Java, where a large number of grabens and half- grabens formed during rifting stages of the Eocene (56 to 36 Ma) to Early Oligocene (35 to 30 Ma). Following a period of quiescence, a phase of local deformation and active volcanism began in the late Miocene (7 Ma) (Doust & Noble, 2008). Rapid sedimentation produced a thick sedimentary package, including over-pressured clay layers at depth. The regional scale conceptual model (Figure 47) includes a heat source from a magma chamber and a proposed dike intrusion (Mazzini et al., 2012), and an overall hydrogeological model with fluid flow driven by hydraulic gradients provided by the Arjuno-Welirang volcanic complex, situated between 10 km for the Penanggungan to 20 km considering the rest of the complex, SW of Lusi. The geological stratigraphy of the region (Figure 47) described in Mazzini et al., 2007; Mazzini et al., 2012 and Samankassou et al., 2018 is given by the Pucangan Formation (yellow) , the Bluish Grey clay (brown) from the Upper Kalibeng Formation, the Volcanoclastics (red) from the Upper Kalibeng Formation, the Kujung/Prupuh/Tuban Formations (blue) and the Ngimgbang Formation (green).

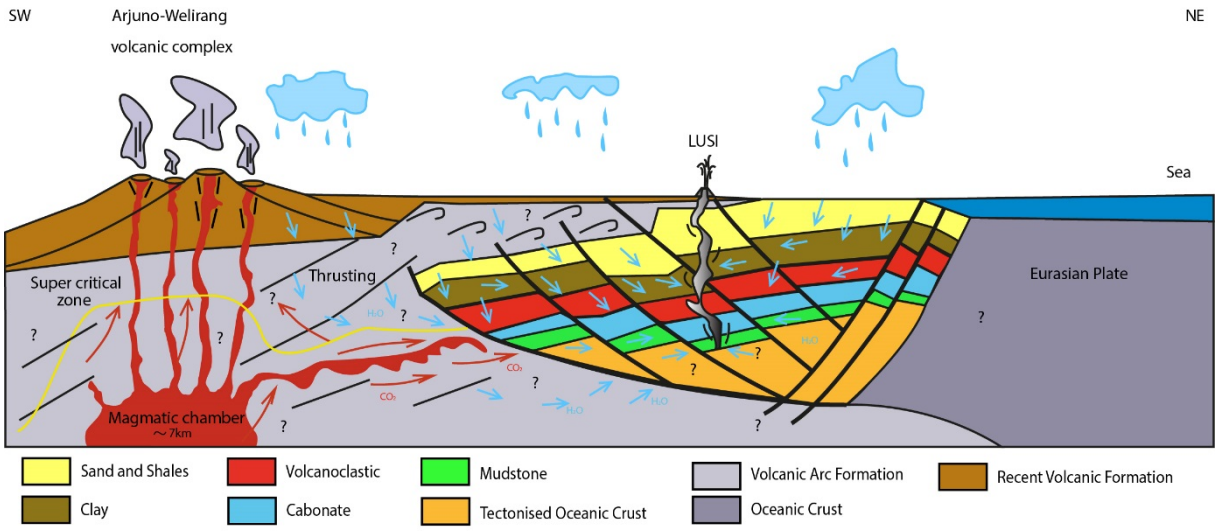

Figure 47: Conceptual hydrogeological framework of East Java shown as a SW-NE cross-section of the sedimentary basin of where Lusi occurred.

4.1.3 Conceptual model

From previous studies (Istadi et al., 2012; Kusumastuti et al., 2002), we combine the geological history of the region with geochemical analyses (Inguaggiato et al., 2018; Malvoisin et al., 2016; Mazzini et al., 2012; Mazzini et al., 2018; Sciarra et al., 2018; Vanderkluisen et al., 2014;) to establish a conceptual and numerical framework to understand in 3D the Lusi geyser system. The dynamics of this system are driven by groundwater flow and CO_2, typical of geyser systems. Understanding the fate of the fluids requires determining their origin and temperature at depth, and the underlying hydrogeology. One of the Lusi mud breccia sources are the bluish grey clays of the Upper Kalibeng Formation present between from 900 - 1830 m depth (Mazzini et al., 2007), while isotopic compositions of hydrocarbons and CO_2 contained in the boiling fluids suggest an additional deeper origin of the fluids controlled by the Watukosek strike slip system and the Siring antithetic faults system (Mazzini et al., 2012, 2017). This additional source is confirmed by the presence of two fluid sources determined from surface deformation (Shirazaei et al., 2015). The stratigraphic units, the temperature and the composition of the fluid in the two sources are well-constrained (Mazzini et al., 2018).

Analysis of major ions shows that the Lusi water is enriched in most elements, particularly Na, Cl and Li with low Mg and K. The ^{3}H results show meteoric water age prior to the 1950's, and ^{14}C results give ages around 16'000 years, indicating mixing of deep fluids and meteoric water. Stable isotopes used to trace the source of water molecules indicate illitization of the clay present in the Upper Kalibeng Formation, and the mixing of seawater and water of volcanic origin. Lithium enrichment suggests a contribution from the mixing of hydrothermal water and seawater. Comparison of various parameters indicates that the erupted Lusi water is a mix of fluids originating from different levels and formations comprising meteoric fluids, dehydration fluids, seawater entrapped fluids, and hydrothermal fluids (Mazzini et al., 2018).

The Kujung and Prupuh Formations, at a depth of between ~ 3 to 4 km (Moscariello et al., 2018), is likely highly permeable and could conduct a large amount of water necessary for the large outflow observed at the surface. The Arjuno-Welirang volcanic complex, situated between 10 km to 20 km SW of Lusi, and the entire sedimentary basin of East of Java could offer the hydraulic gradient necessary to drive the erupted deep fluids (Figure 48).

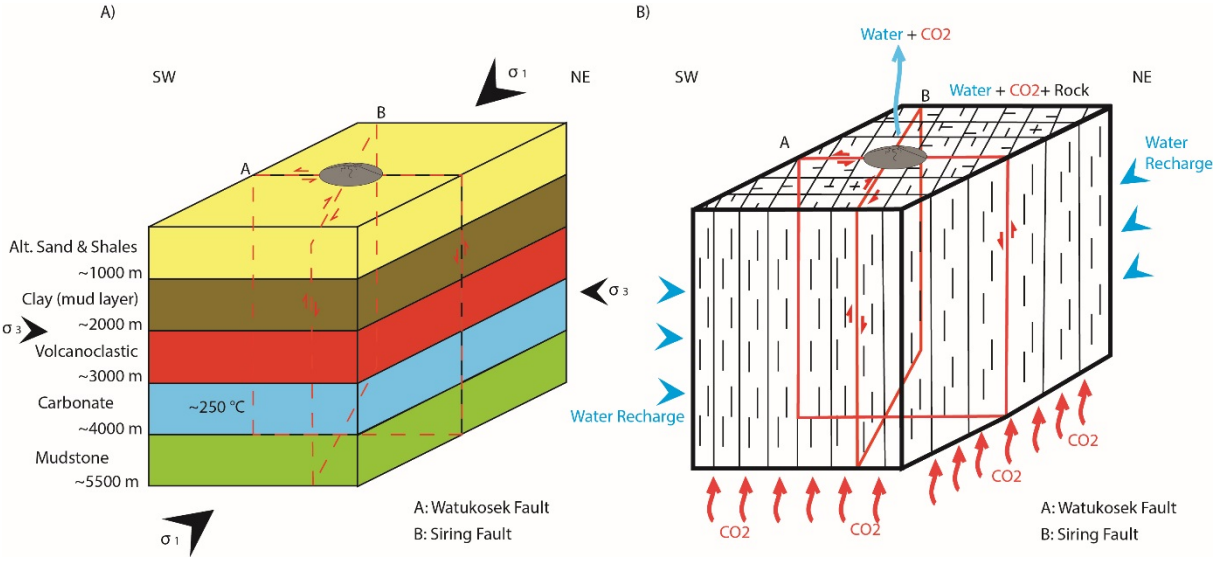

Figure 48: A) 3D structural conceptual model considering five main hydrostructures and two main major shear zone on the Lusi site due to the geodynamic constrains. B) 3D fluid dynamic conceptual model into fractured porous media considering two fluids (Water & CO_2) filling the entire Lusi system.

4.2 Methods

4.2.1 Geological modelling

The methods used to construct the geological model have been described in detail elsewhere (Lajaunie et al., 1997; Calagno et al., 2008). A simplified stratigraphy was modelled to capture only the main hydrodynamic structures for large-scale modelling. Five main units were previously described in the literature for the basin, and we identified these units in the seismic data and use them as basis for the geological model (Figure 49). These include the altered sand, shales and clay from the Pucangan Formation (yellow), the Bluish Grey clay from the Upper Kalibeng Formation (brown), the Volcanoclastics from the Upper Kalibeng Formation (red), the carbonates from the Kujung/Prupuh/Tuban Formations (blue), and the mudstones from the Ngimgbang Formation (green). We also included in the model two major faults or shear zones (red) crossing Lusi, the Watukosek strike slip system and the Siring antithetic faults system (Istatdi et al., 2012). The 3D model was constructed using several seismic lines and the information provided by the boreholes Porong-1 and BJP-1. The role of these five main geological layers and the two major shear zones / faults have a significant impact on the rising of the fluids (water/brine and CO_2) for the entire system.

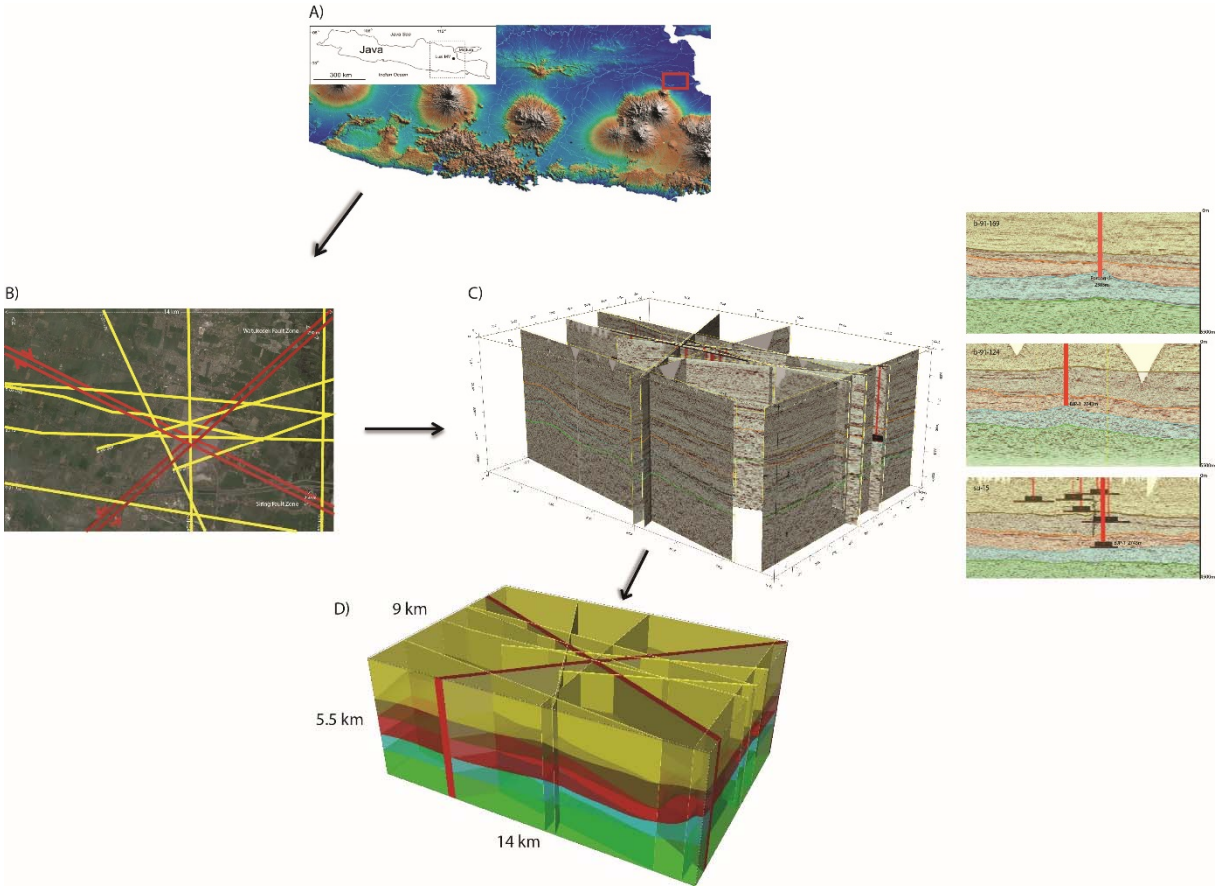

Figure 49: 3D geological model workflow for Lusi, A) Constrain the geology of the Lusi site in Indonesia, East Java ,B) Prepare and interpret the data, C) Import seismic lines and the borehole information into the model, and D) Create a realistic 3D geological model based on limited data.

At the Lusi site, where data acquisition is a major challenge, numerical simulation is a powerful tool for testing competing hypotheses. We attempt to understand this complex system at the large scale considering some of the coupled physical processes. Recognising that, at this stage, including all likely processes operating would not be possible, we simplify the problem from computational viewpoint. Using several hydro/geological properties constrained for Lusi up to 3-3.5 km depth (Tanikawa et al., 2010), we also consider a larger scale up to 5.5 km from interpreting seismic lines. Fine details of the different sediment layers may have an influence locally, but our aim is to constrain the large-scale hydrogeology.

4.2.2 Adaptive Mesh Refinment (AMR) hexahedra numerical grid using HULK

We adapted the geological model to a numerical grid by utilizing a recently developed, fully automatic octree refinement 3D mesh generator using binary space partitioning (BSP), called HULK (Jansen et al., 2017). We exported the geological model using the StereoLithography (STL) format, which can be found in many export options of almost any geological modellers

or computer-aided design (CAD). The HULK algorithm is an efficient technique to reduce the number of grid cells while also minimizing the information lost between the different sedimentary layers and tectonic structures. A comparison of Figure 49 and Figure 50 show that the geological information remains intact using this technique. Modelling fluid flow in the volcanic sedimentary basin hosting Lusi requires estimating properties and parameters for the rock/porous media of each of the main sedimentary or tectonic structures.

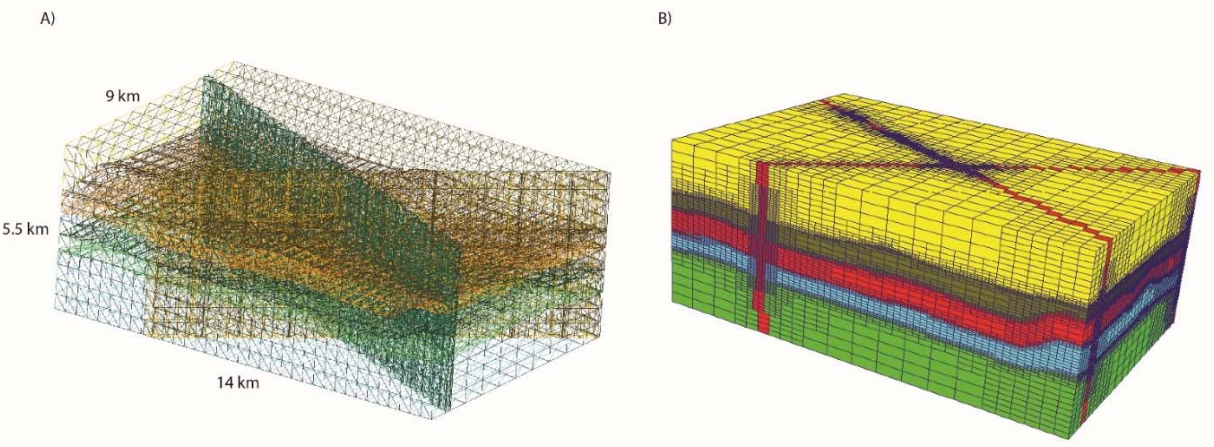

Figure 50: Transfering the 3D structural volume information from a geological modeller to a numerical grid for FD, FV or FE method calculation. A) Creating a 3D "STL" STereLithography volume file. B) Generate a 3D hexahedral mesh using HULK.

4.2.3 Fluid dynamics of a CO_2 - rich aqueous fluid for a geyser system

A typical rock mass within the context of moderate to high enthalpy systems includes solid porous media, brine, and supercritical CO_2. The governing equations include contributions of the individual constituents and their interactions. Multiphase/multicomponent flow in porous media involves many thermodynamic states and variables, and is employed in many different fields. In petroleum engineering, for example, the terms wetting and non-wetting phases are used to describe the water phase and the oil or gas phases, respectively. Here, the phases are named based on the main constituent.

The number of phases in the fluid is not known a priori. Therefore, we used thermodynamic calculations to determine the nature and composition of the fluid expelled at Lusi. Measurements of fluid composition at the crater reveal that the fluid expelled at Lusi is a 3% CO_2 – 97% H_2O (molar) mixture with a salinity of 0.4 g/L (Mazzini et al., 2012, 2018; Vanderkluysem et al., 2014). Therefore, we used the Equation of State from Duan & Sun, 2003 for a CO_2-bearing aqueous NaCl solution to predict the state and the number of phases in the fluid at Lusi (Figure 6) assuming hydrostatic fluid pressure. As expected for the high temperature of the fluid measured at the eruption site (e.g ~100°C, Mazzini et al., 2018), the fluid is a H_2O-CO_2 gaseous mixture at the surface. However, for the temperature gradient measured by Malvoisin et al., 2016 , the fluid is found to rapidly unmix in a two phases mixture in the first meters below the eruption site due an increse in pressure. This mixture is composed of a CO_2-rich gas and a H_2O-rich fluid at least up to a depth of 3'000 meters.

For lower temperature gradients or higher CO_2 content in the fluid, the two-phase fluid may extend to deeper levels (Figure 51). At depths below approximately 5'000 meters, the CO_2 saturation curve is reached and the fluid becomes a one phase H_2O-CO_2 liquid mixture.

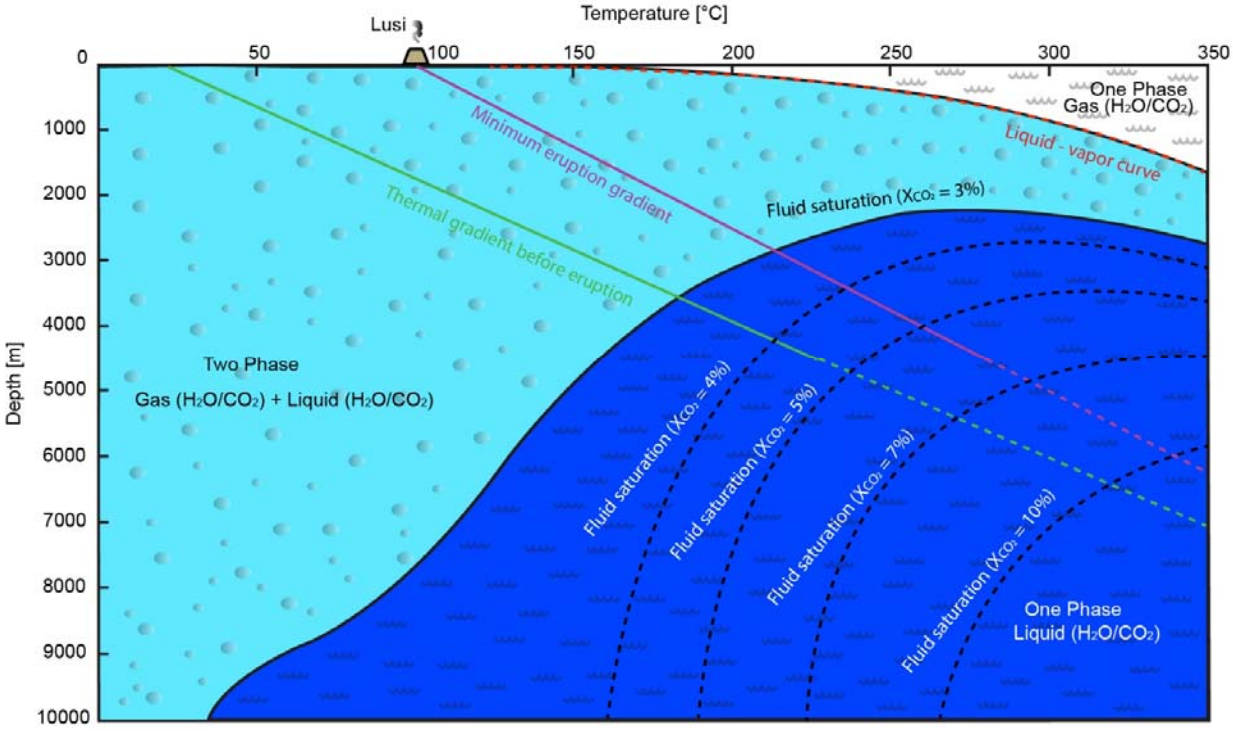

Figure 51: Temperature versus depth diagram, assuming a hydrostatic pressure gradient. The light blue field represents conditions at which 3% CO_2 - 97% H_2O (molar) fluid will unimix to form a water-dominant liquid and a CO_2- rich gaz phase (Duan et al., 1992).

Based on these thermodynamic calculations, the model consist of a two phase fluid with a liquid water phase and a CO_2 gaseous phase. In detail, the water phase is a mixture of brine and dissolved CO_2 whereas the CO_2 phase is a mixture of supercritical CO_2 and water vapor. The term water phase is used to indicate brine water with dissolved CO_2, and the term CO_2 phase to indicate a supercritical CO_2 phase with dissolved water vapor. A component represents an independent chemical element, molecular substance or a mixture of different substances.
If no chemical reactions occur, the components are independent of each other so the mass of each individual component is conserved by the mass balance equation. Components of a phase are described by the mass fraction of the component, X_α^k, where k is a component within the α phase. For a volcanic hydrothermal system, four mass fractions are involved, with X_w^{CO2} and X_w^w representing the mass of the CO_2 component in the water phase and water component in water phase, respectively, and X_{CO2}^{CO2} and X_{CO2}^w that represent the mass of water component in the CO_2 phase and the CO_2 component in the CO_2 phase.
Phase changes can occur in the reservoir under certain pressure and temperature conditions. Water is most likely present in a gas or liquid state. However, CO_2 can also change from gas or liquid to supercritical fluid, or vice versa, under typical reservoir pressure and temperature

conditions. CO_2 changes to a supercritical state if its temperature and pressure exceed the critical values, T_C^{CO2} = 30.85 °C and P_C^{CO2} = 7.38 MPa.
To model the physical and chemical processes occurring at the macro-scale of a porous media, we use the Representative Elementary Volume (REV) averaging theory (Hassanizadeh & Gray, 1979; Hassanizadeh & Gray, 1990). In REV averaging theory, macroscopic quantities are obtained from local volume averaging of corresponding microscopic quantities. Exchange of mass, momentum and energy between the constituents are explicitly accounted for from interfacial effects. The averaging process is conducted by integrating the involved microscopic quantities over a REV of volume *dv* and area *da*. The REV is chosen larger than the constituent individual size scales and at the same time smaller than the size scale of the physical system.

4.2.4 Theory for multiphase flow in fractured porous media

Thermodynamic calculations show that Lusi is a two-phase (Water/CO_2) flow system, and we do not yet consider mixing of the two phases or any chemical reactions. We consider two immiscible fluids simultaneously flow in the pore space with the mass conservation equation for each phase given by:

$$\phi \frac{\partial}{\partial t} S_\alpha + \nabla \cdot v_\alpha = -q_\alpha \qquad \alpha = Water, CO_2 \tag{4.1}$$

Where α is the phase index, S_α [-] is the phase saturation; Φ [-] is the porosity; and q_α is the source term. It is assumed that the phase velocity v_α is governed by the generalized of Darcy's Law for multiphase flow.

$$v_\alpha = -\frac{1}{\mu_\alpha} \mathbf{K}_\alpha \cdot (\nabla p_\alpha - \rho_\alpha g) \tag{4.2}$$

With the definition of the relative permeability $k_{r\alpha}$, we can set up a relation between the conductivity for the phase α, K_α and the intrinsic permeability, **K**, which is fluid independent.

$$\mathbf{K}_\alpha = k_{r\alpha} \mathbf{K} \tag{4.3}$$

The relative permeability $k_{r\alpha}$ can be considered as a scaling factor that depends on the saturation of the phases present and satisfies the following constraint (Bear, 1972; Helmig, 1997):

$$0 \leq k_{r\alpha} \left(S_1, \dots, S_{nphase}\right) \leq 1 \quad \forall \alpha \tag{4.4}$$

The generalized Darcy's Law is therefore:

$$v_\alpha = -\frac{k_{r\alpha}}{\mu_\alpha}\,\mathbf{K}\cdot(\nabla p_\alpha - \rho_\alpha g) \tag{4.5}$$

If we consider an H_2O-CO_2 flow system for Lusi under isothermal conditions, we can apply the pressure-saturation formulation with modifications (Helmig, 1997). With a constitutive relationship for the relative permeabilities of $k_{r\alpha} = k_{r\alpha}(S_\alpha)$, and the saturation constraint $S_{water} + S_{CO2} = 1$, we have a complete system of equations for the unknown variables p, S_{water} and S_{CO2}.

We employ a pressure-saturation formulation to solve this system of equations. Summing up the two mass-balance equations for water and CO_2, we obtain the pressure equation:

$$\nabla\cdot(\lambda_{tot}\nabla p) = q_{tot} \tag{4.6}$$

where $\lambda_{tot} = \lambda_{water} + \lambda_{CO2}$ is the total mobility tensor and $q_{tot} = q_{water} + q_{CO2}$ the total source term. Once the pressure is computed, the saturation is obtained by solving the mass-balance equation for one of the two phases (e.g., water phase):

$$\phi\frac{\partial}{\partial t}S_{water} + \nabla\cdot[f_{water}(S_{water})v_{tot}] = -q_{water} \tag{4.7}$$

where the total velocity is defined as:

$$v_{tot} = v_{water} + v_{CO2} = -\lambda_{tot}\nabla p \tag{4.8}$$

and the fractional flow function is given by:

$$f_{water} = \frac{\frac{k_{rwater}}{\mu_{water}}}{\frac{k_{rwater}}{\mu_{water}} + \frac{k_{rCO_2}}{\mu_{CO_2}}} \tag{4.9}$$

Eqs. (4.6) to (4.13) result in a nonlinear system of differential equation solved here by using a sequentially implicit scheme (Künze & Lunati, 2012).

4.2.5 Modelling the hydrological response to slip on the Watukosek fault system

We are interested in gaining some insight into the evolution of fluid flow through an assumed slipping Watukosek fault system to explore the hypothesis that the Yogyakarta earthquake fluidized some of the sedimentary layers beneath Lusi (Lupi et al., 2013), which then injected into, and induced slip, on the Watukosek fault system. We couple a simple mechanical model to the 2-phase flow model to investigate flow up through the shear zone in response to slip on that fault.

We use the same approach as found elsewhere (Miller et al., 2004; Miller, 2015), and use a Mohr-Coulomb frictional failure criterion, an effective stress-dependent permeability, and step-wise increase in permeability when the failure criterion is satisfied. We also assume a range of slip surface orientations of existing faults loaded by the far-field stress state.
The dependence of permeability on the effective normal stress is needed to approximate the change in crack aperture that accompanies both slip and increasing fluid pressure (Miller et al., 2004). Grid points "fail" when:

$$\tau - \mu\sigma_{eff} > 0 \tag{4.10}$$

where τ is the shear stress [Pa], μ is the friction coefficient, and σ_{eff} [Pa] is the effective normal stress, defined as:

$$\sigma_{eff} = \sigma_n - P_f \tag{4.11}$$

The time and location of each model "event" is catalogued. The effective normal stress σ_{eff} and shear stress τ acting on a plane through a point are:

$$\sigma_{eff} = \frac{\sigma_1 + \sigma_3 - 2P_f}{2} + \frac{\sigma_1 - \sigma_3}{2}\cos(2\theta) \tag{4.12}$$

$$\tau = \frac{\sigma_1 - \sigma_3}{2}\sin(2\theta) \tag{4.13}$$

where σ_1 and σ_3 are the maximum and minimum principal stresses acting in the far field, and θ is the angle measured from the plane normal to the direction of σ_1.

4.3 Results

4.3.1 Coupling 2-phase flow model to a toggle switch permeability model

The 3-dimensional model is still under development, so we use a 2D profile from the 3D numerical grid. We adopt the model for permeability as a highly non-linear function of the effective normal stress and allow a stepwise increase in permeability when the Mohr-Coulomb failure condition is reached (Miller et al., 1996; Miller et al., 2004; Miller, 2015). In our model, the Watukosek fault and the Siring fault represent shear zones or conduits where the permeability increases concomitant with slip on the fault (Figure 52).

The initial conditions at Lusi are unknown, so we assume a normal distribution of incipient slip planes relative to the far-field stresses. This results in a complex stress state, shown in Mohr-Coulomb space (Figure 53A), where each dot represents the state of stress acting on the plane at angle θ from the normal to σ_1 and passing through the point represented by computational nodes. When fluid pressures rise due to CO_2 injection originating from a hypothesized magmatic intrusion, the effective stress state moves, at different rates, towards the failure condition (Figure 53 B-D). The rate of stress state migration depends on the permeability structure within the numerical domain. We do not currently model the stress changes that accompany slip, but the important aspect of the model is applying a stepwise increase in permeability when failure condition is reached (Miller & Nur, 2000).

We use the Finite Volume Method (FVM) assuming an incompressible and immiscible two-phase (Water/CO_2) flow system, considering gravity coupled with a simplified mechanical model. We use the FVM based on the subdivision of the domain in volumes to control and integrate the governing conservation equations (Künze & Lunati, 2012). This method has been developed over the last decade to efficiently solve large-scale reservoir systems.

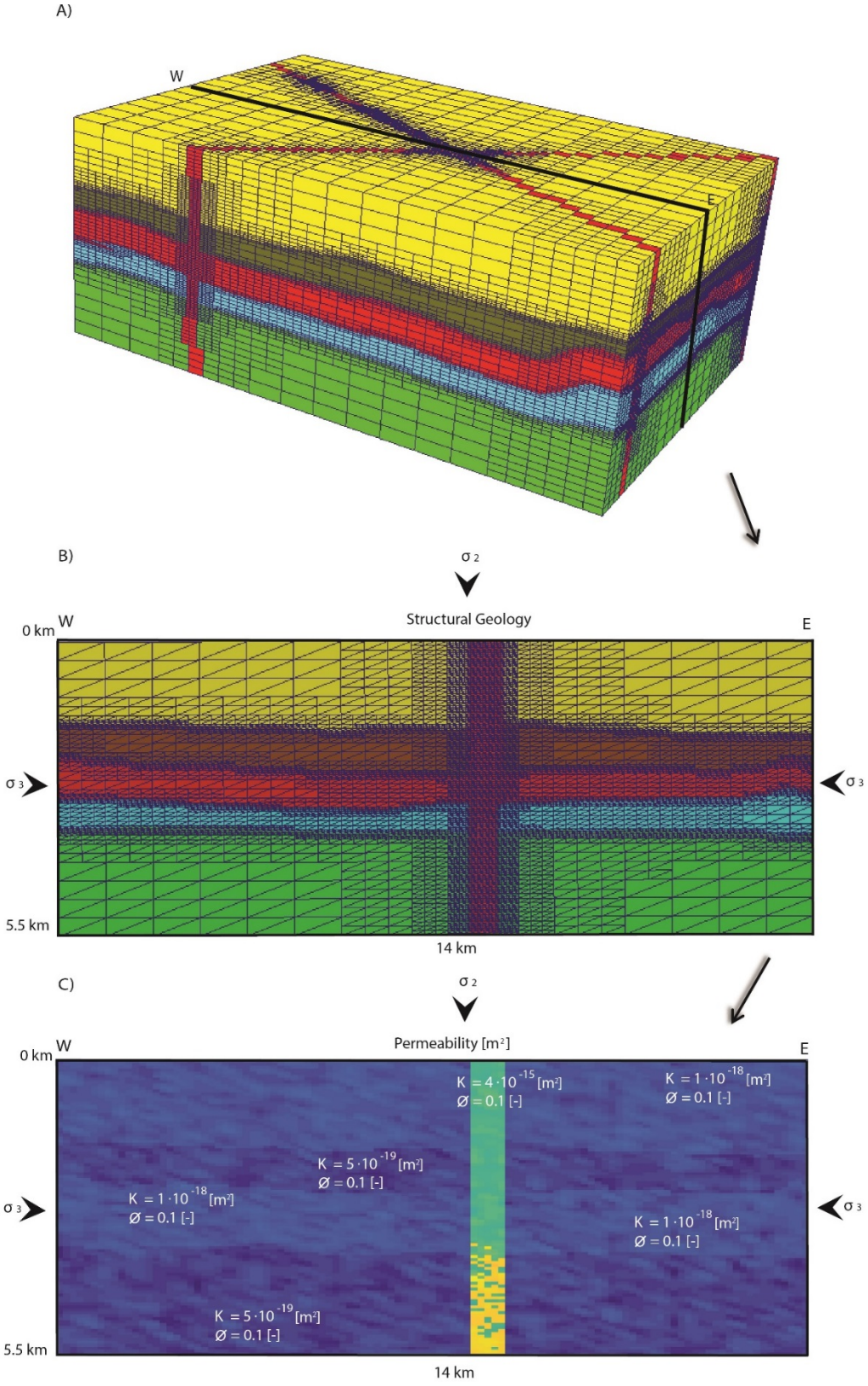

Figure 52: The 3D model A) is cut into a 2D slice on which the simulation take place B). C) Initial permeability field of the numerical model of a 2D cross-section of the Lusi system with already some hours of simulation increasing the permeability (yellow) by a factor of 10^3 into the shear zone. Shear and effective normal stresses acting on virtual slip planes are calculated using Eqs. 4.12 and 4.13.

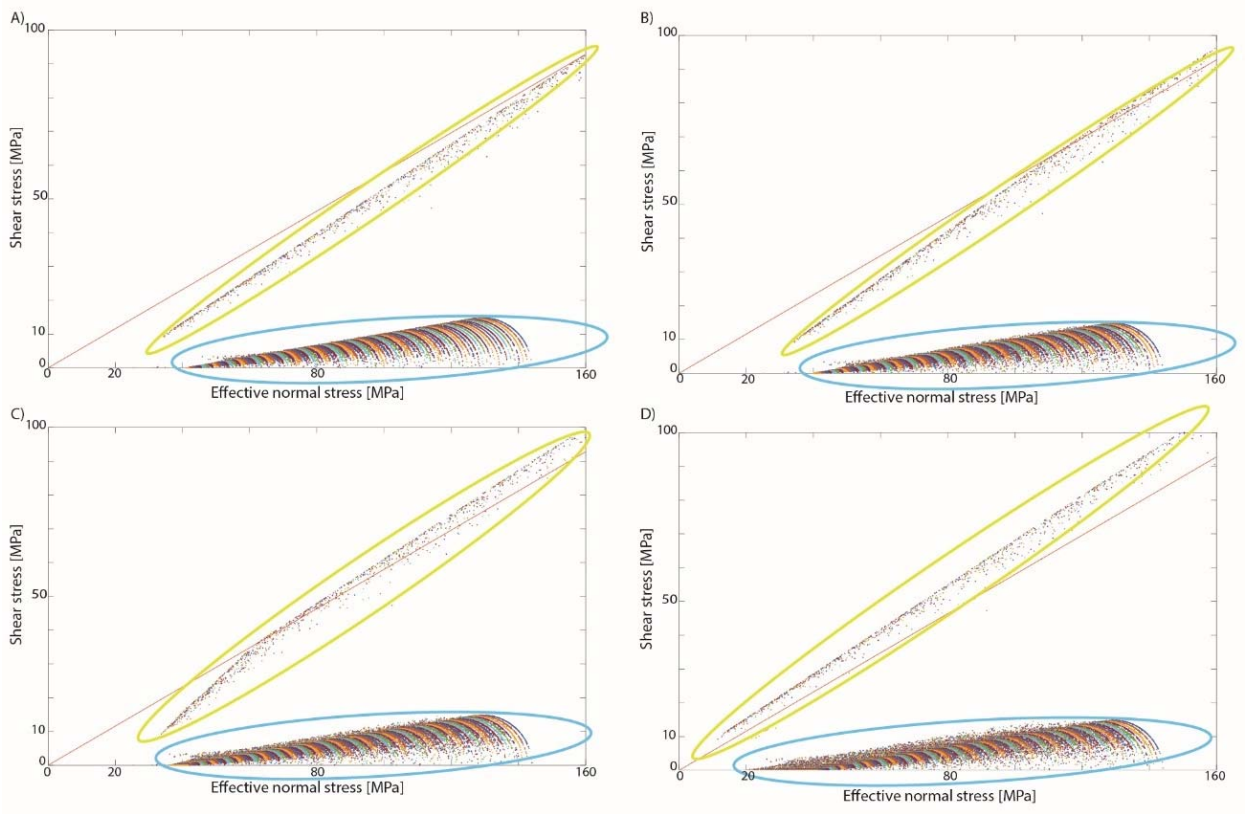

Figure 53: Evolution of the stress state. A) Dots represent the state of stress on each numerical grid cell, with the entire model beneath the Mohr-Coulomb failure condition. Fluid pressure (Water and CO_2) increases in the model B) to D), numerical grid cells "fail" when they reach the failure condition and a model "earthquake" is recorded. Time are A) 0 hour, B) 10 hours, C) 20 hours and D) 40 hours when Lusi erupted. Two zones are described, the shear zones in yellow and the rest of the system in blue.

We investigated under what conditions of flow would result in the 40 hours separating the Yogyakarta earthquake and the first appearance of mud breccia outflow at the surface. We consider two primary hydrologic structures, the clay layer (brown) and the carbonate layer (blue) (Figure 52). The CO_2 originates from an over-pressured source of deep fluids (water and CO_2) and driven by gravity. A source of fluid (water) is also imposed in the clay layer representing the "mud" source fluidized by the earthquake. We currently ignore the mud/water viscosity and assume water viscosity. We apply a zero pressure boundary on the top surface, and 55 MPa (hydrostatic) pressure to the bottom surface. Water inflow is a Neumann boundary of $1 \cdot 10^{-8}$ [m^3/s] for both layers. The fluid properties have typical characteristics for water (brine) and CO_2 (Duan & Sun, 2003). The rock proprieties used are shown in Figure 52. The permeability increase of a factor 10^3 in the shear zone if a grid cell is "failing" in the toggle switch model. Due to the incompressibility assumption of the fluids and the applied boundary conditions, the fluid pressure does not decrease at failure, as would be more reasonable. Nevertheless, this simple model provides a general concept of the possible hydrodynamics during the 40 hours following the Yogyakarta earthquake by considering hydro-mechanical processes and a 2-phase fluid.

Figure 54 show the fluid pressure field after 40 hours of simulation and Figure 55 shows model results of CO_2 saturation at the onset of the eruption. The whole fault zone (conduit) is mechanically altered and increased in permeability in the initial 40 hours. The CO_2 concentration is generally low but reaches up to 60% in the deeper levels. The influence of fresh water inflow (water recharge) is visible about the two layers where the CO_2 concentration decreases, which may explain that the eruptive fluid at the Lusi crater should be mainly water from the carbonate layer and "water mud" from the clay layer. The incoming deep fluids should also bring deeper "water mud" from the mudstone layer between the 4 to 5.5 km depths, as recently confirmed from geodetic measurements (Rudolph et al., 2013), petrographic measurements of erupted clasts (Malvoisin et al., 2016), InSAR investigation (Shirzaei et al., 2015) and water geochemistry (Mazzini et al., 2018).

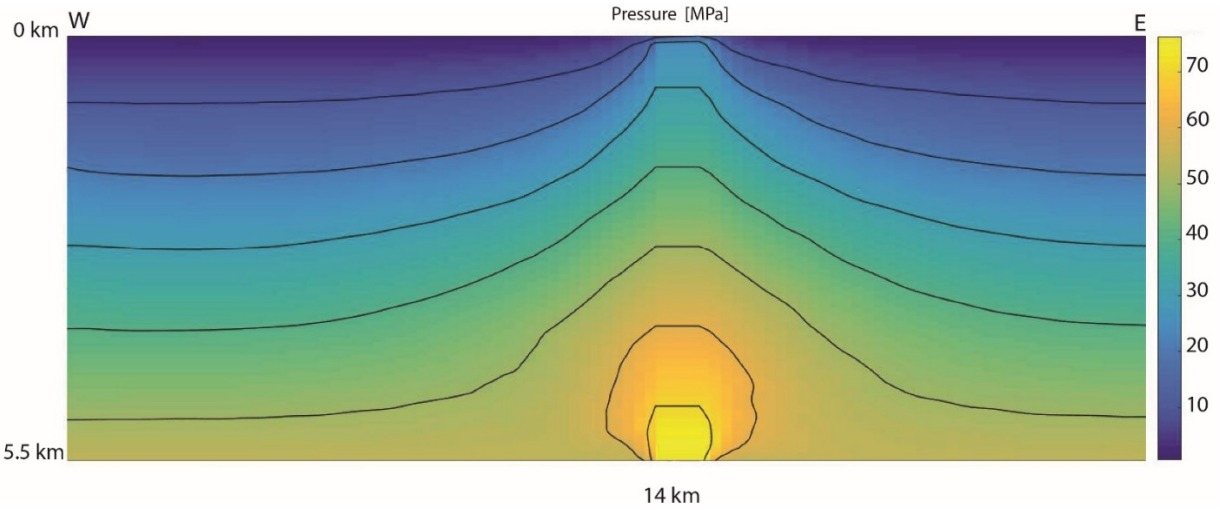

Figure 54: Evolution of the fluid pressure field, above hydrostatic, showing high pressures propagating in the shear zone (conduit) after 40 hours of simulation.

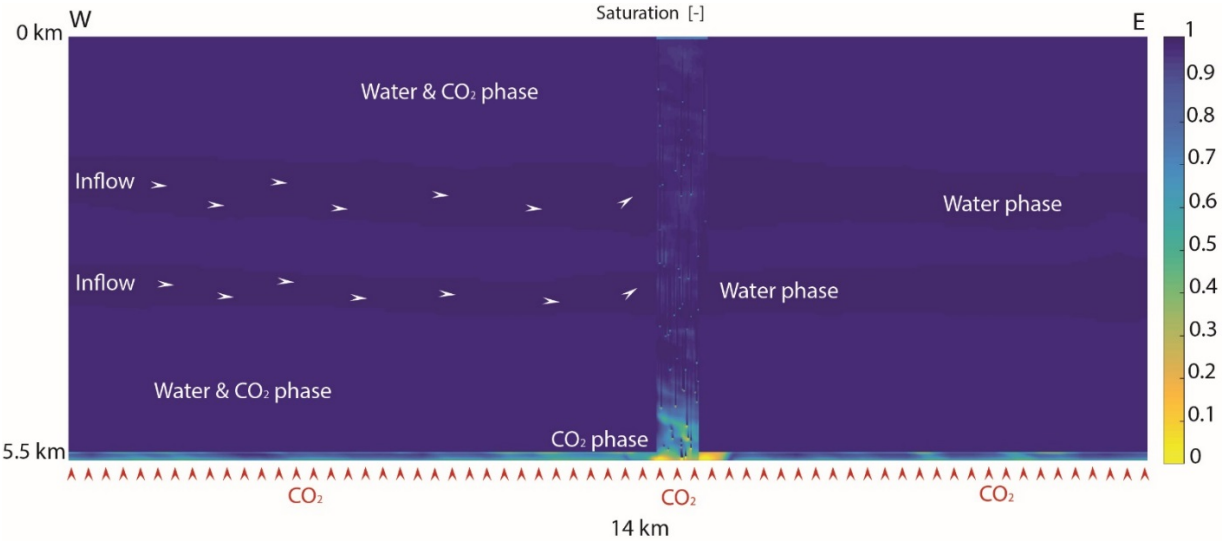

Figure 55: Based on the structure shown in Figure 52, a hydro-mechanical multiphase (Water/CO_2) simulation of Lusi through the shear zone delimitated by the two major fault crossing the Lusi zone. It represents the fluids passing through the reactivated shear zone 40 hours after the earthquake considering the recharge of the two main hydro-geologic structures that could be source of fluids (clay layer (brown) and carbonate layer (blue) and CO_2 transport from volcanic origin through the system.

4.4 Conclusions and outlooks

The objective of this work was to present an approach and some initial results for modelling and understanding the dynamics of the Lusi sediment-hosted hydrothermal system. Our long-term goal is to develop a 3D numerical model, based on a geological model, which couples mechanics with the hydraulics and thermal processes driving Lusi. To date, we have utilized a recently developed algorithm "HULK" and created a 3D numerical grid that approximates the dominant lithology and faults in the region, but are currently constrained to 2D profiles of the 3D grid. We determined from a thermodynamic calculation for CO_2 solubility in aqueous NaCl solution system that Lusi is a 2-phase system of water (brine) and CO_2. This must be incorporated into any future studies because the 2 phases ultimately control the flow properties within the system. The small percentage of CH_4 does not significantly impact the flow system, but would be of interest to study its geochemical significance. A coupled 2-phase model with a model of mechanics investigated under what conditions mud would arrive about 40 hours after presumably being perturbed by the Yogyakarta earthquake. We find that using reasonable permeability values, influx rates and outflow rates of the overall hydrogeological system can reproduce the 40 hours interval between the earthquake and the first appearance of water, CO_2 and also mud at the surface.

These first results provide a basis for more sophisticated studies, eventually in 3D, and we introduced a workflow necessary to achieve this objective. Future work focuses on heat transport coupled with the multiphase (Water/CO_2) hydro-mechanical model presented here and adding chemical reactions and dehydration reactions into the model for long-term simulations. Furthermore a more realistic treatment of the underlying thermodynamics and a deeper investigation of the role of fluid properties on fluid flow dynamics would generate valuable insight. Our long-term goal is code parallelization suitable for High Performance Computing (HPC) to achieve high-resolution simulations to more fully understand the complex dynamics of this system.

5. Multi-GPU based 3D numerical modelling of the Lusi geyser system in Java, Indonesia

"We know more about traveling across our Universe than drilling through our Earth's interior."
Thinking about Earth and Planetary Sciences…

This article is in preparation for submission to the Journal of Volcanology and Geothermal Research, April 2018
Reza Sohrabi, Benjamin Malvoisin, Adriano Mazzini, Stephen A. Miller

5.1 Introduction

The Lusi hydrothermal system, erupting since the 29th of May 2006 in East Java, elicited debate in science and politics (Drake, 2016; Van Noorden, 2006). During the early phases a sequence of aligned clastic eruptions appeared through factures that followed the same orientation of the Watukoesk fault system (Figure 56). Fluids quickly flooded large part of the Sidoarjo regency urban area, permanently displacing 60,000 people (Richards, 2011). Twelve years later the Lusi eruption is still ongoing displaying a perpetual geysering behavior (Karyono et al., 2017) and flow rate of ~80,000 m^3/day with significant earthquake triggered increases up to ~120,000 m^3/day (Miller and Mazzini, 2018). This fascinating system displays complex interactions between hydrothermal fluids, carbonate- and clay-rich formations in an active tectonic setting framed by volcanic complex. Here we will not discuss the mechanisms behind Lusi's triggering, but will rather focus on the long time evolution of this fascinating hydrothermal system and its potential use for geothermal resources.

3D numerical modelling is a powerful tool for investigating processes occurring in the Earth's interior such as hydrothermal circulation or geothermal reservoirs. The dynamics of such heterogeneous complex systems entails coupled and nonlinear flow, heat transport, deformation and reaction. The quantitative analysis of these systems are challenging and depends on numerical solutions of coupled partial differential equations (PDEs). A considerable effort was made in last decades to use different kinds of numerical tools to model and calculate accurate dynamic behaviors. However, scientists and engineers have not been able to adapt 3D software and numerical algorithms to the changes in hardware evolution. Many 3D applications and algorithms are as a result not well suited for the available hardware, which implies performances far below the hardware's peak. Here we report a series of numerical simulations using multi-GPU computing to model physical processes involved in an eruptive clastic system. The impacts of reaction and temperature changes on porosity and fluid pressure are taken into consideration in order to determine the evolution of fluid flow. Today, 3D numerical modelling of hydrothermal systems represent a major challenge due to the multiphysics processes involved (Ingebristen et al., 2010; Jeanne et al., 2014). Many processes are involved regarding short or long term mechanisms (Bowen, 1979; Ingebritsen & Sanford, 1999; Lowenstern & Hurwitz, 2008; Hurwitz & Manga, 2017; White, 1957). This manuscript investigates the evolution of the Lusi system exploring the hydrothermal fluids circulation and the connected hydro-thermo-chemical interactions. The investigation of the complex system requires the development of long-term computational multiphysics approaches at high resolution in 3D.

We present results showing that the evolution of the hydrothermal eruption of Lusi is connected to the generation of high fluid pressures by dehydration reactions as proposed by Mazzini et al. (2007, 2012, 2018). We demonstrate the validation of this hypothesis with two different scenarios considering magmatic intrusion at 500°C and 1000°C beneath Lusi

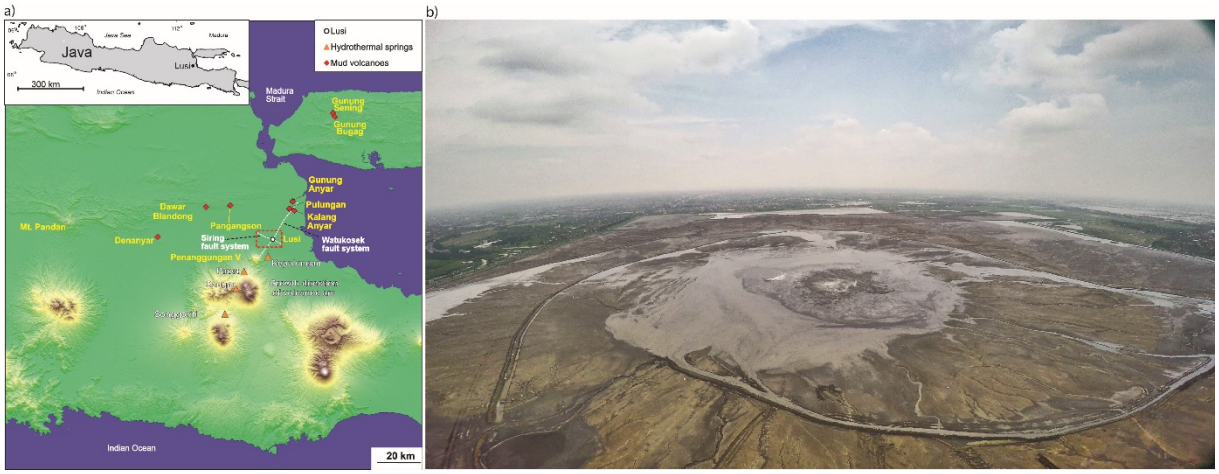

Figure 56: a) Inset map of Indonesia and topographic map showing the Arjuno-Welirang volcanic complex to the south with some of the surrounding hydrothermal springs. To the north of the island inside the sedimentary basin are located Lusi and other mud volcanoes. b) Aerial image from the Lusi drone. Erupting craters are visible in the central part of the inaccessible hydrothermal pond.

5.2 Methodology and model set-up

We combined a 3D geological model proposed by Sohrabi et al. (2018) which include altered sand, shale and clay from the Pucangan Formation (blue), the Bluish Grey clay from the Upper Kalibeng Formation (purple), the volcanoclastics from the Upper Kalibeng Formation (red), the carbonates from the Kujung/Prupuh/Tuban Formations (orange), and the mudstones from the Ngimgbang Formation (yellow). The model also includes two major faults or shear zones (red) crossing Lusi, the Watukosek strike slip system and the Siring antithetic faults system (Figure 57a). This 3D heterogeneous geological numerical model is then implemented in a newly developed numerical High Performance Computing (HPC) tool for subsurface fluid dynamics (Sohrabi et al., 2018).

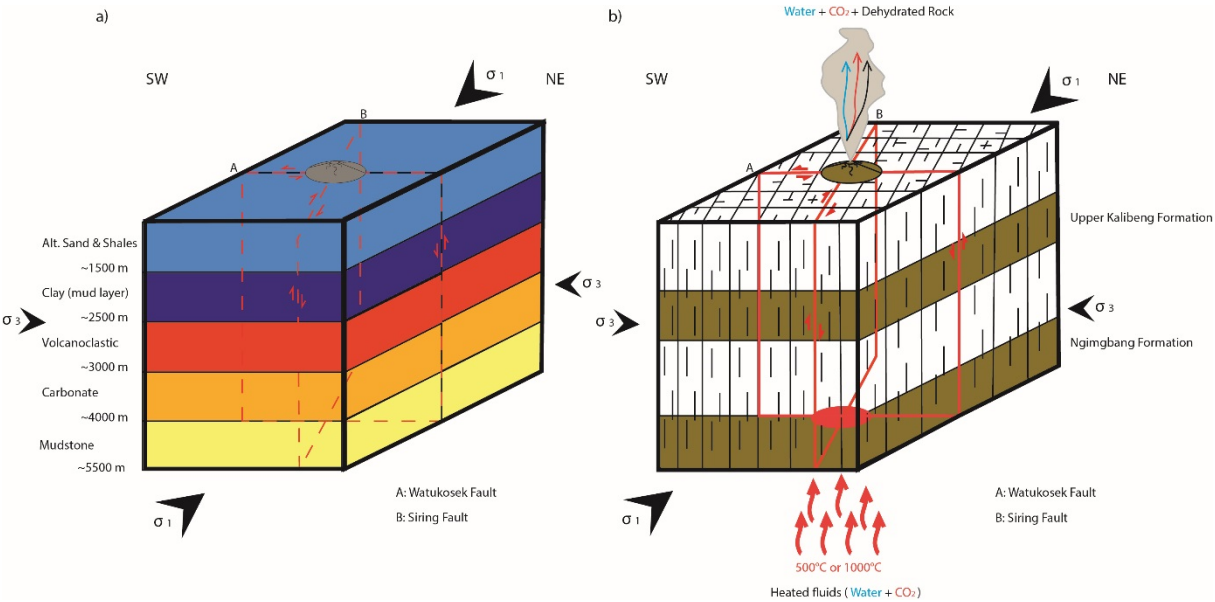

Figure 57: Conceptual model for a fluid pressure increase-controlled by dehydration in deep hydrothermal system or geothermal reservoir. Under conditions of increasing temperature and pressure, dehydration reactions begin for clay minerals. a) 3D structural conceptual model considering five main hydrostructures and two main major shear zones/fractures at Lusi site due to the geodynamic constrains. b) 3D fluid dynamic conceptual model into fractured porous media considering deep hot fluids filling the entire Lusi system.

The Lusi hydrothermal 3D model considers an initial conductive geothermal gradient of 42°C/km (Mazzini et al., 2007) with a fluids intrusion emplaced at 5.5 km with an overpressure of 10 MPa. We simulate two scenarios with a different temperature of the fluid intrusion: a) 500°C and b) 1000°C. The surface temperature is set to 27°C (Svensen et al., 2018). For the rock properties, we used parameters found in Svensen et al. (2018) for the lithology combing with the analyses from Mazzini et al. (2012) and Tanikawa et al. (2010).We also calibrated the simulations with the parameters proposed by the authors mentioned above. We assume that flow properties of supercritical CO_2 at the pressure and temperature conditions is ten times more compressible than water, but it is of the same order less viscous, resulting in similar flow properties (Miller et al., 2004). The potential clay dehydration, fluid flow, mass and heat transport in fractured porous media linked to porosity and permeability changes due to dehydration reactions may have an impact on the outflow at the surface. Fluids production in the future regarding the two main geological clay layers (Upper Kalibeng Formation and Ngimgbang Formation) considered in the 3D system (Figure 57b) may change hydrodynamic properties in a complex system like Lusi.

5.2.1 Physical model

We use a continuum porous media approach to describe the Lusi hydrothermal system. The highly nonlinear equations are solved with a Finite Difference (FD) method (Patankar, 1980). The prevailing view in a large-scale hydrothermal system like Lusi is that dehydration clay reactions can play a substantial role in porosity and permeability evolution or even in seismicity. These changes modify the pore pressure state and can thus change the pore pressure gradients. We use the 3D model proposed by Sohrabi et al. (2018) for clay dehydration in large-scale hydrothermal systems or geothermal reservoirs. We used the 3D geological model proposed by Sohrabi et al. (2018) for generating a complex distribution of porosity and permeability. We simulated the multiphysics in response of clay dehydration using a newly developed multi-GPU simulator (Sohrabi et al., 2018). Our tool computes the pressure (P_f), the temperature (T), the porosity ($\emptyset$), the permeability (k) and the fluid release from clay rock layers using the following equation (i.e. amount of fluid bound to the solid (Xs)).

5.2.1.1 Mass conservation

Total mass conservation in a porous and reacting medium is:

$$\frac{\partial(\rho_f\phi + \rho_s(1-\phi))}{\partial t} + \nabla\cdot\left(\rho_f\phi v_f + \rho_s(1-\phi)v_s\right) = 0 \tag{5.1}$$

where ϕ, ρ, v are the porosity (volume fraction of fluid), the densities and the velocities, respectively. The subscripts *'s'* and *'f'* denote the properties of the solid and the fluid, respectively.

Mass of nonvolatile species is conserved as well (Malvoisin et al., 2015):

$$\frac{\partial(\rho_s(1-X_s)(1-\phi))}{\partial t} + \nabla\cdot(\rho_s(1-X_s)(1-\phi)v_s) = 0 \tag{5.2}$$

where the amount of fluid into the solid X_s is calculated at the equilibrium with a fit of the data of Vidal and Dubacq (2009) giving Xs as a function of temperature in the smectite/illite system.

5.2.1.2 Conservation of momentum

The conservation of fluid momentum is expressed by the Darcy's law:

$$\phi(v_f - v_s) = -\frac{k_0 \phi^3}{\mu_f}(\nabla P_f - \rho_f g) \tag{5.3}$$

where the permeability is related to the porosity through the Kozeny-Carman relationship with an exponent 3 and a constant background permeability k_0 (Carmen, 1937, 1956; Kozeny, 1927). μ_f is the fluid viscosity, g is the gravitational constant and P_f is the fluid pressure

The fluid pressure considering the impact of rock dehydration on volume change (rock density ρ_s constant without viscous deformation) can be expressed as (Malvoisin et al., 2015):

$$\nabla \frac{k_0 \phi^3}{\mu_f}\left(\nabla P_f - \rho_f g\right) = \beta_{eff} \frac{dP_f}{dt} + \left(1 - \frac{\rho_s}{\rho_f}\right) \cdot \frac{1-\phi}{1-X_s} \cdot \frac{dX_s}{dt} \tag{5.4}$$

β_f and β_s are the fluid and pore (crack) compressibility. The effective compressibility β_{eff} is described by:

$$\beta_{eff} = \beta_f + \frac{\beta_s}{1-\phi} \tag{5.5}$$

The hydromechanical porosity change due to fluids extraction from the rock by metamorphism can be expressed by (Malvoisin et al., 2015):

$$\frac{d\phi}{dt} = \beta_s \frac{dP_f}{dt} - \frac{(1-\phi)}{(1-X_s)} \cdot \frac{dX_s}{dt} \tag{5.6}$$

5.2.1.3 Energy conservation

The energy heat conservation over an elemental volume of medium (solid and fluid phase) at thermal equilibrium, $T = T_s = T_f$ (Nield et al., 2006):

$$\Big((1-\phi)\rho_s c_s + \phi\big(\rho_f c_f\big)\Big)\frac{\partial T}{\partial t} + \big(\rho_f c_f\big)v_f \cdot \nabla T = \nabla \cdot \Big(\big((1-\phi)\lambda_s + \phi\lambda_f\big)\nabla T\Big) + \big((1-\phi)q_s + \phi q_f\big) \tag{5.7}$$

where c is the specific heat of the phase, λ is the thermal conductivity and q is the heat production per unit volume. Equations 5.1 to 5.7 results in a highly nonlinear system of differential equation solved here by using a Finite Deference (FD) method (Patankar, 1980).

The general coupled parameters used for simulations are shown in Table 6. Parameter values chosen for the fully coupled 3D numerical model are inputs measured and calculated from previous studies (Mazzini et al., 2018; Svensen et al., 2018).

Table 6: Fully coupled modelling parameters

Symbol	Definition	Units
P_f	Fluid pressure	Pa
ρ_f	Density of fluid	kg·m^{-3}
ρ_s	Density of solid	kg·m^{-3}
v_f	Velocity of fluid	m·s^{-1}
β_f	Compressibility of fluid	Pa^{-1}
β_s	Compressibility of solid	Pa^{-1}
β_{eff}	Effective Compressibility	Pa^{-1}
∅	Porosity	-
k	Permeability	m^2
X_s	Mass fraction of fluid in solid	wt %
T	Temperature	°C
c_f	Fluid specific heat	J/kg·K
c_s	Solid specific heat	J/kg·K
λ_f	Fluid thermal conductivity	W/ m·K
λ_s	Solid thermal conductivity	W/ m·K
q_f	Fluid heat production	J/ m^3/ s
q_s	Solid heat production	J/ m^3/ s
g	Gravity acceleration	m^{2}s^{-1}

5.3 Results

We generated a structural grid for multi-GPU computing from the 3D geological model (Figure 58).

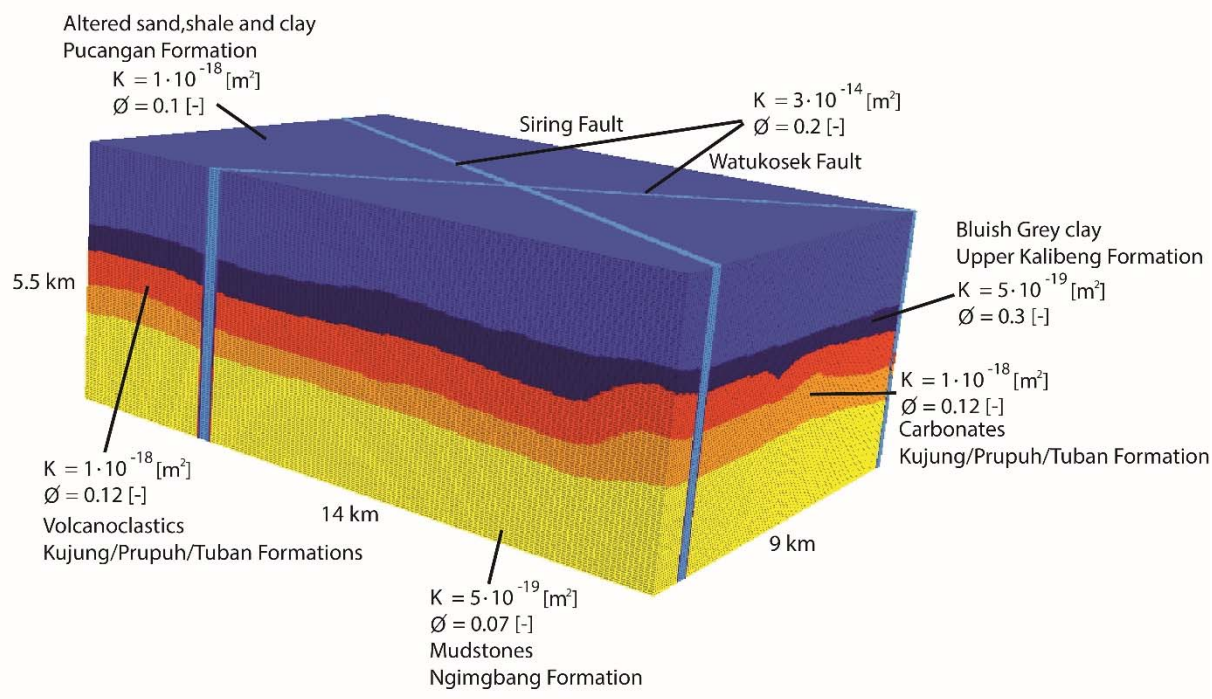

Figure 58: Generation of a 3D structural numerical grid with initial parameters with heterogeneity (permeability (k) and porosity (Ø)) at high resolution for multi-GPU calculation. This numerical grid is based on the 3D geological model of Lusi presented in Sohrabi et al. (2018).

To quantify the impact of the two different clay layers (Upper Kalibeng Formation (purple) and the Ngimgbang Formation (yellow)) considering clay dehydration, we performed 3D simulations in space and time. To compare them to data measured, we investigated two scenarios with different temperature of magmatic intrusion (500°C and 1000°C). We computed numerical simulations considering the metamorphism of the two geological clay layers from the 3D Lusi model (Figure 57) with a starting time when Lusi began to erupt in 2006. On Figure 59 and Figure 60, we present the calculated parameters through the shear zones/faults (conduit) as pressure (P_f), temperature (T), porosity (Ø), permeability (k) and the quantity of fluid into the solid (X_s) filing the fractured porous media in the Lusi system. We compare the numerical simulations to the hypotheses proposed by Mazzini et al. (2007, 2012, 2018).

The 3D high resolution numerical results are shown on Figure 61, Figure 62, Figure 63 and Figure 64. We simulated up to 200 years of the entire system to see the long term effect on the calculated parameters and on the fluid outflow. Nevertheless, we display only the first 50 years

of simulation because the results reached a steady-state after that time due to the irreversibility of the physical processes involved.

Figure 59e and Figure 60e show that the deeper clay layer from the Ngimgbang Formation has been already dehydrated up to 88% and that the clay layer from the Upper Kalibeng Formation up to 82% before Lusi starts to erupt. The illitization of the minerals have already been metamorphosed by the geothermal gradient and hydrostatic pressure initial condition of the entire system. But through the 50 years of simulation, we observed that the Ngimgbang Formation may still generate a certain quantity of water liberation 2%. And on the other hand, the Upper Kalibeng clay Formation may liberate an amount of 8% which in term of volume of water quantity is not negligible. This amount of release water has a consequence on the hydromechanics of the porosity and the permeability through the shear zones/faults (conduit) (Figure 59c,d and Figure 60c,d). In addition, we observe that there is an over pressure in the Upper Kalibeng clay Formation up to 5-10MPa (Figure 59b and Figure 60b).

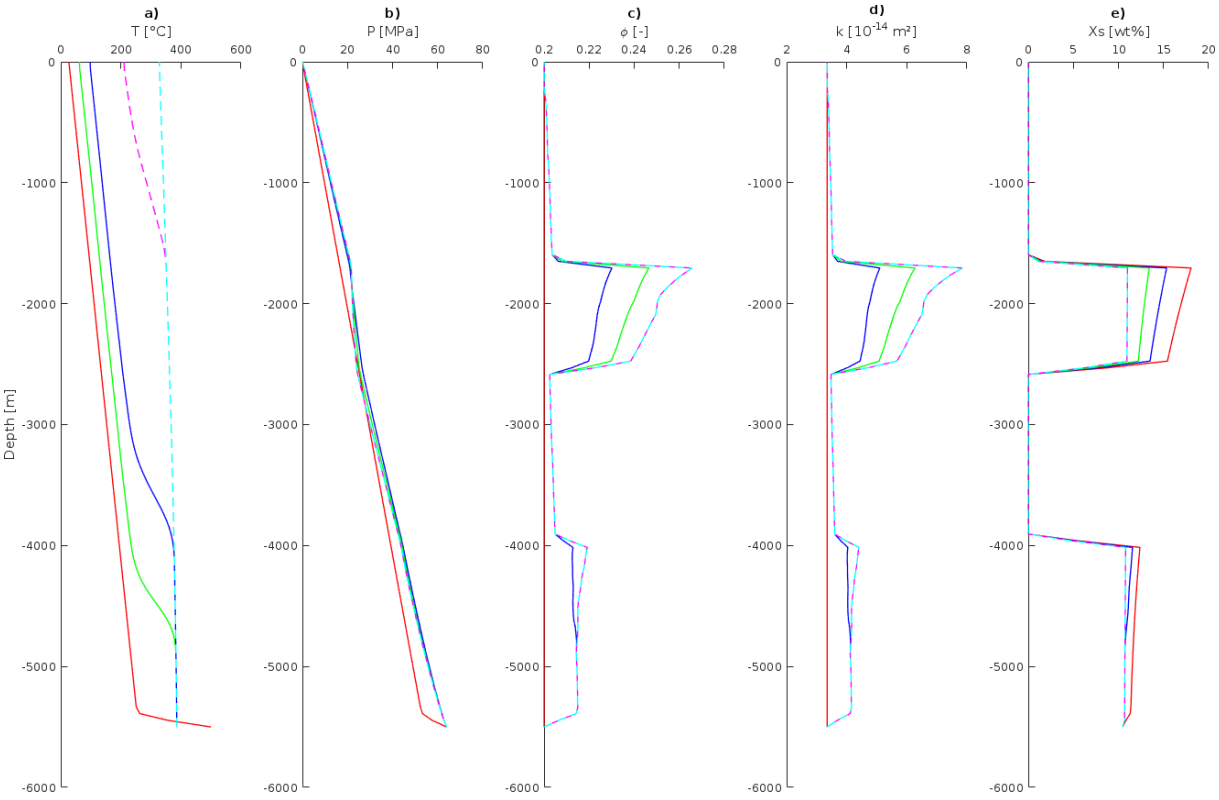

Figure 59: Evolution of the calculated parameters a) temperature, b) pressure, c) porosity, d) permeability and e) water liberation through the Lusi shear zones/ faults (conduit) considering a fluids intrusion at 500°C over different times: 0 years (red), 5 years (green), 10 years (blue), 25 years (dashed magenta) and 50 years (dashed cyan).

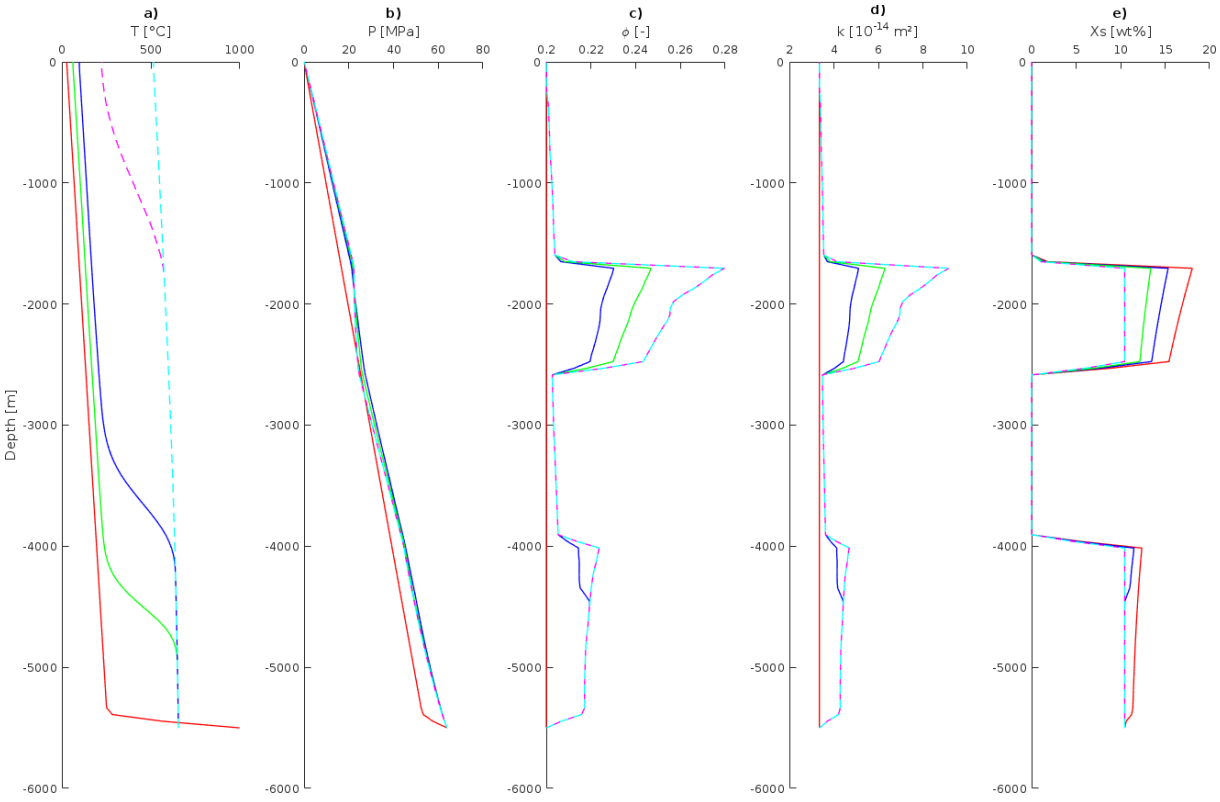

Figure 60: Evolution of the calculated parameters a) temperature, b) pressure, c) porosity, d) permeability and e) water liberation through the Lusi shear zones/ faults (conduit) considering a fluids intrusion at 1000°C over different times: 0 years (red), 5 years (green), 10 years (blue), 25 years (dashed magenta) and 50 years (dashed cyan).

Figure 61 and Figure 62 show the evolution of the temperature through the entire Lusi system, and Figure 63 and Figure 64 the porosity through the two shear zones/faults (Watukosek and Siring faults) at high resolution, since 2006 during 50 years. We observe that the temperature initial condition (500°C or 1000°C) has not a fundamental impact on the special distribution of the temperature in the 3D system. The diffusive effect of a magmatic intrusion in such large-scale system came to equilibrium after a certain time. The calibration of the simulation have shown that a constant heated source at 5.5 km depth is not a valid assumption (e.g. magmatic chamber). The fluids temperature measured at the Lusi vent would be too high with such hypothesis and is not consistent with the field measurement. The porosity evolution shows that with an intrusion impose at 500°C the hydro-fractures effect is less strong than with and intrusion impose at 1000°C, but the calculated parameters are in the same order of magnitude (Figure 59 and Figure 60). We see also that the rest of the illitization of the minerals generate less changes into the rock properties of the Ngimgbang Formation than in the Upper Kalibeng clay Formation.

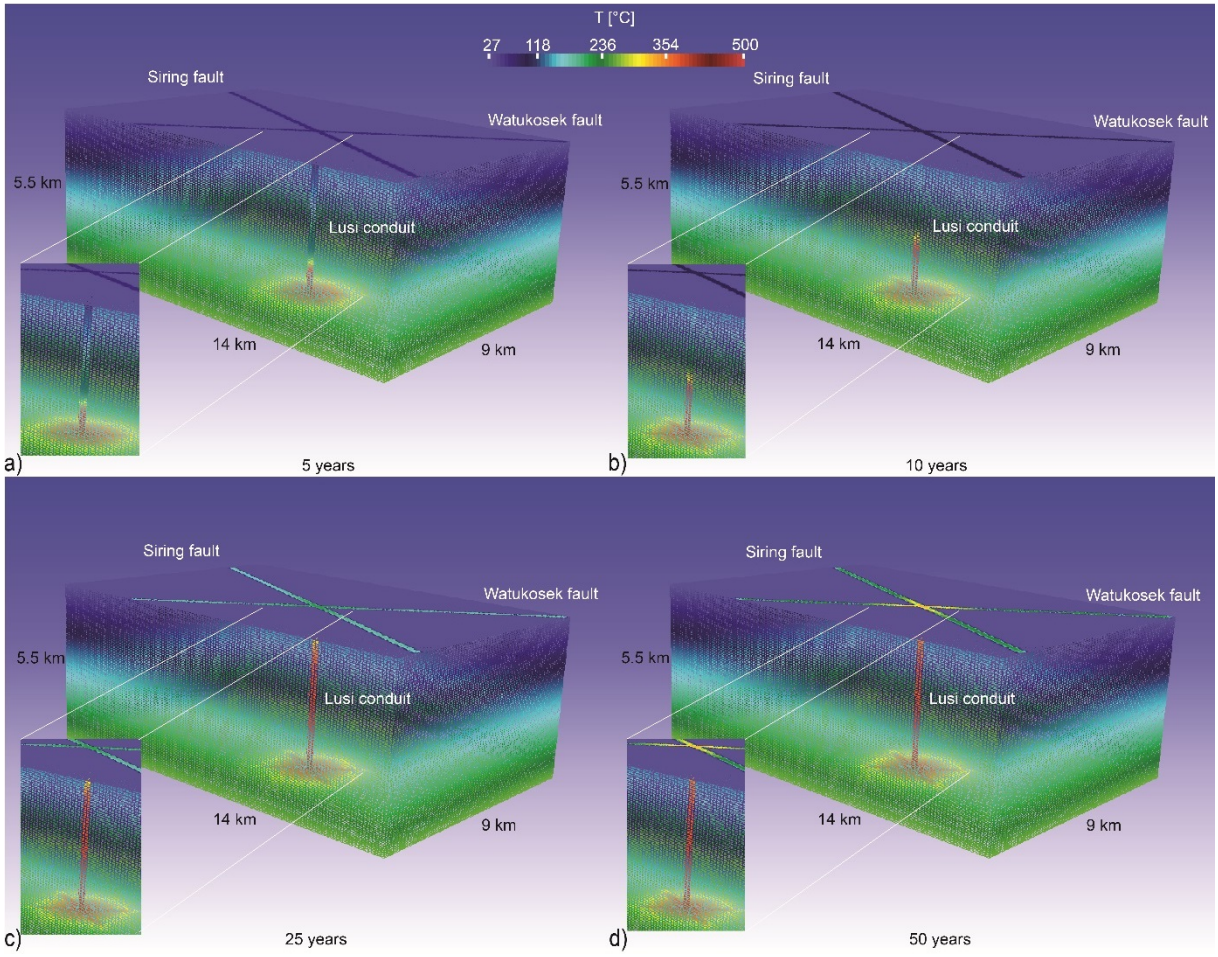

Figure 61: Evolution of the temperature considering a geothermal gradient of 42°C through the entire system and a fluid intrusion at 500°C with input parameters presented in the 3D geological model (Figure 58) with a focus on the Lusi conduit. Time simulations are calculated since Lusi erupted.

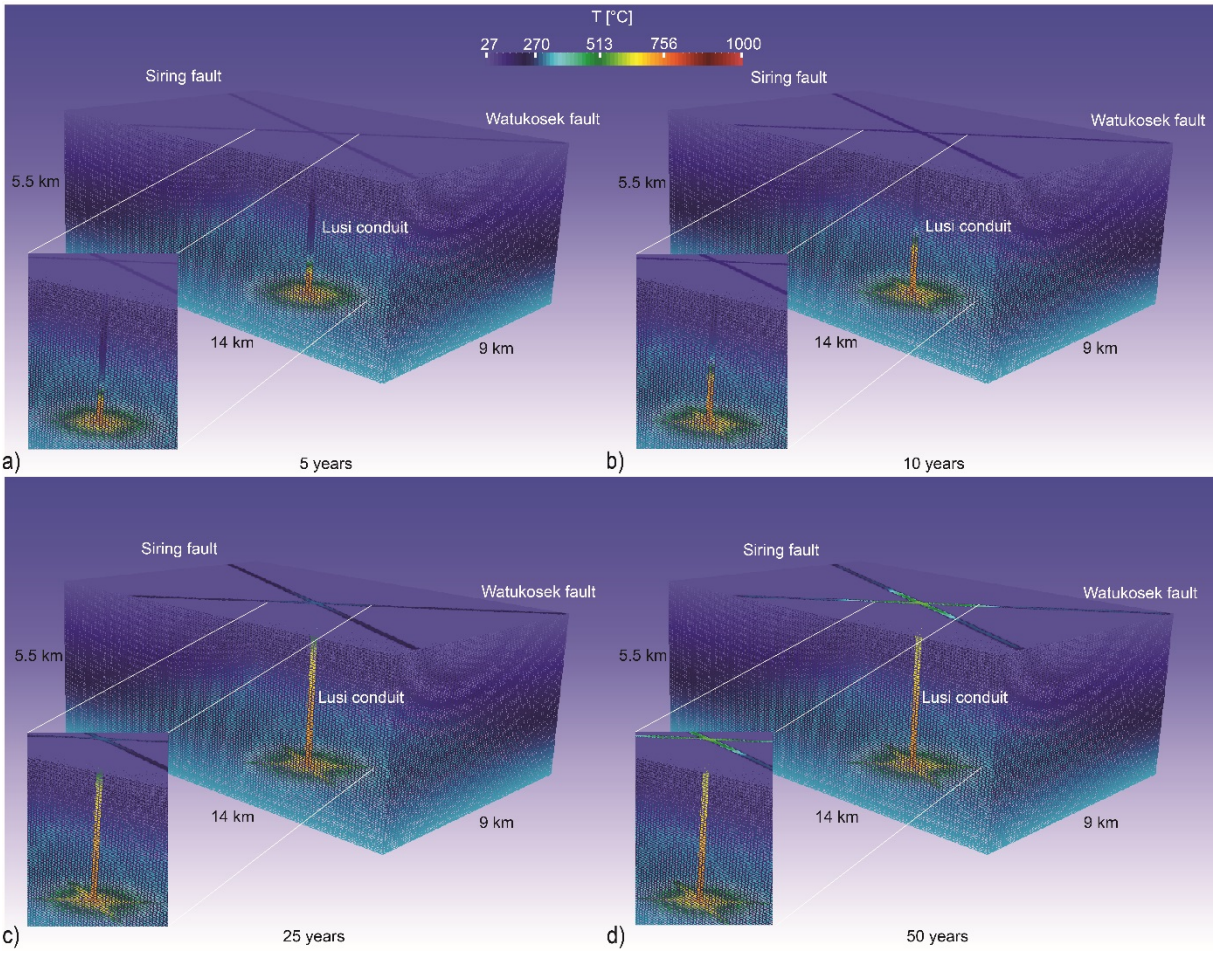

Figure 62: Evolution of the temperature considering a geothermal gradient of 42°C through the entire system and a fluid intrusion at 1000°C with input parameters presented in the 3D geological model (Figure 58) with a focus on the Lusi conduit showing the fluids temperature evolution. Time simulations are calculated since Lusi erupted.

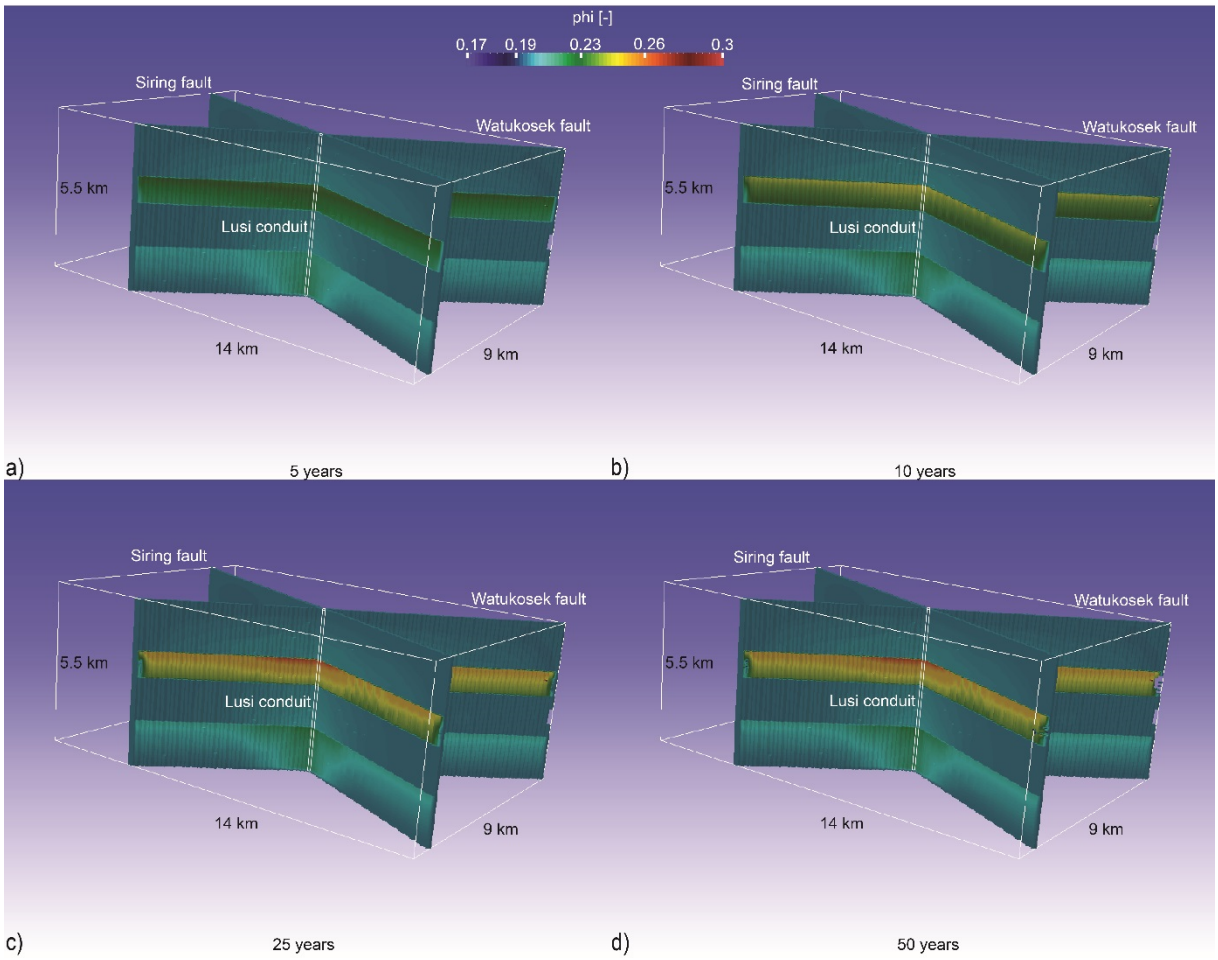

Figure 63: Evolution of the porosity considering a fluid intrusion at 500°C with input parameters presented in the 3D geological model (Figure 58). The two shear zones/faults are shown with a focus on the two clay layers (Upper Kalibeng Formation and Ngimgbang Formation). Time simulations are calculated since Lusi erupted.

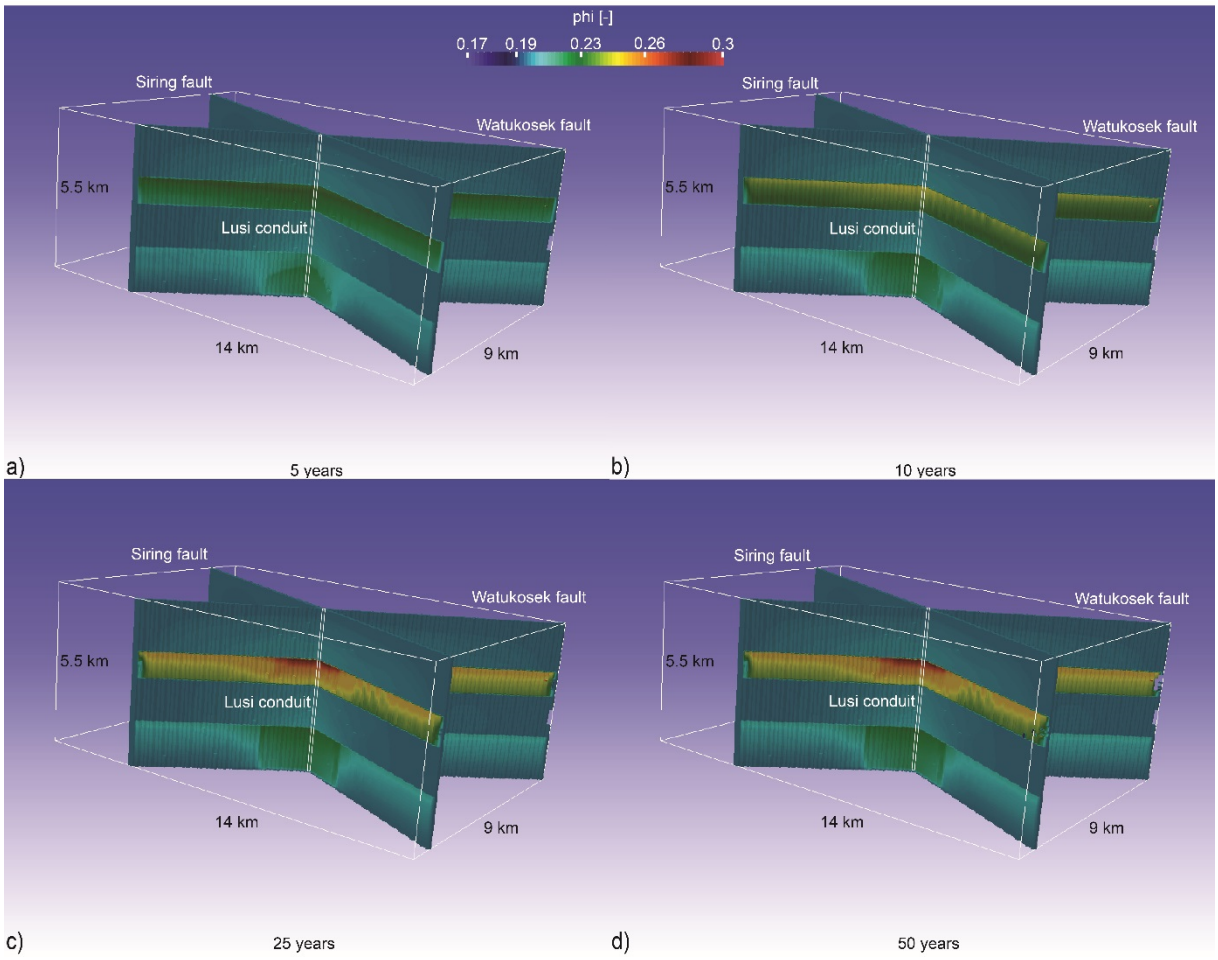

Figure 64: Evolution of the porosity considering a fluid intrusion at 1000°C with input parameters presented in the 3D geological model (Figure 58). The two shear zones/faults are shown with a focus on the two clay layers (Upper Kalibeng Formation and Ngimgbang Formation). Time simulations are calculated since Lusi erupted.

We calculate in terms of volume, the amount of fluids released at Lusi in the two different clay layers (Upper Kalibeng Formation and Ngimgbang Formation) after Lusi starts to erupt (Figure 65). Respectively, the Upper Kalibeng Formation release four time (~4x) more water than the Ngimgbang Formation. The results found within the first decade overestimate of a factor of ~2 to 3 the measured outflow of fluids at the Lusi site (Mazzini et al. 2007; Mazzini et al. 2012). The volume of water released is of 240,000 m^3/day for a magmatic intrusion at 1000°C and of 230,000 m^3/day for a magmatic intrusion at 500°C during the first decade. We calculated the outflow caused by clay dehydration around 60,000 m^3/day after 25 years and 343 m^3/day after 50 years for a magmatic intrusion at 1000°C. With a magmatic intrusion at 500°C, we estimate the water release caused by clay dehydration around 51,000 m^3/day after 25 years and 184 m^3/day after 50 years. After that time, the Lusi fluids outflow eruption will mainly reach a steady-state in term of dehydration and no more clay mineral from the Upper Kalibeng Formation and the Ngimgbang Formation will be illitizated.

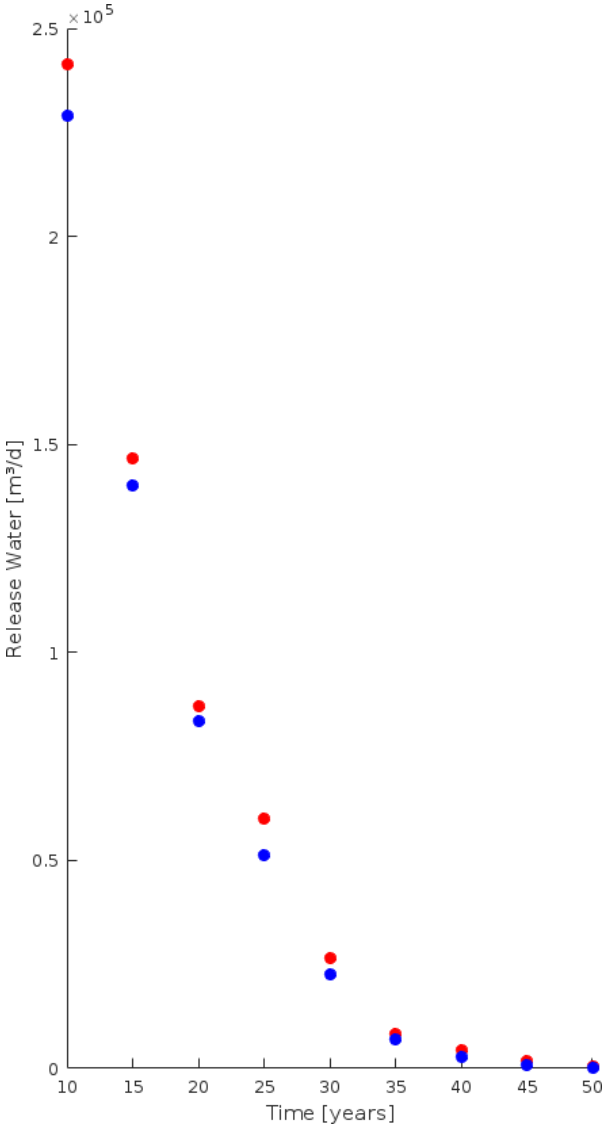

Figure 65: Release water due to the dehydration of the two main clay layers over 50 years after Lusi started to erupt in 2006. The red points shows the magmatic intrusion at 1000 °C and the blue points the magmatic intrusion at 500 °C.

5.4 Discussion

5.4.1 Geyser system of Lusi: evolution and lifetime

This article integrates previous field data measurement and previous calculations showing that the Lusi system is still active and may continue to dehydrate the two main geological clay layers (Upper Kalibeng Formation and Ngimgbang Formation) observed by many studies (Mazzini et al. 2007; Mazzini et al. 2012; Mazzini, 2018). If we consider the physical processes present in chapter 5.1, we see also that the Lusi system is of potential geothermal interest on the long term, whatever the heated fluid intrusion has as initial temperature. The temperature and other physical parameters calculated may be used in future for potential geo-resources at different level of depth or different reservoir targets (e.g. carbonates). The geothermal gradient could increase in the following years because of its geodynamics and volcanic situation, but simulations has shown that Lusi is heated by a magmatic intrusion and not a constant heated fluid source.

As it is presented in this article, the additional dehydration of the underlaying clay layers around ~1500m and ~5000m (Upper Kalibeng Formation and Ngimgbang Formation) may be still active in the future. The numerical simulations proposed two possibilities for the Lusi's evolution. The calculated outflow for the two scenarios overestimates (by a factor of 2-3x) the fact that we calculate the total potential water release of the Lusi geyser system, while the measurements on the Lusi site were done only considering the outflow of the satellite seeps around the main vents (Sciarra et al. 2018). Nevertheless, the large part of the water erupted goes also instantaneously into vapour (e.g. flashing effect) as soon as it reaches the surface.

The calculations of water liberation may have different issues, regarding to the geological 3D structure uncertainties. Generating new geological 3D models based on more detailed geophysical studies would be of main interest to analyse further fluid dynamics and reduce uncertainties. The one presented by Sohrabi et al. (2018) is a first proposed 3D geological model and additionally the one proposed by Moscariello et al. (2018) should add inputs and precisions on the geophysical and structural point of view (Karyono et al., 2017; Fallahi et al., 2017). It should also be interesting to consider several scenarios on the study scale area in 3D with a smaller or larger conceptual scenario to perfectly set initial and boundary conditions for any further numerical models to characterise reservoir properties for different geothermal purposes. We must mention that the physics applied do not take exothermic reactions from the dehydration of the clays (Eqs 5.1 to 5.7) into consideration and that we haven't included as an initial condition meteoritic water filling the system, which may cooldown the system in the shallowed surface and the surrounding Lusi vent. This explains why the results found in Figure 3a and Figure 4a are somehow overestimate the potential temperature in the shear zones/faults zone (conduit) during the time evolution simulation. Groundwater recharge from the sedimentary-hosted system and groundwater flow in the shallowed surfaces linked to the Arjuno-Welirang volcanic complex should also be quantified and taken into account, considering different hydrogeological scale calculations.

If in the future, we see an important increase of the geothermal gradient of the entire sediment-hosted hydrothermal system of East Java, we will have to recalculate and re-estimate the impact

of such new initial conditions and if the fluids outflow at the Lusi site do not decrease with the observed measurements, that would certify that the water filling the Lusi vent is also a recharge from the groundwater at different depth levels and this should be considered in different kinds of model scaling. However, the calculated physical parameters coincide with the observed field data measured on the Lusi site.

5.4.2 Implications for potential geothermal resources

Geyser systems can be found in many places and may be used as geothermal resources like in Italy (Lardarello), Iceland (Blue Lagoon) or in the U.S.A, California (The Geysers). Unfortunately none of them are alike. Each of them has a specific geological environment and as well as their own complexity. The underground beneath Lusi has a geological specificity and in its sedimentary configuration rock, dehydration may have an important impact. The Salton Sea (California, U.S.A) a sediment-hosted hydrothermal system (Svensen et al., 2007) may bear some resemblance with Lusi (Mazzini et al., 2018). However, this system has been erupting for quite a while in geological time compared to Lusi. The structural clay dehydration can cause porosity evolution at different scale as is shown in this article, if deep heated fluids fill the system. The water released from the clay rock induces porosity and permeability changes over several years. In our case, after 50 years since the incipient of Lusi in 2006, the physical rock changes are irreversible considering our implemented physics, but the dynamics of the fluids and the thermodynamics are clearly dependent on this processes. Regarding this analogy, we can perceive that Lusi may evolve like other sediment-hosted hydrothermal system.

Our high resolution 3D numerical simulations replicate the physical characteristic of the hydrodynamic display in the Lusi system with large-scale 3D geological structure environment. They illustrate how the considered processes takes place in 3D space and time evolution related to heated fluids source from depth regarding the actual observed geothermal gradient. In addition, they track the controlled rock property changes where dehydration occur and clarify how these changes progress over 50 years. Deducting from these models, it may be possible to evaluate a first estimation of the potential geothermal evolution of the Lusi system. The models suggest that the clay dehydration should reduce after 25 years of activity and even reach a steady-state after 50 years. If the geothermal gradient of the sediment-hosted hydrothermal system does not exceed 42°C/km in the future as it is observed today, in the East Java region, which will correspond more or less to a magmatic pulse intrusion since the birth of Lusi, we should be able to quantify the potential geothermal resource for this kind of sedimentary basin geo-resource. The complex volcanic structure in the vicinity of Lusi should be able to fill the sedimentary-hosted hydrothermal system over several years and might offer a chance for energy supply for the surrounding population as it can be observed on the temperature space distribution (Figure 61 and Figure 62). The simulations reveal characteristic property profiles which allow first diagnosis of the evolving host rock and estimate a first thermo-hydromechanical structure over time. Considering this, we can expect some challenges studies to potentially quantify the geo-resource of the Lusi system, and a part of the sedimentary basin system of East Java.

5.5 Conclusions

Here we present 3D numerical simulations using multi-GPU computing of fluid thermodynamics with porosity and permeability evolution from a hypothetical hydrothermal fluid intrusion at 5.5 km depth below the active Lusi eruption. We demonstrate the aspects of the system considering 3D geological structures since the incipient stage of Lusi reach an eventual steady-state after 25 to 50 years of geysering activity of clay dehydration rock at different level of depth. As explained the illitization of the minerals have already been metamorphosed by the geothermal and hydrostatic initial condition of the entire system. But the dehydration of the Upper Kalibeng Formation and a smaller part of the Ngimgbang Formation is still evolving through space and time. This process is irreversible and reach a complete steady-state for porosities and permeabilities evolution after 50 years. Due to initial conditions of the system, the Upper Kalibeng Formation structure has still fluids trapped into the rock and these fluids will produce hydro-fractures which will allow a preferential pathway driving more fluids to the surface.

- We have modelled in 3D space and time the dehydration of the two main clay formations (Upper Kalibeng Formation and Ngimgbang Formation) present below the Lusi vent. The simulations are consistent with data observed on the Lusi site.

- Under conditions of increasing temperature and pressure, dehydration reactions is still on going for clay minerals. The conceptual model proposed is applicable to the Lusi system for a fluid pressure-controlled by dehydration in deep hydrothermal systems or geothermal reservoirs, and have shown that the porosity and permeability evolution in time can have a no-negligible impact.

- The temperature difference of the fluids intrusion (500°C or 1000°C) impose as initial condition do not have a fundamental influence on the dehydrated system and demonstrate that the heated fluids come from a magmatic intrusion and not from a magmatic chamber underneath Lusi. If it had been a magmatic chamber beneath Lusi the entire system temperature would have been increase more rapidly and the measured temperature outflow at the vent would have also increase during the first decade of the Lusi activity. If no more fluids migration moves beneath the system, Lusi should stay as a moderated enthalpy system and continue its geyser behavior through the next century regularly. The 10 MPa overpressure and the heated fluids coming from 5.5 km mainly control the dehydration of the rock clay in the long term and that should be continually monitored during time evolution of the Lusi system.

- Starting from 2006, the results show that Lusi is going to produce less outflow fluids due to the two clay layers (Upper Kalibeng Formation and Ngimgbang Formation) dehydration in the next decades. Lusi will already reach a steady-state of water release after 25 years of activity.

- We conclude that the scenarios with a fluids intrusion emplaced at 5.5 km depth under Lusi is a relevant hypothesis to explain the water released by the two main clay layers observed, supported as well by available hydrogeological, geophysical and geochemical data analyses. 3D numerical calculations consolidate this hypothesis, but as all numerical simulations the initial and boundary conditions are essential. Those proposed have to be confirmed and validated by data field measurement.

- New borehole investigations even deeper than the existent ones in East Java need to be planned. Borehole campaigns for geothermal purposes is the way for energy demand. The debate would be virulent on the justification of such complex inquiries, but without drilling deeper new boreholes and studying them in detail, it will be impossible to use this potential heat reservoir as an energy supply. Decisions have to be made in the long term and in the direction or not to use renewable energy of such geothermal resources.

6. Conclusions and outlooks

"In geothermics, you should not crack underpressure!"

Analogy with geothermal energy exploitation and extreme sports.

6.1 Conclusions and outlooks

This thesis compiles studies of computational and geothermal sciences in natural hydrogeological settings. Numerical tools are presented, which enable realistic simulations of hydrothermal systems or geothermal reservoirs like geysers. The simulations presented in this work are important as they help to test the physical realism of scenarios from field observations and also guide field-based studies by predicting measurable phenomena. Geyser systems are difficult to study where 3D data acquisition is a major challenge. Modelling such complexity can be solved step by step, including or excluding certain physical phenomena. Considering the multiphysics of such system is crucial for fundamental insights for scientists and engineers.

The two newly developed computational tools using High Performance Computing (HPC) allow realistic 3D simulations for hydrothermal system or geothermal reservoirs and have been applied here to the Lusi geyser system in Java, Indonesia, for the first time. The results give new and surprising insights in the natural behaviors of this large-scale sediment-hosted hydrothermal system.

The two numerical tools developed in this dissertation, *HULK* and *GEYSER*, have shown their potential for high resolution problems and high speed simulation calculations for complex large-scale underground. Presented models highlight the importance of numerical simulations to understand the physics of complex hydrothermal systems or geothermal reservoirs using High Performance Computing (HPC). They showed that accurately accounting for non-linearity in governing equations is primordial in order to understand the physics related to thermal, hydrodynamic, mechanic and chemical processes involved in deep hydrogeological settings and can explain many observations of natural complex systems.

Moreover, results confirm that Lusi is a complex geyser system and that the metastable hydrogeological underground of the complex has to be studied even more in detail in the long term, for its future evolution. The dynamic instability of Lusi can directly explain variation in measured field data. Simulations reveal new mechanisms to either trap or mobilize fluids through the system. The main shear zones or faults crossing the system have created a corridor/conduit bringing hot fluids water and CO_2 from depth, which has a major impact on the mechanism of Lusi. These predicted behaviors with relative stability or instability is a function of water release from the two major underlying clay layers (Upper Kalibeng Formation and Ngimgbang Formation). The fluctuation of the processes from this moderate to high enthalpy system can be explained by the physics and dynamics of the heated fluids and the mechanical rock property changes with a period of fluctuation depending on the permeability of the conduit which drive the main fluids at Lusi. The results provide a simple explanation of how the evolution of the rock properties can trigger fluids behaviors fluctuations. The thermo-hydro-mechanic-chemical processes fundamentally change rock properties during the transient phase of this geyser system.

The most surprising result presented in the Lusi environmental study is the extremely unstable geological clay layers at depth, which brought many debates through the scientific community. Lusi will more or less reach a steady-state after several years of activity. The geyser activity

will certainly not stop in the future, but fluids release from the two main geological clay layers (Upper Kalibeng Formation and Ngimgbang Formation) will decrease over time. It is obvious, that the natural geofluids recharging this complex system will maintain the geysering activity of Lusi. The hydrothermal fluids have an expected residence time of several hours up to several years or decades.

Hydrothermal systems and geothermal reservoirs are of major interests to human population worldwide. The Lusi geyser is a rare phenomenon and is still gaining wide interest across the scientific community. The complexity of this deep hydrothermal system and the potential of this geothermal reservoir is huge for its scientific, energetic and economic potential. Understanding these natural phenomena is an important duty for society. Hydrological tracer experiments would be of interest and possible in an acceptable timeframe, but the optimal location would be in the vicinity of Lusi which is challenging today. These tests would provide critical data on permeability, porosity and flow paths to fine-tune more detailed and sophisticated numerical models for the transient evolution of Lusi. The LusiLAB machines have the potential to make new measurements in such a hostile environment. These measurements would be very helpful to constraint or even to calibrate numerical transient simulations. Additionally, Lusi needs to be studied in detail and confirmed by new borehole investigations even deeper than the existent ones in East Java. Borehole investigations for geothermal purposes is the way for energy demand. The debate would be virulent on the justification of such complex inquiry, but without drilling new deeper boreholes and studying them in detail, it will be impossible to use this potential heat reservoir for energy supply. Decisions have to be made in the long term and in the direction or not to use renewable energy of such geothermal resources. In comparison today through many countries, many systems similar to Lusi (e.g. Philippines, Iceland, U.S.A, etc.) are being studied for their geothermal potential. Risks have to be considered and detailed studies have to be made using appropriate tools.

The tools presented can still be improved by adding more physical processes. Future computational studies should be performed to investigate the optimal approach to handle more complexity of such systems considering multicomponent, multiphase changes, stress dependency or poro-elasticity processes in a fully 3D computational approach. These challenging simulations should follow the computational evolution of hardware performance and use the state-of-the-art technology advancement. Adding an in-situ visualization software enabling to connect directly to running simulation and allowing to visualize intermediate or final simulation results continually would be a benefit for post-processing analyses. The access to the data directly in memory would be very helpful for improving the work time for scientist and engineers using numerical tools.

The Lusi geyser system shows emerging, powerful, interactions between multidisciplinary sciences. The link between observations and realistic numerical high resolution models opens the possibility of studying the evolution of these complex coupled systems and accurate analyses can be performed. Faster numerical models that include most physics of the underlying processes have for decades been the goal in hydrogeological or geothermal sciences. This dissertation has provided a number of new fundamental insights into the first order physics for

hydrothermal systems or geothermal reservoirs. Multi-GPU technology allows faster simulations at high resolution in 3D, considering many processes. The work presented here is another step in the development of such computational and natural scientific research. More simulations are still required to fully understand the complex multiphysics acting at the Lusi geyser site. These challenging simulations need to consider the use of this immense geothermal potential. The Lusi geyser is naturally fascinating and understanding its beauty and force from an engineering approach will be an important step for supplying heat and electricity energy on the island of Java in Indonesia.

References

Abate, A.F., Nappi, M., Riccio, D., Sabatino, G. 2d and 3d face recognition: a survey**.** Pattern Recognit. Lett., 28 (14) (2007), pp. 1885-1906

Ayachit, U., Bauer, A., Geveci, B., O'Leary, P., Moreland, K., Fabian, N., & Mauldin, J. (2015, November). Paraview catalyst: Enabling in situ data analysis and visualization. In Proceedings of the First Workshop on In Situ Infrastructures for Enabling Extreme-Scale Analysis and Visualization (pp. 25-29). ACM.

Ayachit, U., Bauer, A., Geveci, B., O'Leary, P., Moreland, K., Fabian, N., & Mauldin, J. (2015, November). Paraview catalyst: Enabling in situ data analysis and visualization. In Proceedings of the First Workshop on In Situ Infrastructures for Enabling Extreme-Scale Analysis and Visualization (pp. 25-29). ACM.

Bangerth, W., Hartmann, R., & Kanschat, G. (2007). deal. II—a general-purpose object-oriented finite element library. ACM Transactions on Mathematical Software (TOMS), 33(4), 24.

Bangerth, W., Heister, T., Heltai, L., Kanschat, G., Kronbichler, M., Maier, M., & Turcksin, B. (2016). The deal. II library, version 8.3. Archive of Numerical Software, 4(100), 1-11.

Bear, J. (1972). Dynamics of fluids in porous media. Courier Corporation.

Bárdossy, G., & Fodor, J. (2001). Traditional and new ways to handle uncertainty in geology. Natural Resources Research, 10(3), 179-187.

Botella, A., Lévy, B., & Caumon, G. (2016). Indirect unstructured hex-dominant mesh generation using tetrahedra recombination. Computational Geosciences, 20(3), 437-451.

Bowen, Robert. (1979). Geothermal resources. London: New York: Applied Science Publishers; Halsted Press

Burstedde, C., Wilcox, L. C., & Ghattas, O. (2011). p4est: Scalable algorithms for parallel adaptive mesh refinement on forests of octrees. *SIAM Journal on Scientific Computing*, *33*(3), 1103-1133.

Calcagno, P., Chilès, J. P., Courrioux, G., & Guillen, A. (2008). Geological modelling from field data and geological knowledge: Part I. Modelling method coupling 3D potential-field interpolation and geological rules. *Physics of the Earth and Planetary Interiors*, *171*(1), 147-157.

Carcione, J. M., & Tinivella, U. (2001). The seismic response to overpressure: a modelling study based on laboratory, well and seismic data. Geophysical Prospecting, 49(5), 523-539.

Carman, P. C. (1937). Fluid flow through granular beds. Transactions-Institution of Chemical Engineeres, 15, 150-166.

Carman, P. C. (1956). Flow of gases through porous media. Academic press.

Casarotti, E., Stupazzini, M., Lee, S. J., Komatitsch, D., Piersanti, A., & Tromp, J. (2008). CUBIT and seismic wave propagation based upon the spectral-element method: An advanced unstructured mesher for complex 3D geological media. In Proceedings of the 16th International Meshing Roundtable (pp. 579-597). Springer Berlin Heidelberg.

Chan, C. T., & Anastasiou, K. (1997). An automatic tetrahedral mesh generation scheme by the advancing front method. Communications in Numerical Methods in Engineering, 13(1), 33-46.

Chong, C. S., Kumar, A. S., & Lee, H. P. (2007). Automatic mesh-healing technique for model repair and finite element model generation. Finite Elements in Analysis and Design, 43(15), 1109-1119.

Christie, M. A., & Blunt, M. J. (2001). Tenth SPE comparative solution project: A comparison of upscaling techniques. In SPE Reservoir Simulation Symposium. Society of Petroleum Engineers.

Chueh, C. C., Secanell, M., Bangerth, W., & Djilali, N. (2010). Multi-level adaptive simulation of transient two-phase flow in heterogeneous porous media. Computers & fluids, 39(9), 1585-1596.

Chueh, C. C., Djilali, N., & Bangerth, W. (2013). An h-adaptive operator splitting method for two-phase flow in 3D heterogeneous porous media. SIAM Journal on Scientific Computing, 35(1), B149-B175.

CREGE (2014). Laboratoire de Géothermie, Programme GeoNE-Développement de la géothermie profonde dans le canton de Neuchâtel. Rapport final de la Phase 1.

Colman-Sadd, S., & Scott, S. A. (1994). Newfoundland & Labrador traveller's guide to the geology: guidebook to stops of interest. Gouvernement of Newfoundland and Labrador.

Connolly, J. A. D., Holness, M. B., Rubie, D. C., & Rushmer, T. (1997). Reaction-induced microcracking: An experimental investigation of a mechanism for enhancing anatectic melt extraction. Geology, 25(7), 591-594.

Drake, P. (2016). Multiple visions of Indonesia's mud volcano: understanding representations of disaster across discursive settings. Disasters, 40(2), 346-364.

Datta, K., Williams, S., Volkov, V., Carter, J., Oliker, L., Shalf, J., & Yelick, K. (2009). Auto-tuning the 27-point stencil for multicore. In In Proc. iWAPT2009: The Fourth International Workshop on Automatic Performance Tuning.

Davies, R.J., Swarbrick, R.E., Evans, R.J., Husse, M. (2007). Birth of a mud volcano: East Java, 29 may 2006. Gsa Today, 17 (2), p. 4

Davies, R.J., Brumm, M., Manga, M., Rubiandini, R., Swarbrick, R., Tingay, M. (2008).The East Java mud volcano (2006 to present): an earthquake or drilling trigger? Earth Planet. Sci. Lett., 272 (3–4), pp. 627-638

Davies, R.J., Manga, M., Tingay, M., Lusianga, S., Swarbrick, R.E. (2010). Discussion: Sawolo et al. (2009) the Lusi mud volcano controversy: was it caused by drilling? Mar. Petrol. Geol., 27 (7), pp. 1651-1657, 10.1016/j.marpetgeo.2010.01.019

Denbigh, K. (1966). The principles of chemical equilibrium. Cambridge University Press, Cambridge, 287.

Doust, H., & Noble, R. A. (2008). Petroleum systems of Indonesia. Marine and Petroleum Geology, 25(2), 103-129.

Du, Q., & Wang, D. (2006). Recent progress in robust and quality Delaunay mesh generation. Journal of Computational and Applied Mathematics, 195(1), 8-23.

Duan, Z., Møller, N., & Weare, J. H. (1992). An equation of state for the CH4-CO2-H2O system: II. Mixtures from 50 to 1000 °C and 0 to 1000 bar. Geochimica et Cosmochimica Acta, 56(7), 2619-2631.

Duan, Z., & Sun, R. (2003). An improved model calculating CO2 solubility in pure water and aqueous NaCl solutions from 273 to 533 °K and from 0 to 2000 bar. Chemical geology, 193(3), 257-271.

Eigestad, G. T., Dahle, H. K., Hellevang, B., Riis, F., Johansen, W. T., & Øian, E. (2009). Geological modeling and simulation of CO 2 injection in the Johansen formation. Computational Geosciences, 13(4), 435-450.

Ericson, C. (2004). Real-time collision detection. CRC Press.

Ernst, M., & Greiner, G. (2008). Multi bounding volume hierarchies. In Interactive Ray Tracing, 2008. RT 2008. IEEE Symposium on (pp. 35-40). IEEE.

Fuchs, H., Kedem, Z. M., & Naylor, B. F. (1980). On visible surface generation by a priori tree structures. In ACM Siggraph Computer Graphics(Vol. 14, No. 3, pp. 124-133). ACM.

Fallahi, M. J., Obermann, A., Lupi, M., Karyono, K., & Mazzini, A. (2017). The plumbing system feeding the Lusi eruption revealed by ambient noise tomography. Journal of Geophysical Research: Solid Earth, 122(10), 8200-8213.

Galvan, B. (2012). Modeling the spatio-temporal evolution of fracture networks and fluid-rock interactions in GPU: Application to lithospheric geodynamics. PhD thesis 1-118.

Galvan, B., & Miller, S. (2013). A full GPU simulation of evolving fracture networks in a heterogeneous poro-elasto-plastic medium with effective-stress-dependent permeability. In GPU Solutions to Multi-scale Problems in Science and Engineering (pp. 305-319). Springer, Berlin, Heidelberg.

Geddes, P. (1915). Cities in evolution an introduction to the town planning movement and to the study of civics.

Gerya, T. (2009). Introduction to numerical geodynamic modelling. Cambridge University Press.

Geuzaine, C., & Remacle, J. F. (2009). Gmsh: A 3-D finite element mesh generator with built-in pre-and post-processing facilities. International journal for numerical methods in engineering, 79(11), 1309-1331.

Griebel, M., & Zaspel, P. (2010). A multi-GPU accelerated solver for the three-dimensional two-phase incompressible Navier-Stokes equations. Computer Science-Research and Development, 25(1), 65-73.

Gysi, T., Osuna, C., Fuhrer, O., Bianco, M., & Schulthess, T. C. (2015). STELLA: A domain-specific tool for structured grid methods in weather and climate models. In High Performance Computing, Networking, Storage and Analysis, 2015 SC-International Conference for (pp. 1-12). IEEE.

Hammond, G. E., Lichtner, P. C., Lu, C., & Mills, R. T. (2012). Pflotran: reactive flow & transport code for use on laptops to leadership-class supercomputers. Groundwater reactive transport models, 141-159.

Hammond, G. E., Lichtner, P. C., & Mills, R. T. (2014). Evaluating the performance of parallel subsurface simulators: An illustrative example with PFLOTRAN. Water resources research, 50(1), 208-228.

Hassanizadeh, S. M., & Gray, W. G. (1979). General conservation equations for multi-phase systems: 1. Averaging procedure. *Advances in Water Resources*, *2*, 131-144.

Hassanizadeh, S. M., & Gray, W. G. (1990). Mechanics and thermodynamics of multiphase flow in porous media including interphase boundaries. *Advances in water resources*, *13*(4), 169-186.

Helmig, R. (1997). Multiphase flow and transport processes in the subsurface: a contribution to the modeling of hydrosystems. Springer-Verlag.

Henderson, A., Ahrens, J., & Law, C. (2004). The ParaView Guide (pp. 1-276). Clifton Park, NY: Kitware.

Ho-Le, K. (1988). Finite element mesh generation methods: a review and classification. Computer-aided design, 20(1), 27-38.

Hoppe, H. (1999). New quadric metric for simplifiying meshes with appearance attributes. In Proceedings of the conference on Visualization'99: celebrating ten years (pp. 59-66). IEEE Computer Society Press.

Hurwitz, S., & Manga, M. (2017). The fascinating and complex dynamics of geyser eruptions. Annual Review of Earth and Planetary Sciences, 45, 31-59.

Ingebritsen, S. E., & Sanford, W. E. (1999). Groundwater in geologic processes. Cambridge University Press.

Ingebritsen, S. E., Geiger, S., Hurwitz, S., & Driesner, T. (2010). Numerical simulation of magmatic hydrothermal systems. Reviews of Geophysics, 48(1).

Inguaggiato, S., Mazzini, A., Vita, F., and Sciarra, A. (2018). The Arjuno-Welirang Volcanic Complex and the connected Lusi system: geochemical evidences: Marine & Petroleum Geology, 90, 67-76.

Istadi, B. P., Sunardi, E., Wibowo, H. T., Sawolo, N., & Hadi, S. (2012). Mud volcano and its evolution. INTECH Open Access Publisher.

ISOR, Iceland Geosurvey.

Jansen, G., Sohrabi, R., & Miller, S.A. (2017). HULK - Simple and fast generation of structured hexahedral meshes for improved subsurface simulations. Computers and Geosciences, 99, 159-170.

Jasak, H., Jemcov, A., & Tukovic, Z. (2007). OpenFOAM: A C++ library for complex physics simulations. In International workshop on coupled methods in numerical dynamics (Vol. 1000, pp. 1-20). IUC Dubrovnik, Croatia.

Jeanne, P., Rutqvist, J., Vasco, D., Garcia, J., Dobson, P. F., Walters, M., & Borgia, A. (2014). A 3D hydrogeological and geomechanical model of an Enhanced Geothermal System at The Geysers, California. Geothermics, 51, 240-252.

Joseph, D. D. (1976). Stability of Fluid Motions II, Springer, Berlin. [2.3, 6.3, 6.4]
Karyono, K., Obermann, A., Lupi, M., Masturyono, M., Hadi, S., Syafri, I., Abdurrokhim, A., and Mazzini, A., 2017, Lusi, a clastic-dominated geysering system in Indonesia recently explored by surface and subsurface observations: Terra Nova, v. 29, p. 13-19.

Kolditz, O., Bauer, S., Bilke, L., Böttcher, N., Delfs, J. O., Fischer, T., ... & Park, C. H. (2012). OpenGeoSys: an open-source initiative for numerical simulation of thermo-hydro-mechanical/chemical (THM/C) processes in porous media. Environmental Earth Sciences, 67(2), 589-599.

Kozeny, J. (1927). Uber kapillare leitung der wasser in boden. Royal Academy of Science, Vienna, Proc. Class I, 136, 271-306.

Krotkiewski, M., & Dabrowski, M. (2013). Efficient 3D stencil computations using CUDA. Parallel Computing, 39(10), 533-548.

Kusumastuti, A., Van Rensbergen, P., & Warren, J. K. (2002). Seismic sequence analysis and reservoir potential of drowned Miocene carbonate platforms in the Madura Strait, East Java, Indonesia. AAPG bulletin, 86(2), 213-232.

Künze, R., & Lunati, I. (2012). An adaptive multiscale method for density-driven instabilities. Journal of Computational Physics, 231(17), 5557-5570.

Lajaunie, C., Courrioux, G., & Manuel, L. (1997). Foliation fields and 3D cartography in geology: principles of a method based on potential interpolation. Mathematical Geology, 29(4), 571-584.

Li, Q., Ito, K., Wu, Z., Lowry, C. S., Loheide, I. I., & Steven, P. (2009). COMSOL Multiphysics: A novel approach to ground water modeling. Groundwater, 47(4), 480-487.

Lichtner, P. C., & Carey, J. W. (2006). Incorporating solid solutions in reactive transport equations using a kinetic discrete-composition approach. Geochimica et Cosmochimica Acta, 70(6), 1356 1378. https://doi.org/10.1016/j.gca.2005.11.028

Lichtner, P. C., & Kang, Q. (2007). Upscaling pore-scale reactive transport equations using a multiscale continuum formulation. Water Resources Research, 43, W12S15. https://doi.org/10.1029/2006WR005664

Lin, M., & Gottschalk, S. (1998). Collision detection between geometric models: A survey. In Proc. of IMA conference on mathematics of surfaces (Vol. 1, pp. 602-608).

Lindsay, M. D., Aillères, L., Jessell, M. W., de Kemp, E. A., & Betts, P. G. (2012). Locating and quantifying geological uncertainty in three-dimensional models: Analysis of the Gippsland Basin, southeastern Australia. Tectonophysics, 546, 10-27.

Lizarralde, D., Soule, S. A., Seewald, J. S., & Proskurowski, G. (2011). Carbon release by off-axis magmatism in a young sedimented spreading centre. Nature Geoscience, 4(1), 50-54.

Löhner, R. (1996). Progress in grid generation via the advancing front technique. Engineering with computers, 12(3), 186-210.

Lowenstern, J. B., & Hurwitz, S. (2008). Monitoring a supervolcano in repose: Heat and volatile flux at the Yellowstone Caldera. Elements, 4(1), 35-40.

Lupi, M., Saenger, E. H., Fuchs, F., & Miller, S. A. (2013). Lusi mud eruption triggered by geometric focusing of seismic waves. Nature Geoscience, 6(8), 642-646.

Malvoisin, B., Mazzini, A., & Miller, S.A. (2016). Constraining the thermal structure beneath Lusi: insights from temperature record in erupted clasts. EGU General Assembly 2016. EGU2016-16421.

Malvoisin, B., Podladchikov, Y. Y., & Vrijmoed, J. C. (2015). Coupling changes in densities and porosity to fluid pressure variations in reactive porous fluid flow: Local thermodynamic equilibrium. Geochemistry, Geophysics, Geosystems, 16(12), 4362-4387.

Marechal, L. (2001). A New Approach to Octree-Based Hexahedral Meshing. In IMR.

Marechal, L. (2009). Advances in octree-based all-hexahedral mesh generation: handling sharp features. Proceedings of the 18th International Meshing Roundtable, 65-84.

Mazzini, A. (2018). 10 years of Lusi eruption: Lessons learned from multidisciplinary studies (LUSI LAB). Marine and Petroleum Geology, 90, 1-9.

Mazzini, A., Etiope, G., & Svensen, H. (2012). A new hydrothermal scenario for the 2006 Lusi eruption, Indonesia. Insights from gas geochemistry. Earth and Planetary Science Letters, 317, 305-318.

Mazzini, A., Nermoen, A., Krotkiewski, M., Podladchikov, Y., Planke, S., and Svensen, H. (2009). Strike-slip faulting as a trigger mechanism for overpressure release through piercement structures. Implications for the Lusi mud volcano, Indonesia: Marine and Petroleum Geology, 26, 1751-1765.

Mazzini, A., Scholz, F., Svensen, H., Hensen, C., & Hadi, S. (2018). The geochemistry and origin of the hydrothermal water erupted at Lusi, Indonesia. Marine and Petroleum Geology, 90, 52-66.

Mazzini, A., Svensen, H., Akhmanov, G. G., Aloisi, G., Planke, S., Malthe-Sørenssen, A., & Istadi, B. (2007). Triggering and dynamic evolution of the LUSI mud volcano, Indonesia. Earth and Planetary Science Letters, 261(3), 375-388.

Mauri, G., Husein, A., Mazzini, A., Irawan, D., Sohrabi, R., Hadi, S., Prasetyo, H. & Miller, S. A. (2018). Insights on the structure of Lusi mud edifice from land gravity data. Marine and Petroleum Geology, 90, 104-115.

Micikevicius, P. (2009). 3D finite difference computation on GPUs using CUDA. In Proceedings of 2nd workshop on general purpose processing on graphics processing units (pp. 79-84). ACM.

Michéa, D., & Komatitsch, D. (2010). Accelerating a three-dimensional finite-difference wave propagation code using GPU graphics cards. Geophysical Journal International, 182(1), 389-402.

Miller, S. A. (2015). Modeling enhanced geothermal systems and the essential nature of large-scale changes in permeability at the onset of slip. Geofluids, 15 (1-2), 338-349.

Miller, S. A., Collettini, C., Chiaraluce, L., Cocco, M., Barchi, M., Kaus, B.J.P. (2004). Aftershocks driven by high-pressure CO2 source at depths. Nature, 427, 724-7.

Miller, S. A., Nur, A., & Ogaard D.L. (1996). Earthquakes as a coupled shear stress high pore pressure dynamical system. Geophysical Research Letters, 23, 197-200.

Miller, S. A. & Nur, A. (2000). Permeability as a toggle switch in fluid controlled crustal processes. Earth and Planetary Science Letters, 183, 133-46.

Miller, S. A., & Mazzini, A. (2018). More than ten years of Lusi: A review of facts, coincidences, and past and future studies. Marine and Petroleum Geology, 90, 10-25.

Miller, S. A., Van Der Zee, W., Olgaard, D. L., & Connolly, J. A. D. (2003). A fluid-pressure feedback model of dehydration reactions: experiments, modelling, and application to subduction zones. *Tectonophysics*, *370*(1), 241-251

Miller, T. A., Vessilinov, V. V., Stauffer, P. H., Birdsell, K. H., Gable, C. W., & Kues, B. S. (2007). Integration of geologic frameworks in meshing and setup of computational hydrogeologic models, Pajarito Plateau, New Mexico. In New Mex. Geol. Soc. Guid. Book, 58th F. Conf. Geol. Jemez Mt. Reg. III.

Moscariello, A., Do Couto, D., Mondino, F., Booth, J., Lupi, M., & Mazzini, A. (2018).Genesis and evolution of the Watukosek fault system in the Lusi area (East Java): Marine & Petroleum Geology, 90, 125-137.

Nield, D. A., Bejan, A., & Nield-Bejan (2006). Convection in porous media (Vol. 3). New York: springer.

NVIDIA (2017). NVIDIA CUDA C Programming Guide version 9.0, NVIDIA Corporation.

Omlin, S. (2017). Development of Massively parallel near peak performance solvers for three-dimensional geodynamic modelling. PhD thesis 1-176.

Omlin, S., Malvoisin, B., & Podladchikov, Y. Y. (2017). Pore Fluid Extraction by Reactive Solitary Waves in 3-D. Geophysical Research Letters, 44(18), 9267-9275.

Omlin, S., Räss, L., & Podladchikov, Y. Y. (2015). HPC.m - The MATLAB HPC Compiler and its use for solving 3D poromechanics on supercomputers, Platform for Advanced Scientific Computing Conference ETH Zurich, Switzerland.

Owen, S. J., & Shelton, T. R. (2015). Evaluation of grid-based hex meshes for solid mechanics. Engineering with Computers, 31(3), 529-543.

Patankar, S. (1980). Numerical heat transfer and fluid flow. CRC press.

Pitzer, K. S. (1973). Thermodynamics of electrolytes. I. Theoretical basis and general equations. The Journal of Physical Chemistry, 77 (2), 268-277.

Pruess, K. (1991). TOUGH2: A general-purpose numerical simulator for multiphase fluid and heat flow (p. 102). Berekeley, California: Lawrence Berkeley Laboratory.

Pruess, K., Oldenburg, C. M., & Moridis, G. J. (1999). TOUGH2 user's guide version 2. Lawrence Berkeley National Laboratory.
Press, F. & Siever, R. (2004). Understanding earth. Macmillan.

Pollack, H. N., Hurter, S. J., & Johnson, J. R. (1993). Heat flow from the Earth's interior: analysis of the global data set. Reviews of Geophysics, 31(3), 267-280.

Rice, J. R. in Fault Mechanics and Transport properties of Rock (eds Evans, B. & Wong, T.-f.) 476-503 (Academic, San Diego, 1992)

Richards, J. R. (2011). Report into the past, present, and future social impacts of Lumpur Sidoarjo. Humanitus Sidoarjo Fund.

Rudolph, M. L., Shirzaei, M., Manga, M., & Fukushima, Y. (2013). Evolution and future of the Lusi mud eruption inferred from ground deformation. Geophysical Research Letters, 40(6), 1089-1092.

Samankassou, E., Mazzini, A., Chiaradia, M., & Spezzaferri, S. (2018). The carbonate deposits underneath the geysering Lusi eruption (Java, Indonesia): (this volume) Marine & Petroleum Geology.

Sawolo, N., Sutriono, E., Istadi, B. P., & Darmoyo, A. B. (2009). The LUSI mud volcano triggering controversy: Was it caused by drilling?. Marine and Petroleum Geology, 26(9), 1766-1784.

Schneiders, R. (1996). A grid-based algorithm for the generation of hexahedral element meshes. Engineering with computers, 12(3-4), 168-177.

Sciarra, A., Mazzini, A., Inguaggiato, S., Vita, F., Lupi, A., and Hadi, S. (2018). Radon and carbon gas anomalies along the Watukosek fault system and Lusi mud eruption, Indonesia. Marine & Petroleum Geology, 90, 77-90.

Scott, M. A., Earp, M. N., Benzley, S. E., & Stephenson, M. B. (2005). Adaptive sweeping techniques. In Proceedings of the 14th International Meshing Roundtable (pp. 417-432). Springer, Berlin, Heidelberg.

Shephard, M. S., & Georges, M. K. (1991). Automatic three-dimensional mesh generation by the finite octree technique. International Journal for Numerical methods in engineering, 32(4), 709-749.

Shirzaei, M., Rudolph, M. L., & Manga, M. (2015). Deep and shallow sources for the Lusi mud eruption revealed by surface deformation. Geophysical Research Letters, 42(13), 5274-5281.

Smithsonian Institution (2017), https://volcano.si.edu/E3/

Sohrabi, R., Jansen, G., Malvoisin, B., Mazzini, A., & Miller, S. A. (2018). Numerical modeling of the Lusi hydrothermal system: Initial results and future challenges. Marine and Petroleum Geology, 90, 191-200.

Sohrabi, R., Malvoisin, M., Mazzini, A., & Miller, S. A (2018) Multi-GPU based 3D numerical modeling of the Lusi geyser system in Java, Indonesia. Journal of Volcanology and Geothermal Research (in preparation for submission).

Sohrabi, R., Omlin, S., & Miller, S. A (2018) GEYSER: 3D thermo-hydrodynamic reactive transport numerical simulator considering porosity and permeability evolution on multi-GPU technology. Computational Geoscience Journal (in preparation for submission).

Stefano, R. and Hailu, T.S. (2014). Solve. The Exascale Effect: Benefits of Supercomputing Investment for U.S. Industry, Washington, D.C., 2014. http://www.compete.org/reports/all/2695-solve.

Strikwerda, J. C. (2004). Finite difference schemes and partial differential equations. Society for Industrial and Applied Mathematics.

Stupazzini, M., 2004. A Spectral Element Approach for 3d Dynamic Soil–Structure Interaction Problems (Ph.D. Thesis).

Steefel, C. I., DePaolo, D. J., & Lichtner, P. C. (2005). Reactive transport modeling: An essential tool and a new research approach for the Earth sciences. Earth and Planetary Science Letters, 240(3–4), 539–558. https://doi.org/10.1016/j.epsl.2005.09.017

Suisse Energie (OFEN). (2017). Géothermie en Suisse. Une source d'énergie polyvalente.

Sun, H., Feistel, R., Koch, M., & Markoe, A. (2008). New equations for density, entropy, heat capacity, and potential temperature of a saline thermal fluid. Deep Sea Research Part I: Oceanographic Research Papers, 55(10), 1304-1310.

Svensen, H., Hammer, Ø., Mazzini, A., Onderdonk, N., Polteau, S., Planke, S., & Podladchikov, Y. Y. (2009). Dynamics of hydrothermal seeps from the Salton Sea geothermal system (California, USA) constrained by temperature monitoring and time series analysis. Journal of Geophysical Research: Solid Earth, 114(B9).

Svensen, H. H., Iyer, K., Schmid, D. W., & Mazzini, A. (2018). Modelling of gas generation following emplacement of an igneous sill below LUSI, east Java, Indonesia. Marine and Petroleum Geology, 90, 201-208.

Svensen, H., Karlsen, D. A., Sturz, A., Backer-Owe, K., Banks, D. A., & Planke, S. (2007). Processes controlling water and hydrocarbon composition in seeps from the Salton Sea geothermal system, California, USA. Geology, 35(1), 85-88.

Tanikawa, W., Sakaguchi, M., Wibowo, H. T., Shimamoto, T., & Tadai, O. (2010). Fluid transport properties and estimation of overpressure at the Lusi mud volcano, East Java Basin. Engineering Geology, 116(1), 73-85.

Tingay, M., Heidback, O., Davies, R.J., Swarbrick, R.E. (2008). Triggering of the Lusi mud eruption: earthquake versus drilling initiation. Geology, 36 (8), pp. 639-642

Tingay, M., Manga, M., Rudolph, M. L., & Davies, R. (2017). An alternative review of facts, coincidences and past and future studies of the Lusi eruption. Marine and Petroleum Geology (in press).

Tingay, M., Rudolph, M.L., Manga, M., Davies, R.J., Wang, C.-Y. (2015). Initiation of the Lusi mudflow disaster. Nat. Geosci., 8 (7), pp. 493-494

Thore, P., Shtuka, A., Lecour, M., Ait-Ettajer, T., & Cognot, R. (2002). Structural uncertainties: Determination, management, and applications. Geophysics, 67(3), 840-852.

Top500.org. (2017) https://www.top500.org/list/2017/11/

Trefry, M. G., & Muffels, C. (2007). FEFLOW: A Finite-Element Ground Water Flow and Transport Modeling Tool. Groundwater, 45(5), 525-528.

Tu, T., & O'Hallaron, D. R. (2004). Extracting hexahedral mesh structures from balanced linear octrees.

Vanderkluysen, L., Burton, M. R., Clarke, A. B., Hartnett, H. E., & Smekens, J. F. (2014). Composition and flux of explosive gas release at LUSI mud volcano (East Java, Indonesia). Geochemistry, Geophysics, Geosystems, 15(7), 2932-2946.

Van Noorden, R., 2006, Mud volcano floods Java: Nature, v. doi : 10.1038/ news060828-1

Vidal, O., & Dubacq, B. (2009). Thermodynamic modelling of clay dehydration, stability and compositional evolution with temperature, pressure and H2O activity. Geochimica et Cosmochimica Acta, 73(21), 6544-6564.

VisItusers.org, (n.d.). www.visitusers.org (accessed November, 2017).

Wellmann, J. F., Finsterle, S., & Croucher, A. (2014). Integrating structural geological data into the inverse modelling framework of iTOUGH2. Computers & Geosciences, 65, 95-109.

White, D. E. (1957). Thermal waters of volcanic origin. Geological Society of America Bulletin, 68(12), 1637-1658.

Xing, H., Yu, W., & Zhang, J. (2009). 3D mesh generation in geocomputing. Advances in Geocomputing, 27-64.

Xu, T., Sonnenthal, E., Spycher, N., & Pruess, K. (2008). TOUGHREACT user's guide: A simulation program for non-isothermal multiphase reactive geochemical transport in variably saturated geologic media, V1. 2.1 (No. LBNL-55460-2008). Ernest Orlando Lawrence Berkeley National Laboratory, Berkeley, CA (US).

Yerry, M. A., & Shephard, M. S. (1984). Automatic three-dimensional mesh generation by the modified-octree technique. International Journal for Numerical Methods in Engineering, 20(11), 1965-1990.

Yu, W., Zhang, K., & Li, X. (2015). Recent algorithms on automatic hexahedral mesh generation. In Computer Science & Education (ICCSE), 2015 10th International Conference on (pp. 697-702). IEEE.

Zehner, B., Hellwig, O., Linke, M., Görz, I., Buske, S. (2015). A method for converting triangle-mesh-based 3d geological models into hexahedral grids for parallel finite difference simulation. In: 35th Gocad Meeting – 2015 RING Meeting, ASGA.

Zoporowski, A., & Miller, S. A. (2009). Modelling eruption cycles and decay of mud volcanoes. Marine and Petroleum Geology, 26(9), 1879-1887.